CHANGES IN AUDITORY EVOKED RESPONSES DUE TO BLAST AND AGING

by

Emily X. Han

A Dissertation

Submitted to the Faculty of Purdue University

In Partial Fulfillment of the Requirements for the degree of

Doctor of Philosophy

Department of Biological Sciences

West Lafayette, Indiana

May 2021

THE PURDUE UNIVERSITY GRADUATE SCHOOL
STATEMENT OF COMMITTEE APPROVAL

Dr. Edward L. Bartlett, Chair
Department of Biological Sciences

Dr. Alexander A. Chubykin
Department of Biological Sciences

Dr. Michael G. Heinz
Department of Speech, Language, and Hearing Sciences

Dr. Stephanie M. Gardner
Department of Biological Sciences

Approved by:
Dr. Janice P. Evans

To my dear friends, Luyao Che and Vivi Cheng, for their unconditional love and encouragement

And, to my friends at Graduate Rights and Our Well-Being (GROW), whose care and camaraderie pushed me through this unprecedented time.

ACKNOWLEDGMENTS

I would like to express my sincerest gratitude to Dr. Edward Bartlett for his mentorship. Despite all the tribulations I encountered, you have always had faith in me. I will forever be grateful for the knowledge you have imparted, the trainings and opportunities you provided, and the unfailing care and patience along my journey of fulfilling this Ph. D study. In every sense possible, you have rebuilt me as a scholar.

My gratitude also goes to all members of my committee, Dr. Stephanie Gardner, Dr. Mike Heinz, and Dr. Alex Chubykin for their considerate guidance and advice. I would also like to thank Dr. Riyi Shi of Lab of Translational Neuroscience for providing the opportunity, resource, and encouragement for me to work on the blast project.

I would like to thank Purdue University Department of Biological Sciences, Weldon School of Biomedical Engineering, and the Institute for Integrative Neuroscience for providing the resources and a friendly, intellectually stimulating research environment which allowed me to conduct the present study.

I would also like to thank the past and present members of central auditory processing laboratory, especially Aravindakshan Parthasarathy, Brandon Coventry, Jesyin Lai, Caitlin Swanberg, Alex Sommer, Nanami Miyazaki, and Marisa Dowling, for their generous help and advice working together. I would also like to thank Dr. Bjorn Herrmann for helping me overcome several technical obstacles in circular statistics. Special thank also goes to Joseph Fernandez. You have been my brother in arms for a major part of this arduous, but ultimately worthwhile journey.

Last but not the least, I would like to thank my parents, my brother Eric, my best friends Luyao Che and Vivi Cheng, and all my friends at Graduate Rights and Our Well-Being. Without your love and support, none of this would have been possible.

The research of this dissertation was funded by NIDCD DC-011580 (Chapter 3) and Indiana CTSI 11917 (Chapter 4 and 5).

TABLE OF CONTENTS

LIST OF TABLES

LIST OF FIGURES

ABBREVIATIONS

A1	Auditory cortex
ABRs	Auditory brainstem responses
AEP	Auditory-evoked potential
AM	Amplitude modulation
AMFR	Amplitude modulation-following response
AN	Auditory nerve
ANF	Auditory nerve fiber
ARHL	Age-related hearing loss
BF	Best frequency
BIHL	Blast-induced hearing loss
BMF	Best modulation frequency
bTBI	Blast-induced traumatic brain injury
CAP	Central auditory processing
CAS	Central auditory system
CN	Cochlear nucleus
DCN	Dorsal nucleus of CN
EFRs	Envelope-following responses
F344	Fischer 344 (rat strain)
FFRs	Frequency-following responses
FFTs	Fast Fourier Transforms
IC	Inferior colliculus
ICC	Central nucleus of the inferior colliculus
IHC	Inner hair cell
IRN	Iterated rippled noise
LFP	Local field potential

LL	Lateral lemniscus
MFs	Modulation frequencies
MLRs	Middle latency responses
MGB	Medial geniculate body
NIHL	Noise-induced hearing loss
PH	Period histogram
PSTH	Peristimulus time histograms
rBMF	Best modulation frequency for rate
SOC	Superior olivary complex
TBI	Traumatic brain injury
VCN	Ventral nucleus of CN
VS	Vector strength

ABSTRACT

Hearing loss of various types is increasingly plaguing our modern world (Geneva: World Health Organization 2018). As the life expectancy increased in the industrialized world, age-related hearing loss (ARHL) has become more prevalent. The wars and terrorism of the modern world also created a significant body of blast-induced hearing loss (BIHL) patients. Both types of hearing loss present significant challenges for listeners even at suprathreshold sound levels. However, increasing bodies of clinical and laboratory evidence have suggested that the difficulties in the processing of time-varying auditory features in speech and other natural sounds may not be sufficiently diagnosed by threshold changes and simple auditory electrophysiological measures (Snell and Frisina 2000; Saunders et al. 2015; Bressler et al. 2017; Guest et al. 2018).

Studies have emphasized that excitatory/inhibitory neurotransmission imbalance plays important roles in ARHL (Caspary et al. 2008) and may also be key in BIHL, as hinted by the strong presence of GABA regulation in non-blast TBI (O'Dell et al. 2000; Cantu et al. 2015; Guerriero et al. 2015). The current studies focus on age-related and blast-induced hearing deficits by examining changes in the processing of simple, brief stimuli and complex, sustained, temporally modulated sounds.

Through post hoc circular analysis of single-unit, *in vivo* recording of young and aged inferior colliculus (IC) neurons responding to amplitude modulation (AM) stimuli and modulation depth changes, we observed evidence of central compensation in the IC manifesting as increased sensitivity to presynaptic input, which was measured via local field potentials (LFPs). We also found decreased sensitivity to decreasing modulation depth. Age-related central gain in the IC single units, while preserving and even overcompensating for temporal phase coding in the form of vector strength, was unable to make up for the loss of envelope shape coding.

Through careful, longitudinal measurements of auditory evoked potential (AEP) responses towards simple sounds, AM and speech-like iterated rippled noise (IRN), we documented the development and recovery of BIHL induced by a single mild blast in a previously established (Song et al. 2015; Walls et al. 2016; Race et al. 2017) rat blast model over the course of two months. We identified crucial acute (day 1-4 post-exposure) and early recovery (day 7-14) time windows in which drastic changes in electrophysiology take place. Challenging conditions and broadband, speech-like stimuli can better elucidate mild bTBI-

induced auditory deficits during the sub-acute period. The anatomical significance of the aforementioned time windows was demonstrated with immunohistochemistry methods, showing two distinct waves of GABA inhibitory transmission changes taking place in the auditory brainstem, the IC, and the auditory thalamus. These changes were in addition to axonal and oxidative damage evident in the acute phase. We examined the roles and patterns of excitatory/inhibitory imbalance in BIHL, its distinction compared to that of ARHL, and demonstrated the complexity of its electrophysiological consequences. Blast traumatizes the peripheral auditory system and auditory brainstem, evident through membrane damage and acrolein-mediated oxidative stress. These initial traumas kickstart a unique, interlocking cascade of excitatory/inhibitory imbalances along the auditory neuraxis that is more complex and individually varied than the gradual, non-traumatic degradations in ARHL. Systemic treatment with the FDA-approved acrolein scavenger Hydralazine (HZ) was attempted with limited effects.

Taken together, the current study provided insights into the similarities and distinctions between the mechanisms of ARHL and BIHL and called for innovative and individual diagnostic and therapeutic measures.

CHAPTER 1. INTRODUCTION

Hearing loss is a malady that plagues the modern world, with more than 15% of the population affected by any form of auditory deficits (Felix et al. 2018). WHO estimated that around 466 million people suffer from disabling hearing loss globally (Geneva: World Health Organization 2018). Notably, the growing life expectancy in the industrialized world indicates an increasing prevalence of age-related hearing loss (ARHL), while blast-induced hearing deficits have become a major source of lasting trauma, threatening the quality of life of survivors from military and civil instabilities. In diagnosing and treating these forms of hearing deficits, the changes in the central auditory system (CAS) are often overlooked in contrast to the more easily assessed peripheral changes in auditory threshold. However, clinical and laboratory studies have noted that the difficulties in the processing of time-varying auditory features encountered may not be closely correlated to absolute thresholds (Snell and Frisina 2000; Guest et al. 2018), and instead may come from more central sources along the auditory pathway (Plack et al. 2016; Grose et al. 2019). Specifically, the subcortical CAS has been attracting the attention of hearing deficit researchers over the past two decades (Frisina 2001; Caspary et al. 2008; Anderson et al. 2013a; Felix et al. 2018). The systematic changes that occur alongside age-related and blast-induced hearing deficits both encompass subcortical CAS (Burianova et al. 2009; Cho et al. 2013b; Race et al. 2017; Caspary and Llano 2019). Therefore, it is imperative that we examine how these changes relate to the development of auditory deficits, and vice versa.

This dissertation will first investigate the age-related changes in single-unit temporal coding in the auditory midbrain region of the inferior colliculus (IC). With that knowledge, we will then examine blast-induced auditory deficits as exhibited by the auditory responses of various subcortical auditory locales, and correlate to the changes in anatomical features, especially neurochemical excitatory/inhibitory imbalance. Our hypothesis is that similar to ARHL, the changes in excitatory/inhibitory neurotransmissions, both *de novo* and in response to peripheral damage, are a major driver of the temporal deficits in the blast-exposed subcortical CAS.

1.1 Specific aims

The subcortical CAS mechanisms of ARHL, especially the temporal processing aspect, have been hypothesized to be driven prominently by neurochemical excitatory/inhibitory

imbalance (Caspary et al. 2008; Caspary and Llano 2019). Age-related hearing deficits share certain parallels in peripheral neurodegeneration and central neurochemical changes with the lesser-understood blast-induced central auditory deficits. Chapter 2 provides a literature review on the background related to subcortical CAS and means to reveal central auditory deficits. This chapter will also establish the similarities between age-related and blast-induced hearing loss. The subsequent chapters contain research performed to investigate temporal processing mechanisms in age-related and blast-induced hearing deficits, as well as the potential role of excitatory/inhibitory changes. The research will be divided into three aspects, as presented in three specific aims:

In the first specific aim, we addressed the changes in phase-locking ability, a significant temporal property, as well as rate coding of aged and young rat IC neurons towards amplitude modulation (AM) depth stimuli using circular statistical analysis algorithms. We will discuss potential models for the effect of excitatory-inhibitory imbalance on single-unit temporal processing in the IC. The result and interpretation of this study are presented in Chapter 3.

In the second specific aim, a series of longitudinal auditory evoked potential recordings of various auditory parameters were conducted on blast-exposed and sham rats. We documented a detailed time course of the development of auditory deficits post-blast exposure by various auditory-evoked potentials (AEPs) and identified time windows in which drastic central changes take place. The results are presented in Chapter 4 and are under revision for publication (Han et al. 2020).

In the third specific aim, we examined the central gain of multiple auditory regions after blast injury by analyzing auditory brainstem response (ABR) and middle-latency response (MLR) wave ratios. We compared electrophysiological recordings to various immunohistochemistry results in order to understand the impact of acute and longer-term subcortical CAS excitatory/inhibitory changes to auditory parameters. The result and interpretation are presented in Chapter 5. We will also briefly discuss potential treatment options in this chapter.

CHAPTER 2. GENERAL BACKGROUND

2.1 Subcortical Central Auditory System

The subcortical Central Auditory System (CAS), consisting of the cochlea, the auditory nerve (AN), auditory brainstem, auditory midbrain, and the auditory thalamus, plays a major role in the relaying and processing of temporal auditory information. A schematic of rat CAS is shown in Figure 2.1. Neural signals from the cochlea pass through the AN to the cochlear nucleus (CN). Neurons in the dorsal and ventral nucleus of CN (DCN and VCN, respectively) then project to the inferior colliculus (IC) in the auditory midbrain through lateral lemniscus (LL). The ventral nucleus of CN also projects to the superior olivary complex (SOC), which then also converges at the IC (Malmierca 2003; Caspary et al. 2008). Ascending signals are then projected from the IC to the medial geniculate body (MGB) in the thalamus and the primary auditory cortex (A1) (Bartlett 2013).

Although the interest in central auditory processing (CAP) has traditionally been focused on the auditory cortex, a growing body of evidence suggests that subcortical CAS contributes significantly to the extraction, processing, and relay of complex auditory features, especially temporal features (Felix et al. 2018). While some subcortical auditory locales such as the inferior colliculus and the auditory thalamus were less understood in their precise functions and coding schemes, later studies have refined the knowledge about these structures, and researchers are increasingly aware of the role subcortical CAS plays in central auditory processing (Malmierca 2004; Caspary et al. 2008; Wang et al. 2008; Bartlett 2013). Through the interlocking projections and local networks of excitatory and inhibitory neurons, subcortical locales such as the IC and MGB are able to converge, transform and relay auditory information, utilizing rate coding, temporal coding, feature selectivity, feature enhancement, among other diverse coding schemes (Koch and Grothe 1998; Frisina 2001; Caspary et al. 2008; Pollak et al. 2011; Caspary and Llano 2019).

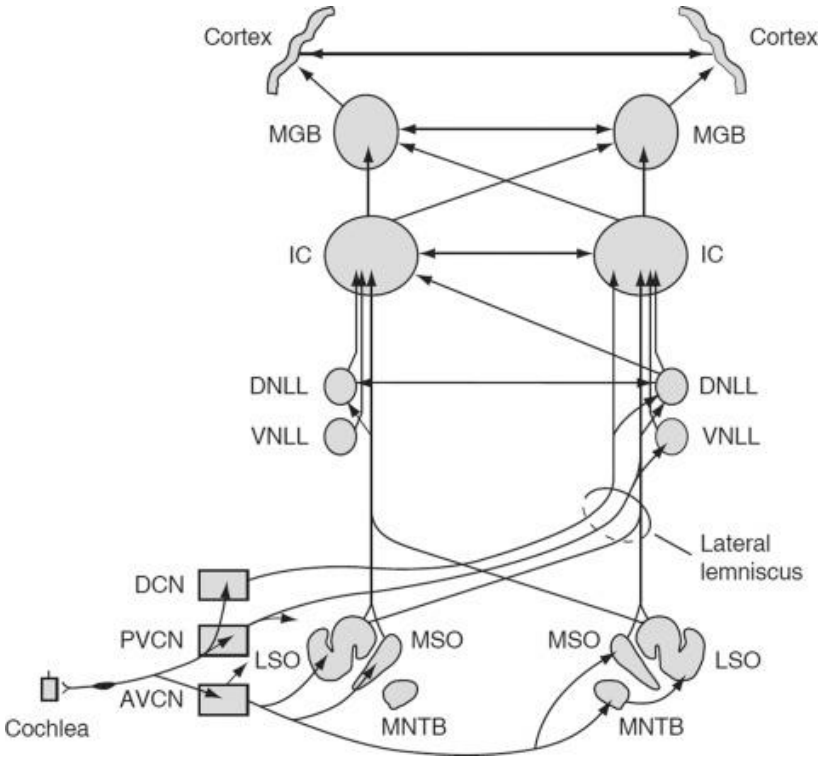

Figure 2.1. A schematic of the main ascending pathways of the rat central auditory system. Many minor pathways, including many inhibitory pathways, are not shown. Figure adapted from Pickles (2015).

2.1.1 Auditory Nerve

The AN is the sole route for acoustic information from the inner ear to enter the central auditory system, where all acoustic information are stochastically coded into the timing and rates of spikes generated in the afferent neurons and projected into the CN through myelinated nerve fibers (Spoendlin and Schrott 1989; Makary et al. 2011; Heil and Peterson 2015). Cochlear neuropathy causes the disconnection of auditory nerve fibers from the cochlea even when the hair cells survived, resulting in an under-sampling of acoustic information not dissimilar to the effect of a vocoder, severely compromising the coding of temporal information (Lopez-Poveda and Barrios 2013; Sergeyenko et al. 2013). On the other hand, demyelination of the auditory nerve fibers, even transient ones, are known to induce electrophysiological alterations in central auditory systems such as the CN and the IC and is being proposed to be another source of hearing loss in individuals with normal audiograms (El-Badry et al. 2007; Wan and Corfas 2017).

The auditory nerve fibers are spontaneously active, highly selective to characteristic frequency, and exhibit robust, high-resolution phase-locking compared to more central structures (Joris et al. 2004). Alterations in temporal precision of envelope coding and

modulation gain, as well as broadened tuning, were observed in noise-impacted AN (Kale and Heinz 2012; Henry et al. 2014), suggesting AN to be a prominent contributor to the distortion of acoustic information in hearing deficits.

2.1.2 Cochlear Nucleus

The cochlear nucleus gives rise to widespread projections into nuclei throughout the brainstem. Cant (2003) described the diverse cast of neurons in the CN and the complex brainstem network it is involved in. The VCN harbors multipolar cells that receive abundant inputs from the AN and contralateral CN, encoding complex features of sounds and are a major source of excitatory input for the IC. The VCN also gives rise to widespread inhibitory projections to the DCN and contralateral CN. The DCN engages in auditory pattern extraction, exhibiting complex excitatory/inhibitory response areas due to the network of inhibitory interneurons (Pickles 2015). Information pertaining to sound location is also coded in the CN. Because of the complexity of auditory information being coded and the intricate excitatory/inhibitory network in the CN, changes in this structure due to aging or traumatic impact are likely to generate substantial alterations in central auditory processing downstream.

2.1.3 Inferior Colliculus

The inferior colliculus is a major convergence point along the central auditory pathway (Malmierca 2004) with virtually all of the processing in lower centers of the auditory brainstem projecting into it (Adams 1979; Frisina et al. 1998). It is known that the superior olivary complex (SOC) and lateral lemniscus (LL) make projections to the tonotopic central nucleus of the IC (ICC) in various animal models (Zook and Casseday 1987; Kelly et al. 1998). Anatomical studies focusing on the IC have highlighted its intricate local circuits and thalamic projections, consisting of glutamatergic excitatory neurons as well as GABAergic inhibitory neurons (Frisina et al. 1997; Ito and Oliver 2012). Aside from these links with direct upstream and downstream structures on the auditory pathway, the IC also receives tonotopic and non-tonotopic projections from the auditory cortex in its dorsal and caudal cortex (Stebbings et al. 2014), the mechanisms of which is beyond the scope of this thesis.

Among this diverse cast of neurons, inhibitory neurons are noted for playing a crucial role in sharpening neural activities in response to rapidly time-varying signals (Frisina 2001). There is evidence that the large GABAergic tectothalamic neurons in the IC are convergence points of lemniscal and local excitatory projections (Ito and Oliver 2014), hinting at their

importance in integrating ascending inputs and generating high temporal precision responses. The MGB of the auditory thalamus also receives excitatory and inhibitory projections from the IC (Bartlett et al. 2000; Ito et al. 2009). Thus, the integrity and balance of excitatory/inhibitory IC circuits, both local and tectothalamic, are key when considering auditory processing in normal and impaired CAS.

2.1.4 Processing of temporally modulated sounds in subcortical CAS

Concerning the representation of time-varying acoustic information in neural activity, it is useful to distinguish both the dimensions of temporal characteristics of sound, as well as two strategies of neural representation in encoding these temporal characteristics.

Based on dominant fluctuation rates in the sonic pressure waveform, the temporal element of natural sounds can be put into three categories: Envelope, periodicity and temporal fine structure (TFS) (Rosen 1992). Envelope refers to temporal fluctuations within the range from 2 Hz to ~50 Hz, which account for a lot of acoustic information in natural sounds, such as the occurrence of speech elements and rhythm of music (Shannon et al. 1995; Stevens 2002; Singh and Theunissen 2003; Rennies et al. 2010). Periodicity refers to fluctuations generally occurring between 50 Hz and 500 Hz for humans, and TFS refers to the rapid fluctuations above 500 Hz. These fast temporal fluctuations determine the spectral content of sounds (Moore 2014), and characterize crucial auditory cues such as fundamental frequencies, formant structure, consonant identity and speaker identity (Bregman et al. 1990; Rosen 1992; Sheft et al. 2008; Chait et al. 2015). It is important to note that the processing of these categories of temporal resolution may not be clearly segregated and may affect the processing of one another (Drullman et al. 1996).

The auditory system has evolved many neural processing mechanisms for encoding the aforementioned temporal elements of sound. While the auditory nerve shows high temporal resolution and robust phase-locked temporal coding of amplitude fluctuations, more central structures, having a lower temporal resolution, rely increasingly on rate coding of periodicity (Frisina 2001; Joris et al. 2004). This shift in strategy along the auditory pathway further exhibits subcortical synthesis of auditory features. The IC, where both strategies are present among different IC single neurons across a substantial range of modulation frequencies (MFs) (Møller and Rees 1986; Rees and Møller 1987), is therefore of key importance in the hierarchical processing of temporal cues in natural sounds.

The coding strategies of temporal elements in CAS can be assessed on single-unit and systems levels. These electrophysiological methods, their advantages, and their shortcomings will be laid out in later chapters.

Pure tone evoked responses

Currently, the most common and accessible way to screen for and diagnose hearing deficit is through generating an audiogram of measured pure-tone hearing thresholds (Davies 2016). A typical audiogram is shown in Figure 2.2. Audiogram configuration confers helpful information regarding peripheral changes in the auditory system and is traditionally used to explain and identify certain auditory pathologies (Dubno et al. 2013; Vaden et al. 2017; Parthasarathy et al. 2020). For example, an epidemiological study suggests that profound self-reported hearing difficulties among older adults are commonly associated with a steep high-frequency slope in audiograms (Hannula et al. 2011). Higher odds of high-frequency hearing loss, low-frequency deficits and general threshold shifts are also observed among veterans with blast-related injuries compared to those with non-blast-related injuries, as exposed through pure-tone audiometric data (Joseph et al. 2018).

Although proven useful in clinical settings, audiogram tests have been noted for their inability to detect hearing deficits whose sources lie in cochlear synaptopathy or changes in more central structures (Kujawa and Liberman 2015; Liberman et al. 2016; Guest et al. 2018; Bramhall et al. 2020). Objective physiological measures that could provide more information about evoked neural activities and neurotransmission between different auditory structures are therefore crucial. Auditory brainstem responses (ABRs), and similarly middle latency responses (MLRs), are fast and non-invasive methods of exposing changes along the auditory pathway through responses to short pure tone pips and clicks (Picton et al. 1974; Özdamar and Kraus 1983; Gorga et al. 1988; Overbeck and Church 1992). Through repeated recordings of the human or animal auditory system in response to these simple, brief sounds, the activities of various auditory structures are reflected as characteristic waves on the ABR/MLR waveform. ABR/MLR parameters such as wave morphology, amplitudes, latencies, and wave ratios have been known to reveal different aspects of central hearing deficits (Gallun et al. 2012a; Mehraei et al. 2016; Bramhall et al. 2017; Race et al. 2017; Schrode et al. 2018).

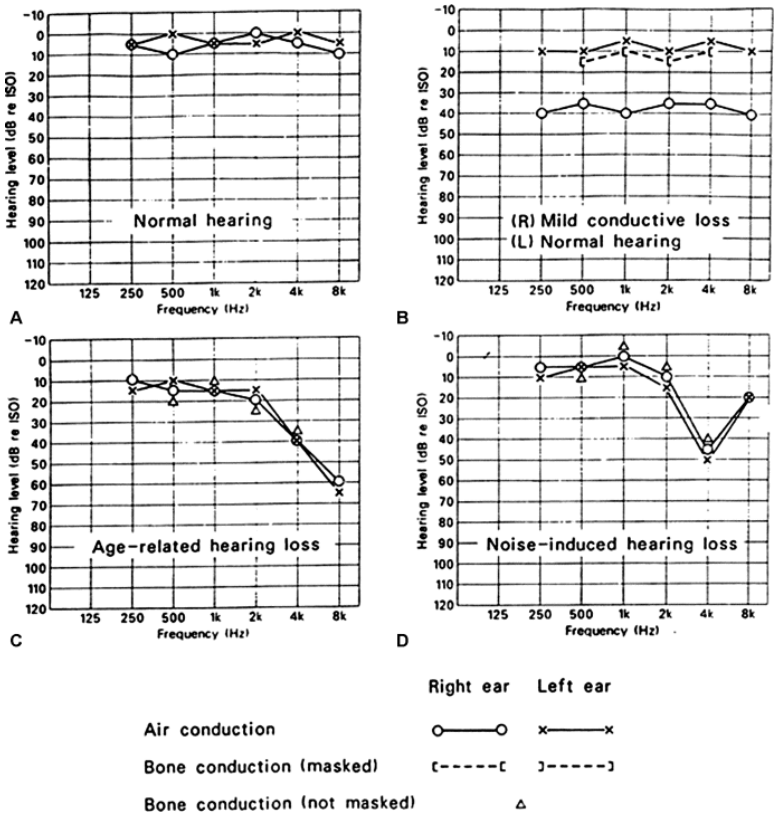

Figure 2.2. Typical audiogram configurations. Figure adapted from Davies (2016).

Moving onto the single-unit level, short Gaussian noise or pure tone stimuli are common tools used for identifying a neuron's basic properties such as threshold, best frequency, and certain firing patterns (Malmierca et al. 2008; Bartlett and Wang 2011; Bartlett et al. 2011; Wallace et al. 2012). These stimuli, aside from providing a quick look at a neuron's frequency response area, are an essential basis for other auditory measurements to be made.

However, in studies concerning noise-induced, age-related, and blast-induced hearing deficit studies, simple evoked responses to pure-tone pips and clicks in quiet are not fully indicative of the extent of hearing deficits and related behavioral complaints of affected individuals (Gallun et al. 2012a; Bharadwaj et al. 2015; Prendergast et al. 2017). Studies correlating simple electrophysiological tests in quiet such as ABR with lifetime noise exposure in individuals with normal audiograms but experiencing hearing difficulties have shown mixed results (Bramhall et al. 2017; Guest et al. 2018; Valderrama et al. 2018). Elderly listeners show evidence of temporal processing deficits even when audiogram results are similar to younger listeners or when hearing threshold has been compensated for (Kathleen Pichora-Fuller et al. 1994; Frisina and Frisina 1997; Strouse et al. 1998). Similar cases can be claimed for patients exposed to high-intensity blasts, where the differences in audiogram results seldom exceeded

the range of test-retest reliability for clinical tests and cannot account for differences between groups on the behavioral and electrophysiological tests (Gallun et al. 2012a). Pure tone responses in quiet provide a very limited reflection of real-world hearing scenarios, where spectral and temporal fluctuations and suboptimal hearing environments pose great challenges for individuals with any type of hearing deficit. Changes in the nuanced mechanisms of central spectrotemporal integration along the auditory pathway cannot be fully exposed through simple auditory stimuli such as click and pure-tone stimuli in quiet. Moreover, although ABR amplitudes are widely used as a reliable tool in studying central hearing deficits in animal models, the high variance of Wave I amplitudes makes ABR findings difficult to translate into human patients (Plack et al. 2016).

Amplitude modulation stimuli

Although brief clicks or tones are instrumental in defining the basic properties of the auditory system, they do not reflect the complexity and challenges posed by sounds we encounter in real-life such as speech and music, and predict responses toward complex sounds poorly (Palmer and Shamma 2006; Skoe and Kraus 2010; Guest et al. 2018). Amplitude modulation (AM) and frequency modulation (FM) are important auditory elements of human speech, animal vocalization and other natural sounds (Shannon et al. 1995; Miller and Hauser 2004). Notably, as time-varying amplitude-modulation carries vital acoustic information, precise temporal processing is necessary for the accurate perception of speech and environmental sounds (Parthasarathy and Bartlett 2011; Anderson et al. 2013a). Therefore, speech understanding, especially in challenging hearing environments, is often associated with impaired auditory temporal processing in older individuals (Frisina and Frisina 1997; Leigh-Paffenroth and Fowler 2006).

Amplitude modulation stimuli, as shown in Figure 2.3, are widely used in studies on auditory temporal processing because they can be manipulated to represent many temporal modulation properties found in speech and other natural sounds. Aside from modulation frequency, which has been instrumental in identifying neuronal temporal properties and even the temporal resolution of various auditory structures (Caspary et al. 2005; Parthasarathy et al. 2010; Parthasarathy and Kujawa 2018), modulation depth and shape are crucial factors that affect speech intelligibility (Drullman et al. 1996; Jørgensen et al. 2015) and have been key in revealing temporal processing mechanisms in normal and aged auditory systems (Krebs et al. 2008; Dimitrijevic et al. 2016; Herrmann et al. 2017). The detection and discrimination of

modulation frequency, modulation depth and modulation shape in AM stimuli has been widely incorporated in laboratory and clinical studies to expose auditory deficits that are otherwise undetected or only subtly detected through simple stimuli (Parthasarathy and Bartlett 2011; Wallaert et al. 2016; Herrmann et al. 2017; Lai et al. 2017; Paul et al. 2017).

Ample studies have been conducted on age-related changes in subcortical AM responses, both on population and single-unit levels. Reduction in EFR amplitudes towards fast, MF>1 kHz AM stimuli suggests that age-related temporal processing deficits may occur as early as cochlear synapses (Parthasarathy and Kujawa 2018). temporal processing Significant age-related changes in the shape and peak vector strength of temporal modulation transfer functions, but not rate functions at the best modulation frequency (BMF, i.e., the modulation frequency to which a neuron responds maximally), were observed in rat DCN, theorized to be the result of age-related disruption of glycinergic inhibitory inputs (Caspary et al. 2005; Schatteman et al. 2008). A Shift to lower amplitude modulation BMF in IC neurons has been noted in mice and rat models as a hallmark of age-related temporal processing change (Palombi et al. 2001; Walton et al. 2002). Most notably, AM frequency response (AMFR) revealed that aged F-344 rats experienced a systematic reduction in subcortical neural population response amplitude, as well as reduced sensitivity to modulation shape and depth (Parthasarathy and Bartlett 2011). A transformation of AM response pattern in aged IC neurons was observed and replicated in a computational model through reduction of GABA inhibitory inputs (Rabang et al. 2012). Reductions in AM response in older human individuals did not reach the level of explaining behavioral differences, and can be mostly accounted for by peripheral threshold shifts instead of central changes (Boettcher et al. 2001; He et al. 2008; Dimitrijevic et al. 2016).

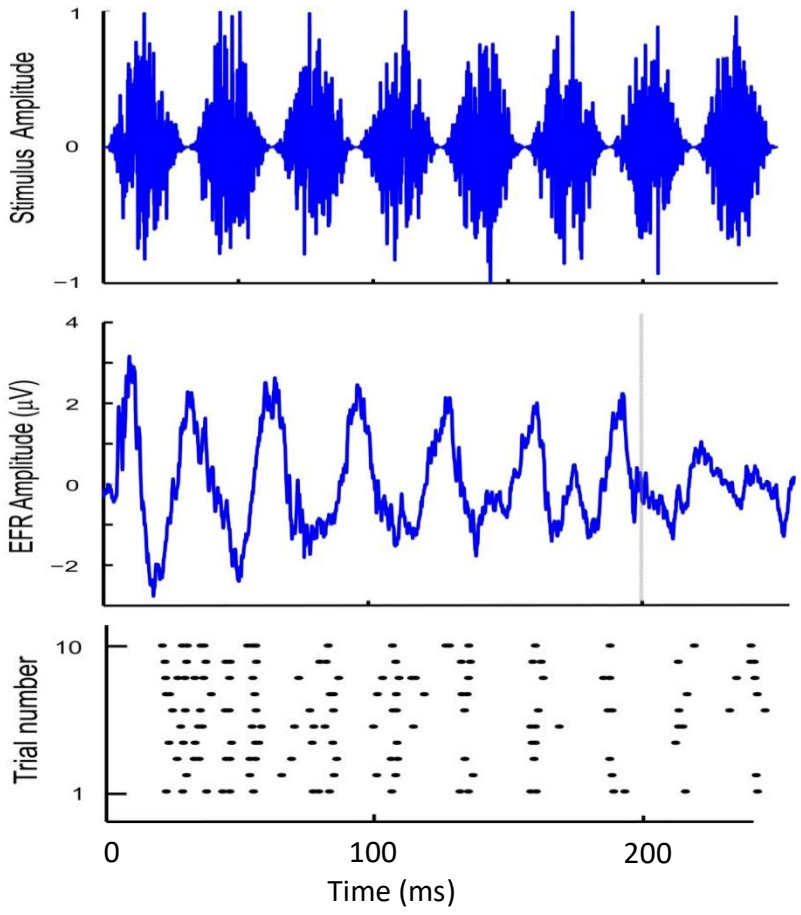

Figure 2.3. A waveform of amplitude modulation stimuli (top panel) and its representation in EFR (middle panel) and IC single−unit recording (bottom panel).

The use of AM stimuli in TBI-related hearing deficit is relatively sparse. Although AMFR recordings at 8 kHz and 80 dB SPL from blast-exposed rats showed reduced response amplitude in a selected few MFs compared to non-blast controls, even at 1-month post−exposure when hearing thresholds were similar (Race et al. 2017), AMFR in blast-exposed human individuals falls within the normal range and cannot account for blast-related sensory-cognitive processing difficulties (Bressler et al. 2017). These results suggest that simple steady-state temporal auditory stimuli such as sinusoidal AM in quiet are also limited in their capacity to reveal central changes associated with real-life hearing difficulties.

More recently, it has been noted that although responses to temporally modulated stimuli in quiet were predictive to the performances of speech processing in noise for normal-hearing individuals (Mepani et al. 2021), they are less representative for hearing-impaired individuals (Bressler et al. 2017; Guest et al. 2018). While the response towards AMFR stimuli is similar for young and aged animals in quiet, it diverges substantially with the addition of

background noise (Parthasarathy et al. 2010). The presence, levels and spectrotemporal properties of noise simultaneous to AM stimuli present a whole array of factors that may differentially impact individuals affected by different hearing deficits. For example, Lai and Bartlett (2018) observed that while young animals maintain dual AM representations better than older animals overall, high-pass noise may impact AMFR amplitude in young animals more than aged by reducing the contributions of high-frequency-sensitive inputs that are more robust in young animals. Conversely, oversensitive neural envelope coding in the human cortex and auditory brainstem may be linked with worse performance in speech recognition (Goossens et al. 2018). These observations, taken together, necessitate the use of AM-in-noise stimuli when assessing temporal processing changes in various forms of hearing deficits.

Speech and speech-like stimuli

Because of the limitation of simple auditory stimuli in revealing real-life hearing difficulties encountered by older or TBI-affected individuals, stimuli incorporating speech or speech-like elements are extremely valuable means of exposing central auditory deficits in laboratory and clinical studies. The strength and limitation of speech and speech-like stimuli vary depending on the type and construction of each stimulus, as well as the subject of each study, providing a wide array of angles through which to understand the neural mechanisms of hearing loss.

Psychoacoustic methods utilizing real speech recognition represent real-life hearing scenarios with the highest fidelity. These methods are especially invaluable in screening the abilities in performing everyday hearing tasks in hearing-loss-affected individuals (Saunders et al. 2015) but is limited in their compatibility with various animal models due to the differences in hearing range and animal's lack of language cognition.

Speech-like stimuli focusing on the time-varying elements in speech, on the other hand, are widely used in studies that compare behavioral performances human steady-state ABR/AEP recordings (Gallun et al. 2012a; Shearer et al. 2018; Daube et al. 2019) and single-unit/multi-unit recordings in human (Mesgarani and Chang 2012; Mesgarani et al. 2014) and animal models (Engineer et al. 2008; Reed et al. 2014). These moderately abstract stimuli such as speech envelopes and consonant-vowel pairs were valuable in uncovering age-related changes in the subcortical CAS that affects temporal processing of speech (Tremblay et al. 2003; Harkrider et al. 2005; Anderson et al. 2012; Goossens et al. 2018; Roque et al. 2019),

and the electrophysiological components can be translated to animal models with relatively ease (Herrmann et al. 2017; Parthasarathy et al. 2019b).

Simpler broadband stimuli extracted from speech can also be utilized in temporal processing studies for their compatibility with animal models that possess hearing ranges different from humans. Voice Onset Time (VOT) tests, for example, were used to reveal age-related increases of sensitivity to the sound's onset and temporal regularity (i.e., periodicity envelope) in the output of inferior colliculus neurons, relative to their synaptic inputs, potentially due to central inhibitory loss in the IC (Parthasarathy et al. 2019b). This overexcitability in the subcortical CAS may have been disruptive towards overall temporal precision, partially explaining the age-related changes observed in speech psychoacoustic and electrophysiological results, such as consonant discrimination, response consistency and AEP phase-locking precision (Tremblay et al. 2003; Harkrider et al. 2005; Anderson et al. 2012).

Among these studies utilizing speech or speech-like stimuli, there are still gaps of understanding between electrophysiological results, psychoacoustic tests, and self-reported hearing difficulties in real life. This suggests that any conclusion on speech processing in the auditory system may be further confounded by changes in other brain regions, a situation that is common in both age-related and TBI-induced hearing deficits (Strouse et al. 1998; Gallun et al. 2012a; Bressler et al. 2017).

Iterated rippled noise

Iterated Rippled Noise (IRN) is a broadband, temporally complex stimuli created by putting a segment of wideband noise (WBN) through a delay-and-add network of custom delay time (τ) and iterations as shown in Figure 2.4. This process creates a temporal periodicity using a broadband carrier, generating a spectrum with sharp peaks at integer multiples of $1/\tau$ and elicit pitch-perception in listeners (Yost 1996a; Shofner 1999). The strength of this “pseudo-pitch” increases with increased iterations (Patterson et al. 1996; Yost 1996b). The temporal processing of IRN periodicity was preserved in many CN unit types regardless of best frequency (Shofner 1999; Wiegrebe and Winter 2001). Therefore, IRN is advantageous as a class of temporally complex stimuli in its capacity to create speech-like periodicity of changing intelligibility, suitable for both human and animal models.

IRN stimuli have long been used in studies understanding subcortical CAS temporal coding mechanisms from CN, SOC to IC (Shofner 1999; Wiegrebe and Winter 2001; Alsindi et al. 2018). More recently, IRN stimuli following pitch patterns of tonal language such as

Mandarin Chinese were used to assess temporal processing of pitch in human cortical and subcortical CAS of normal-hearing individuals (Krishnan and Gandour 2009; Krishnan et al. 2010, 2014, 2017b).

In the recent two decades, more hearing loss and hearing implant studies are conducted using IRN stimuli to assess pitch perception (Leek and Summers 2001; Penninger et al. 2013; Wagner et al. 2017; Shearer et al. 2018). Because of its broadband nature circumventing uncertainties in peripheral damage common in many types of hearing loss, particularly in noise-induced and blast trauma-induced hearing loss, as well as avoiding the differences in AN fiber property in rodent models, IRN presents a unique advantage in studying complex temporal processing in subcortical CAS.

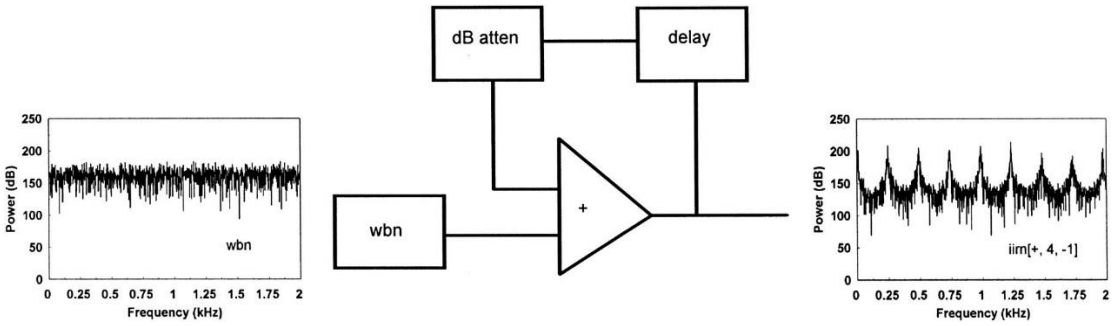

Figure 2.4. Circuit diagram for generating iterated rippled noise with a fixed delay time. Figure adapted from Shofner (1999).

There are myriad other types of auditory stimuli that have been used to reveal the central mechanisms of hearing loss. For example, gap detection performance is known to correlate strongly with decreased temporal acuity and word recognition ability as a result of aging (Kathleen Pichora-Fuller et al. 1994; Phillips et al. 2000; Snell and Frisina 2000). Spectrally complex stimuli such as dynamic moving ripple and random spectrum stimuli are especially ideal in revealing the spectrotemporal receptive field of single neurons with regards to the influence of adjacent neural networks (Escabí and Schreiner 2002; Barbour and Wang 2003; Chen et al. 2012). These stimuli will not be discussed in depth in this thesis but are nonetheless valuable tools in studying auditory mechanisms in the CAS. It should be noted that many spectrotemporally complex stimuli have yet to be widely applied in age-related and TBI-induced hearing loss.

2.1.5 Sensorineural vs. neurochemical elements in hearing loss

Damage or age-related changes in the auditory system can be characterized as sensorineural or neurochemical. Sensorineural damages are irreversible damages, mechanical, biochemical or physiological in nature, caused to the hair cells and supporting cells in the cochlea (Kaźmierczak and Doroszewska 2001; Wong and Ryan 2015; Liberman and Kujawa 2017; Jalali and Nasimidoust Azgomi 2020). Neurochemical changes are the changes in neurotransmission along the auditory neuraxis that affect the processing of acoustic information. The downstream consequences of different classes of peripheral damages, such as mechanical impact, metabolic changes, and age-related cell death and synaptopathy in the cochlea, are likely to manifest in different ways. Moreover, these peripheral changes will interact with mechanical damages or age-related changes in the CAS, further complicating the mechanisms of later stages of hearing deficit development.

Sensorineural damage: cochlear and subcortical neurodegeneration

Sensorineural components consist of the physiological and anatomical changes that are associated with hearing loss, primarily centered around the cochlea but may also extend to subcortical CAS (Lin et al. 2011; Kujawa and Liberman 2015). Mechanical trauma, autoimmune response, noise impact and age-related cochlear degradation lead to peripheral sensorineural loss and, in severe cases, may cause dead regions in the cochlea to manifest (Moore 2007; Kujawa and Liberman 2009; Cho et al. 2013b; Hickman et al. 2018). Altered peripheral input profiles that arise from these cochlear damages are known to cause changes in central auditory regions such as excitatory and inhibitory imbalance, synaptic rewiring and even remapping of tonotopic areas (Yang et al. 2011; Henry et al. 2016; Masri et al. 2018; Liu et al. 2021). Because cochlear and AN synaptopathy often precede cell death and even significant threshold elevation, even seemingly temporary sensorineural hearing loss can lead to lasting changes in ABR and temporal processing in subjects with normal hair cell count and function (Kujawa and Liberman 2009; Bramhall et al. 2017; Liberman 2017).

Sensorineural components such as hair cell death and cochlear synaptopathy also occur with the advance of age, making them prominent aspects of ARHL. The loss of hair cells and afferent neuron degeneration have been observed in human and various animal models, with outer hair cells being the most vulnerable (Helfer et al. 2020). Most recently, cochlear synaptopathy has been observed to precede outer and inner hair cell loss in aged animals, similar to noise-induced hearing loss (Sergeyenko et al. 2013; Parthasarathy and Kujawa 2018).

A typical profile of hair cell loss and the cochlear synaptopathy that precedes can be seen in Figure 2.5. These peripheral declines not only make an early contribution to the degradation of temporal processing but may also instigate compensatory plasticity downstream, leading to distorted representations of temporal cues in speech and other natural sounds (Parthasarathy et al. 2019a).

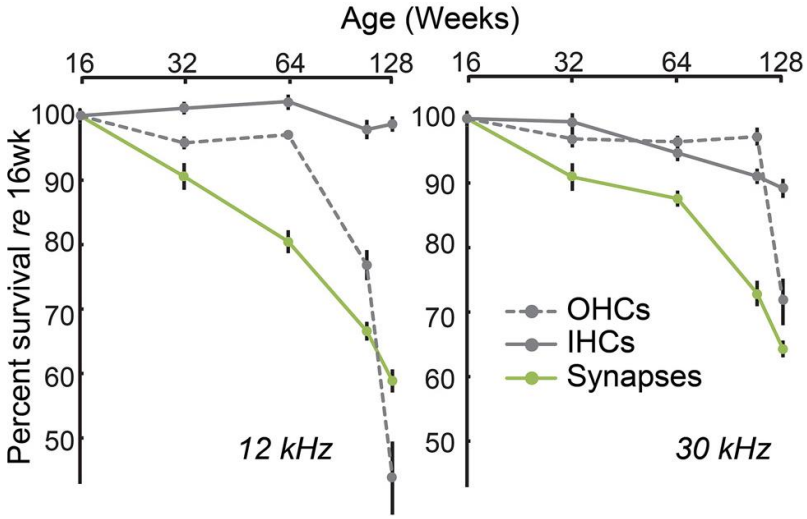

Figure 2.5. Mean±SEM percentage survival of cochlear synapses (green line), inner hair cells (IHCs, gray solid line), and outer hair cells (OHCs, gray dashed line) at 2 cochlear locations and 5 age groups relative to 16-week-old CBA/CaJ mice, showing cochlear synaptopathy preceding hair cell loss. Figure adapted from Parthasarathy and Kujawa (2018).

Neurochemical changes: excitatory/inhibitory imbalance

Here, neurochemical changes refer to the changes to neurotransmitters, receptor compositions and other neurochemical components along the auditory neuraxis that affect the processing of acoustic information. These changes may be *de novo*, or a result of changes in peripheral input. Peripheral deafferentation, for example, is known to induce central gain in various auditory structures through the reorganization of excitatory/inhibitory balance, particularly through downregulation of GABAergic and Glycinergic neurotransmission (Godfrey et al. 2014; Chambers et al. 2016; Heeringa and van Dijk 2016; Schrode et al. 2018).

Conversely, acute enhancement of inhibitory neurotransmission can arise as a result of the sudden traumatic impact. An immediate upregulation of inhibition of the IC is observed following intense acoustic exposure (Abbott et al. 1999). Positive modulation of GABA in the acute period (2-4 days) enhanced the survival and cognitive performance in TBI-impacted rats (O'Dell et al. 2000), suggesting the neuroprotective effect of GABA following traumatic

impact. The upregulation of inhibition in the subcortical CAS can be therefore understood as a potential neuroprotective measure of the brain, that may result in alterations in central auditory processing.

The systematic changes in the excitatory and inhibitory network, both as a result of external impacts and from internal compensation, have been hypothesized to be a major driver of auditory deficits (Caspary et al. 2008; Sturm et al. 2017; Caspary and Llano 2019). Because inhibitory neurotransmission plays an important role in shaping selectivity in the CAS (Burger and Pollak 1998; Razak and Fuzessery 2009; Mayko et al. 2012), a disruption of excitatory/inhibitory balance in the CAS is expected to alter the precise coding of auditory information.

2.2 Concerning Sensorineural and Neurochemical Elements in Age-related and Blast-induced Hearing Loss

2.2.1 Presbycusis

Age-related hearing loss (Presbycusis) consists of gradual sensorineural and neurochemical changes across the Central Auditory Pathway (CAP) as the result of aging. These changes in the auditory system often come intertwined with a general age-related decline of cognitive function (Humes et al. 2012), making it complicated to determine the source(s) of age-related deficits in auditory processing.

Sensorineural hearing loss in the form of age-related hair cell loss and general cochlear neurodegeneration has long been observed as a major part of presbycusis. (Gates et al. 1989; Gates and Mills 2005). However, substantial hearing difficulties in individuals with normal audiograms have long been noticed in clinical practice, theorized to be the result of cochlear neuropathy and consequent central changes. These symptoms are commonly thought to be "hidden" from audiological diagnosis, earning the term "hidden hearing loss" (Schaette and McAlpine 2011; Plack et al. 2016). More recent studies have noted the importance of non-lethal synaptopathy of hair cells and the degeneration of cochlear nerve peripheral axons that may well precede cochlear cell death (Kujawa and Liberman 2015; Viana et al. 2015; Liberman 2017; Wu et al. 2019). This implies that the so-called "hidden hearing loss" in presbycusis may already be taking place and affecting the CAS long before an audiometric diagnosis can detect it.

The age-related excitatory/inhibitory imbalance, specifically age-related decrease of GABA neurotransmission, within the subcortical CAS, was first documented in the 1980s

(Banay-Schwartz et al. 1989). A number of studies have extensively examined the selective and impairment of inhibitory GABAergic neurotransmission in the dorsal cochlear nucleus (DCN) and the central nucleus of the IC, hypothesizing that this inhibitory loss contributes to abnormal auditory perception and processing in ARHL (Caspary et al. 1990; Milbrandt et al. 1996; Helfert et al. 2003; Caspary et al. 2005, 2008; Richardson et al. 2013). Drug studies and computational models simulating the downregulation of GABA have partially recreated aged-like electrophysiology (Bauer et al. 2000; Sun et al. 2009; Rabang et al. 2012), further confirming the key role of excitatory/inhibitory imbalance in ARHL.

2.2.2 Blast-induced Hearing Loss

On the other hand, blast-induced hearing loss (BIHL), which has long been documented mainly at the peripheral level, is recently focused on by many for its central components. Though initially presents as acute sensorineural damage at cochlear and auditory nerve level (Ewert et al. 2012; Cho et al. 2013b), BIHL gradually manifests itself into a series of lasting, multilocal central auditory deficits (Gallun et al. 2012b; Race et al. 2017). Notably, in the subcortical CAS, initial hyperactivity and later hypoactivity in the DCN, as well as hyperactivity in the IC correlated to tinnitus, have been documented in blast-exposed rats (Luo et al. 2014b, 2014a).

There are sparse publications on blast trauma and excitatory/inhibitory imbalance in the CAS. However, studies have reported the dynamic changes of glutamate (excitatory) and GABA (inhibitory) in non-blast controlled TBI models. After an immediate decrease in excitatory neurotransmission immediately post-trauma, the chronic trend in excitatory/inhibitory balance changed direction from the acute trend with GABA interneuron death, GABA receptor dysfunction and upregulation in excitatory receptors (Cantu et al. 2015; Guerriero et al. 2015). The chronic trend of TBI-induced metabolic imbalance has been confirmed in blast trauma by Wang et al. (2018), who observed enhanced excitatory synaptic transmission, reduced inhibitory synaptic transmission, and a loss of parvalbumin-positive (PV+) inhibitory interneurons in blast-exposed mouse hippocampus 10 days post-exposure. This long-term inhibitory loss in BIHL presents a curious parallel to the gradual, age-related inhibitory loss in the CAS. To what extent this two-fold trend in excitatory/inhibitory imbalance contributes to blast-induced hearing deficits has yet to be understood.

Given that blast injury is a compound trauma to the auditory system, consisting of elements of both noise trauma and TBI, it could be expected that blast exposure would present

a unique challenge to the CAS that is more complicated than that of noise trauma and aging. Race et al. (Race et al. 2017) notably documented the sub-chronic (14 days) and chronic (1 month) changes in various auditory electrophysiological parameters throughout the rat auditory neuraxis after a single exposure to mild blast impact, a summary of which is shown in Figure 2.6. These changes include subclinical elevation of ABR thresholds, reduced MLR amplitudes, and reduced cortical/subcortical AMFR at a fixed sound pressure level, suggesting altered brainstem activity, thalamocortical transmission and cortical activation. These results strongly indicate the contribution of a cascade of metabolic changes across the auditory neuraxis as a result of blast TBI.

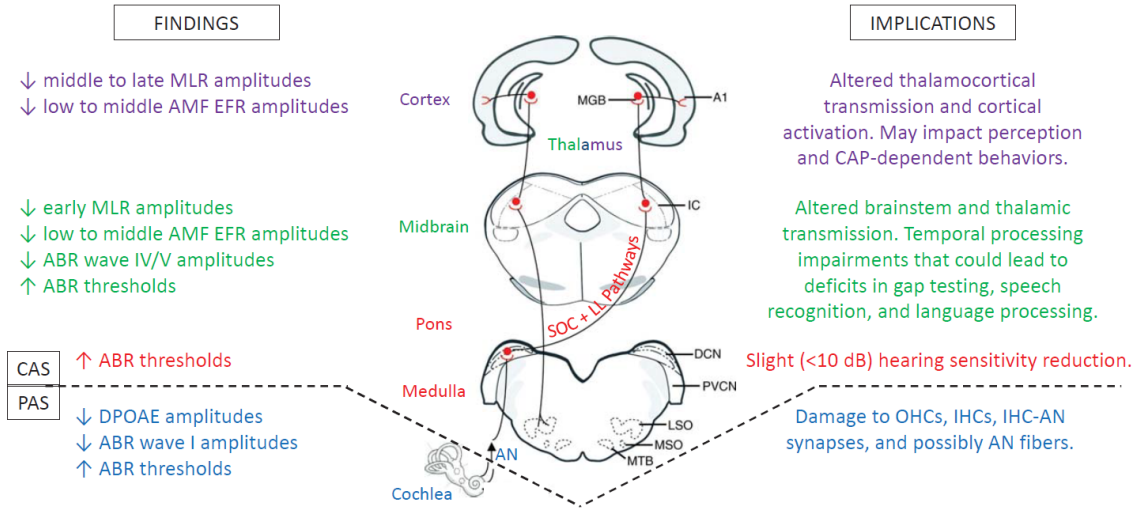

Figure 2.6. Overview of blast-induced auditory pathophysiological findings and implications from the cochlea to the cortex. Figure adapted from Race et al. (2017).

2.3 Knowledge gaps

The response of auditory midbrain neurons to simple stimuli are known to be remarkably resilient to age despite peripheral degradation (Willott et al. 1988a, 1988b), evidence of central compensation in the IC. On a population level, studies have shown an age-related decrease in AMFR amplitudes to at least low and high MFs, as well as increased sensitivity to AM depth (Parthasarathy et al. 2010; Parthasarathy and Bartlett 2011, 2012). AMFR studies suggested that age-related temporal processing deficits of AM stimuli could be observed on a single-unit level, which was predicted by experimental and modeling study (Khouri et al. 2011; Rabang et al. 2012). However, such a deficit in AM processing has not been observed by many previous studies (Burger and Pollak 1998; Caspary et al. 2002). There was also little correlation between

ABR amplitude and AMFR amplitudes in aged animals, contrary to that of young animals (Parthasarathy et al. 2014). It is thus unknown how this central compensation on a single-neuron level organized into the age-related decrease in AM processing observed on a population level, but not evident on the single-unit level. Moreover, how do age-related changes affect the response of IC neurons towards AM stimuli with decreased depth is yet to be analyzed. Through analyzing the firing patterns of aged and young IC neurons in response to AM depth stimuli using circular analysis, this study would attempt to provide a better insight into how age-related changes in temporal processing ability manifest on the single-unit level and translate to the collective responses as observed in AMFR.

Studies have strongly suggested the dual nature of both mechanical and neurochemical damages in BIHL. However, there are distinctly fewer studies pertaining to the precise course of development, from blast-induced peripheral damages, mostly mechanical in nature, to a persistent central change combining sensorineural and neurochemical changes. Most previous studies of this nature usually only assessed one or two time points spread between the acute (1-4 days post-exposure), sub-acute (around 4-10 days) or chronic (around 14 days to 1 month, and onwards) time window (Race et al. 2017; Wang et al. 2020; Witcher et al. 2021). There is a need for a more detailed time course of BIHL development, as well as linking this course of development to the dynamic sensorineural and neurochemical changes in subcortical CAS, in order to achieve better understanding and identify critical windows of intervention. This study would address the need by providing thorough documentation of the time course of mild blast-induced hearing deficit development. Moreover, aided with our knowledge of age-related hearing deficits, we would help reveal the underlying sensorineural and neurochemical mechanisms of blast-induced hearing deficits by comparing auditory electrophysiology to immunohistochemical and other anatomical evidence.

2.4 Methods used in this study

2.4.1 In vivo single-unit recording of the IC

Chapter 3 of the current dissertation that aimed at ARHL and its effect on AM depth coding in the inferior colliculus mainly utilized in vivo single−unit recording. These recordings were conducted using methods similar to our lab's previous studies (Rabang et al. 2012; Herrmann et al. 2015, 2017). Sound-driven single units were sorted visually online and then subsequently identified and isolated offline using the OpenEx interface (TDT). Responses to

100% modulation depth Gaussian noise AM and pure tone AM with carrier tone at the units' best frequency were then recorded for these sound-driven single units in order to identify the best modulation frequency (BMF). Noise and tone AM depth recordings at each unit's BMF were then recorded at a sound level 20–40 dB above the unit's thresholds for respective carriers.

2.4.2 Auditory brainstem response

In the current study, we utilized a two-channel recording method of AEP that has been laid out by Parthasarathy and Bartlett (2012) to efficiently acquire a longitudinal auditory assessment of blast-exposed animals at multiple time points post-blast. This method has the advantage of differentially amplifying the caudal brainstem structures and the more rostral auditory nuclei such as the inferior colliculus and the auditory forebrain on different channels. Typical waveforms of two-channel ABR and human ABR are shown in Figure 2.7. Compared to human ABR, the current electrode configuration was able to obtain not only clear wave I and III on channel 1 (sagittal) but also more robust wave I, IV and V on channel 2 (interaural).

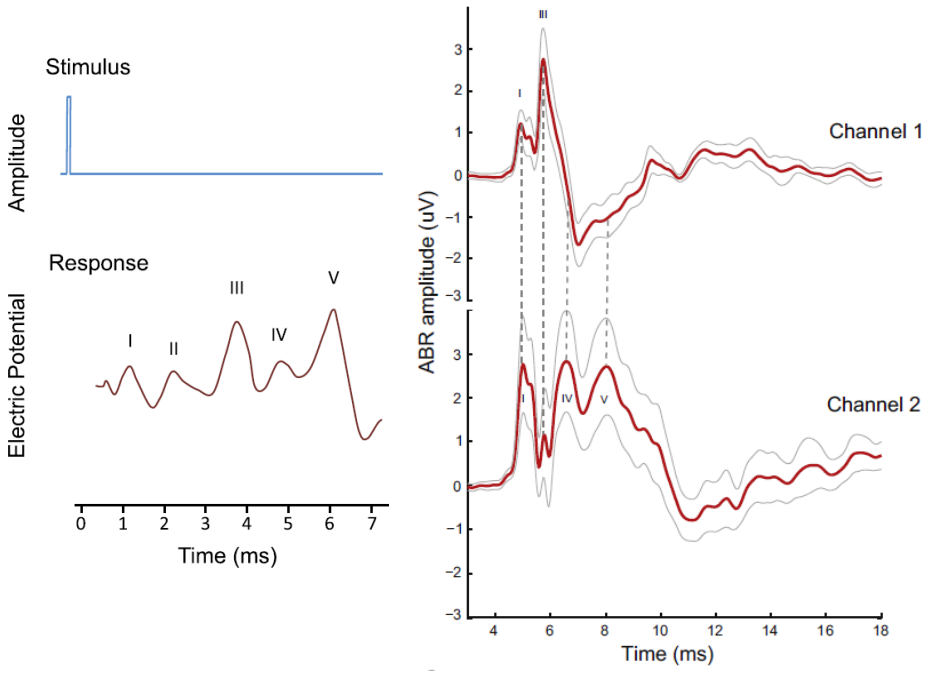

Figure 2.7. Human ABR (left) compared to rat ABR (right) recorded with two-channel AEP setup used in the current study. Edited from Plack et al. (2016) and Parthasarathy and Bartlett (2012).

2.4.3 Envelope following response

EFR recordings of AM and IRN responses were recorded under the same electrode configuration as ABR. This configuration allows for EFR recording under the same setup with

complementary emphasis on different neural generators, enabling a more precise understanding of the sources of central temporal processing deficits. In previous research on the two-channel recording of AMFR, channel 1 was shown to be more sensitive to faster MFs, in the range of 128 Hz-1024 Hz, whereas Channel 2 was more sensitive to slower MFs (Parthasarathy and Bartlett 2012). Analysis of AMFR of MFs below and above 100 Hz was focused on recordings taken from the more sensitive channel, channel 2 and channel 1, respectively.

IRN stimuli used in the current study were modified from Chinese tone IRN used in studies by Krishnan et al. (2010, 2014, 2015). These stimuli followed the rising (tone 2) and falling (tone 4) lexical tones in Mandarin Chinese, with sliding temporal periodicity ranging from ~80 Hz to ~150 Hz. Because of the temporal periodicity range of the stimuli used in the current study, IRN analysis focused on channel 1 in favor of its emphasis on higher MFs.

2.4.4 Immunohistochemistry

Walls et al. (2016) assessed multiple structural and biochemical markers in whole brains subjected to mild blast exposure. Because TBI is known to induce alterations in GABAergic receptors and neurotransmission in the cortex at both acute and chronic phases (Cantu et al. 2015; Guerriero et al. 2015), it is reasonable to hypothesize that changes in GABAergic neurotransmission may also take place in the subcortical CAS. By comparing AEP measurements with immunohistochemistry of GABA at acute, sub-acute and chronic phases post-blast, the present study aimed to provide a better understanding of the role of neurochemical changes in blast-induced hearing deficits.

In the present study, the brain tissue of rats subject to mild blast impact was harvested at various time points of interest. Presynaptic GABA immunohistochemistry was performed on half of the post-blast brain tissue through immunohistochemical labeling of GAD 65/67, similar to the methods used in Rabang et al. (2012). To measure the integrity of the cell membrane after blast exposure, the exclusion of tetramethylrhodamine dextran (TMR) analysis was performed on the same half of the brain prior to sectioning and free-floating immunofluorescent staining of GAD (Hamann et al. 2008b). *In situ* analysis of acrolein was performed on the other half of the brain tissue using 3,3'diaminobenzidine (DAB) assessment (Hashimoto et al. 2001; Hovens et al. 2014). These methods were used in Chapter 5 to provide a systematic look of blast-induced neurochemical changes at different phases post-blast, alongside our detailed documentation of post-blast auditory parameters.

CHAPTER 3. CIRCULAR ANALYSIS OF AGE-RELATED EFFECTS ON SINGLE-UNIT AMPLITUDE MODULATION DEPTH PROCESSING IN INFERIOR COLLICULUS

3.1 Introduction

Amplitude modulation (AM) is an important feature in human speech, music, animal vocalization and environmental sounds (Rosen 1992; Shannon et al. 1995; Miller and Hauser 2004), often exhibiting periodic temporal cues with simple (sinusoidal amplitude modulation) or complex (speech) waveforms. Thus, deficiencies in processing such temporal cues along the auditory pathway will disrupt the perception of these AM-rich sounds. Older individuals exhibited changes in their electrophysiological and psychoacoustic responses towards amplitude modulation even at suprathreshold levels (He et al. 2008; Grose et al. 2009, 2019; Goossens et al. 2016), demonstrating the potential of age-related AM processing difficulties in affecting the quality of life.

Subcortical processing of temporal modulation is critical for understanding hearing in normal and hearing-impaired or aging listeners. The Inferior Colliculus (IC) is the first major integrative auditory center, converging excitatory and inhibitory inputs from several brainstem nuclei to higher levels of central auditory processing (Frisina 2001; Cant and Benson 2003). Anatomical studies at multiple levels of the central auditory pathway, including the IC, have shown significant synaptic and metabolic changes in older individuals (Helfert et al. 1999; Tadros et al. 2007). Such changes are observed most evidently in inhibitory GABAergic and glycinergic synapses, with the GABAergic loss being the most predominant (Caspary et al. 1990, 1999, 2008). Since then, it has been hypothesized that inhibitory loss throughout the aging mammalian auditory system is a major driver of age-related hearing loss through changes in temporal processing and response reliability (Caspary et al. 2008). The changes of excitatory synapses across aging, though noted by many of these studies, are relatively less discussed in this Inhibitory Loss Hypothesis.

GABAergic subunits have been known to partake in the modulation of auditory adaptation in the IC (Pérez-González et al. 2012; Ayala and Malmierca 2018), and the expression of GABAergic receptor subunits is shown to change in the IC following peripheral hearing loss (Holt et al. 2005). The loss of GABAergic neurotransmission has been proposed to be a central adaptation in response to peripheral deafferentation in noise-induced and age-related hearing loss (Caspary et al. 2008; Schrode et al. 2018), compensating for reduced general input activity due to hair cell loss, cochlear synaptopathy and other changes in activity

in the auditory periphery. However, such compensation combined with other excitatory/inhibitory changes often disrupts subtle spectrotemporal processing along the central auditory pathway, as observed by many single-unit and Auditory Brainstem Response (ABR) studies (Walton et al. 2002; Khouri et al. 2011; Parthasarathy and Bartlett 2012; Herrmann et al. 2015; Parthasarathy et al. 2019b). These changes in auditory processing occur despite the preservation of frequency tuning and some aspect of intensity tuning in IC units from older animals (Caspary et al. 1990, 1995; Palombi and Caspary 1996).

Regarding age-related GABAergic loss, there have been ample single-unit studies relating to the potential roles of such loss in shaping AM responses of IC. For example, a single-unit study in bats has shown that blockade of $GABA_A$ and $GABA_B$ subunits does not change the phase-locking rate of bat IC_C neurons towards sinusoidal amplitude-modulated (SAM) stimuli (Burger and Pollak 1998), indicating that age-related GABAergic loss might not be the sole mechanism of decreasing AM phase-locking response in aged IC units. The Caspary group has observed that aging decreases bandpass proportion and increases the low-pass proportion of both rate and temporal modulation transfer functions (rMTFs and tMTFs, respectively) selectivity of AM response in the IC (Palombi et al. 2001). rMTFs and tMTFs are functions relating rate or temporal statistics of responses to modulation frequency. But though the blockade of $GABA_A$ alone consistently increases the selective rate response towards SAM stimuli in chinchilla IC, the temporal tuning properties of these responses are relatively unaffected (Caspary et al. 2002). Notably, none of these studies has looked at the effect of reduced AM depth.

Previous studies from our lab using the *in vivo* Amplitude Modulation Following Response (AMFR) have confirmed the decrease in response amplitude among aged rat IC in response to challenging AM stimuli with modulation frequencies (MF) ranging 8~700Hz, either under the presence of a competing masker (Parthasarathy et al. 2010) or with reduced modulation depth (Parthasarathy and Bartlett 2011). These studies have shown an age-related change in temporal processing accuracy in population response. A previous biophysical modeling study from our lab incorporating adaptation via calcium-activated potassium currents and synaptic depression has recreated major subtypes of modulation frequency (F_{Mod}) preferences in IC neurons and predicted age-related temporal processing deficits as a result of GABA loss (Rabang et al. 2012). However, such changes on a single-unit level have neither been observed by previously cited studies (Burger and Pollak 1998; Caspary et al. 2002) or have not been well demonstrated from *in vivo* single-unit data. EFR studies on young and older human subjects have also found age-related changes in AM response or AM depth response in

quiet, unmasked conditions to be either non-significant, or too weak to be clinically useful (Boettcher et al. 2001; Dimitrijevic et al. 2016). Considering that envelope modulation magnitude is correlated with speech intelligibility (Jørgensen and Dau 2011; Jørgensen et al. 2015), the lack of significant age-related differences in single-unit animal studies and human EFR studies came as surprising.

With the effect of aging on AM response in IC shown in animal AMFR studies and the lack of conclusive difference in aged single-unit AM responses in mind, we were confronted by two knowledge gaps. These gaps are: 1) how does reduced GABAergic neurotransmission in the IC affect AM temporal coding, but not showing at the single-unit level; 2) how do age-related changes affect the response of IC neurons towards AM stimuli with decreased depth.

In this study, we measured the changes in phase-locking ability, a significant temporal property, as well as rate coding of aged and young rat IC neurons, in response to sinusoidally amplitude-modulated carriers of differing modulation depths. We analyzed both single-unit response and local field potentials (LFP), a small, local populational response thought to reflect the summed synaptic inputs to a neuron or local neuronal population to a large degree (Bullock 1997; Buzsáki et al. 2012), using circular statistical analysis algorithms. Circular statistical analysis has the advantage over traditional peristimulus time histograms (PSTHs) and vector strength (VS) analysis of visualizing detailed, aggregate spike distribution within a cycle of modulation. Although aged single units showed higher VS synchronization when isolated, circular statistics revealed that it came at the cost of loss of off-peak coding and suggested a potential mechanism of synchronization loss at multi-unit and population level.

3.2 Methods and Materials

3.2.1 Ethical approval

The experimental procedures described below were approved by the Institutional 116 Animal Care and Use Committee of Purdue University (PACUC #1111000167). The experiments included in this study comply with the policies and regulations described by Drummond (2009). Rats were housed one per cage in accredited facilities (Association for the Assessment and Accreditation of Laboratory Animal Care) with food and water provided ad libitum. The number of animals used was reduced to the minimum necessary to allow adequate statistical analyses.

3.2.2 Surgical procedures

Data from 9 young (4-6 months) and 8 aged (22-24 months) Fischer 344 rats were included in this study. Methods for surgery, sound stimulation and recording are similar to those described in Rabang et al. (2012). Surgeries and recordings were performed in a 9'×9' double-walled acoustic chamber (Industrial Acoustics Corporation). Anesthesia was induced in the animals using a mixture of ketamine (VetaKet, 80 mg/kg for the young, 60 mg/kg for the aged) and medetomidine (Dexdomitor, 0.2 mg/kg for the young, and 0.1 mg/kg for the aged) administered intra-muscularly via injection. The reduced concentration of anesthesia for the aged was to account for their decreased liver function. Anesthesia applied in these protocols reduces overall spontaneous firing in the IC, but appears to not affect temporal firing precision (Ter-Mikaelian et al. 2007). A constant physiological body temperature was maintained with a water-circulated heating pad (Gaymar) set at 37°C with the pump placed outside the recording chamber to eliminate audio and electrical interferences. The animals were maintained on oxygen through a manifold, with pulse rate and oxygen saturation monitored to ensure that they were within normal ranges during surgery. Supplementary doses of anesthesia (20 mg/kg ketamine, 0.05 mg/kg medetomidine) were administered intramuscularly approximately every 4 hours to maintain areflexia and a surgical plane of anesthesia. An initial dose of dexamethasone and atropine was administered before incision to reduce swelling and mucosal secretions. A subdermal injection of lidocaine (0.5 ml) was administered at the site before the first incision. A central incision was made along the midline and the calvaria exposed. A stainless steel head post was secured anteriorly to bregma with an adhesive and three screws drilled into the skull to provide structural support for a head-cap constructed of orthodontic resin (Dentsply). A craniotomy was performed from 9 to 13 mm posterior to bregma, which extended posteriorly to the lambda suture, and 3 mm wide extending to the right from the midline. The dura mater was kept intact, and the site of the recording was estimated stereotaxically with a rat atlas (Paxinos and Watson 2007) as well as internal vasculature landmarks and physiological measurements. At the completion of recordings, animals were euthanized with Beuthanasia (200 mg/kg, intraperitoneal). Once areflexive, they were perfused transcardially with 150–200 ml of phosphate-buffered saline followed by 400–500 ml of 4% paraformaldehyde. The brain was then removed and stored or processed further for Nissl or immunohistochemistry.

3.2.3 Acoustic stimulation

Sound stimuli were generated using SigGenRP (Tucker-Davis Technologies, TDT) at a 97.64 kHz sampling rate (standard TDT sampling rate) and presented through custom-written interfaces in OpenEx software (TDT) in a random order for each repetition. Sound waveforms were generated via a multichannel processor (RX6, TDT), amplified (SA1, TDT), and presented free-field through a Bowers and Wilkins DM601 speaker. The sounds were presented to the animal at azimuth 0° and elevation 0°, calibrated at a distance of 115 cm from speaker to ear, using a Bruel and Kjaer microphone and SigCal software (TDT). All stimuli used had a 5ms cosine squared gate at onset and offset. Search stimuli used were 200ms long band-pass (BP) filtered noise (BPN) with center frequencies from 1 to 36 kHz in five steps per octave with a 0.5-octave bandwidth. The stimuli for the tuning curve were 200ms long pure tones with frequencies from 500 to 40 kHz, with 10 steps per octave. BPN and tuning curve stimuli were presented every 800ms. The rate-level stimuli consisted of 100 or 200ms long pure tones set at the center frequency (CF) of the neuron presented at varying sound levels from 5 to 85 dB SPL in 10 dB steps to determine the thresholds of isolated neurons.

Sinusoidally amplitude-modulated noise (nAM) and pure tone (tAM) stimuli were 750 ms long, and with modulation frequency (MF) ranging from 8 to 1024 Hz in one-octave steps. The nAM stimuli used broadband Gaussian noise as the carrier (0.1–44kHz), while the carrier frequency of the tAM stimuli was set to the CF of the neuron determined by BPN and tuning curve stimuli. AM stimuli were presented every 2000–2500 ms and were 100% modulated.

nAM depth (nAMd) and tAM depth (tAMd) stimuli were also 750 ms long, with modulation frequency set to the neuron's best synchronized AM frequency or highest synchronized frequency determined by nAM and tAM stimuli. The amplitude modulation depth of nAMd and tAMd stimuli was varied in the following steps: 0 dB attenuation (100%), 2.5 dB (75%), 6 dB (50%), 12 dB (25%), 18 dB (12.5%), 24 dB (6.25%), and 30 dB (3.125%). The carrier frequency of the tAMd stimuli was the same of the tAM stimuli used on the same neuron.

3.2.4 Data acquisition and recording

Single unit activity and multiunit activity in the IC were recorded using a tungsten electrode (A-M Systems) encased in a glass capillary that was advanced using a hydraulic micro-drive (Narishige). The IC was identified based on short-latency driven responses to the 1/2 octave band-passed noise search stimuli. The central nucleus of the IC was identified using

the ascending tonotopy, as well as narrowly tuned responses to pure tones of various frequencies. Once an auditory neuron was isolated using the search stimuli, the CF of the neuron was determined using Band Pass Noise (BPN) and tuning curve stimuli. Responses of the neuron to 5–10 repetitions of each sound stimulus were recorded (usually five repetitions for the tuning curve and 10 for other stimuli). Once the CF was determined, the responses of the neuron were obtained to nAM or tAM stimuli with the carrier frequency set at CF. The sound level of presentation for the tAM and nAM stimuli were set at the lowest sound level that produced a robust, sustained response to the tone set at CF. The sound level was usually 20–40 dB above threshold and corresponded to about 60–70 dB SPL for the young and 75–85 dB for the aged, comparable to those used in our lab's previous EFR studies in young and aged animals (Parthasarathy et al. 2010; Parthasarathy and Bartlett 2011, 2012). Neurons with confirmed synchrony towards nAM and/or tAM stimuli were then obtained of nAMd and/or tAMd responses, respectively, under the neuron's best synchronized AM frequency and/or highest synchronized frequency. Local field potentials (LFPs) were simultaneously recorded from the same electrode by sampling at 3,051.8 Hz and band-pass filtering from 3 to 500 Hz. Line noise at 60 Hz was off-line removed from the LFP recordings with an elliptic notch filter (infinite-impulse response; zero-phase lag).

3.2.5 Data analysis

The spontaneous rate was calculated as the mean rate of the 200ms period that preceded each trial of the stimulus presentation. An auditory-driven neuron was defined as a neuron that exhibited an overall firing rate that was at least two standard deviations higher than the spontaneous firing rate during the presentation of the search stimulus. Only neurons that produced a significant sound-evoked increase in firing rate were obtained from AM responses. The ability of a neuron to synchronize with AM stimuli was calculated using the vector strength (VS) of the response at each modulation frequency:

$$VS = \left(\frac{1}{n}\right) * \sqrt{\sum (cos\varphi_i)^2 + \sum (sin\varphi_i)^2}$$

Where n = total number of observed spikes, φ_i = phase of observed spike relative to modulation frequency. Statistical significance was assessed using the Rayleigh statistic to account for differences in the number of driven spikes between neurons (Lu and Wang 2000):

$$\text{Rayleigh} = 2N \times VS^2$$

A Rayleigh statistic value of greater than 13.8 was considered to be statistically significant ($p<0.001$) (Mardia and Jupp 2000). Only AM depth units with Rayleigh>13.8 on at least one depth were considered synchronized and were included in the analysis.

To visualize the group synchrony of multiple units towards AM depth stimuli of the same MF, period histograms (PHs) were generated by dividing the AM period into 60 phase bins (6 degrees each), and all driven spikes are added into bins according to phase, creating a histogram. Directional mean VS was calculated using the above equation with all spikes from all units responding to the same MF, displaying a summed phase. Absolute mean VS referred to the average value of all VS values from each unit of the same modulation frequency, regardless of their phases.

Circular analysis of single-unit AM depth data was conducted using CircStat toolbox for MATLAB (Mathworks) as described by (Berens 2009), which has been implemented for analyzing directional data in neurophysiology. Mean phase was defined as the circular mean value of the phases of all spikes of one depth in one unit. Circular distribution of all spikes in a unit was quantified by the circular standard deviation of all spike phases of the unit, defined as spike jitter. Circular distribution of mean phases was quantified by the circular standard deviation of all units' mean phases in radians, defined as phase jitter.

The analysis for LFP data focused on peak amplitude, latency, FFT (fast Fourier transform) magnitude at the modulation frequency and FFT ratio. The first negative peak amplitude (N_1) and the first two positive peak amplitude (P_a and P_b) of LFP data are calculated of amplitude and latency. Modal frequencies and phase-locking strengths of LFP were calculated using FFTs, and FFT ratios were calculated from peak FFT (highest within ±3 Hz around stimuli frequency) and an average of adjacent (±2~6 Hz around FFT peak frequency) non-stimuli frequency FFTs, as a measurement of FFT signal-to-noise ratio and frequency specificity.

3.3 Results

3.3.1 General properties of AM depth response and depth-dependent changes

A total number of 444 AM frequency-depth combinations were recorded from 198 single-unit recording sites in the ICs of 17 animals (9 young, 8 aged). The distribution of unit

frequencies is listed in Table 3.1. The numbers of tested units with an MF below 8Hz or above 128Hz were too small to draw any statistical conclusion from. These frequencies are excluded from frequency-specific analysis but still included in the general analysis. All units included in the following analyses are synchronized (Rayleigh>13.8) for at least one modulation depth. An example of a typical AM depth response unit is shown in Figure 3.1.

We also briefly analyzed units that do not meet the Rayleigh criterion for any modulation frequency or depth but showed depth-related rate coding. These units consist of 72 units, of which 57 have rate best modulation frequency (rBMF) ≤ 32Hz. These rate-coding but unsynchronized units are slightly overrepresented in young animals (45 compared to 29 in aged), with chi-square test indicating a significantly different distribution compared to synchronized units (p=0.046). These "unsynchronized" units don't have significant temporal coding related to AM modulation or depth but show moderate rate coding and LFP response with strength related to depth, the threshold at -12dB. These units are not included in subsequence analyses of this study.

Table 3.1. General statistics of the modulation frequencies of the collected single units.

MOD FREQUENCY/TYPE	YOUNG	AGED
4	7	0
8	54	32
16	47	40
32	47	65
64	29	47
128	26	28
>128	13	9
nAM	145	123
tAM	78	98
TOTAL	223	221

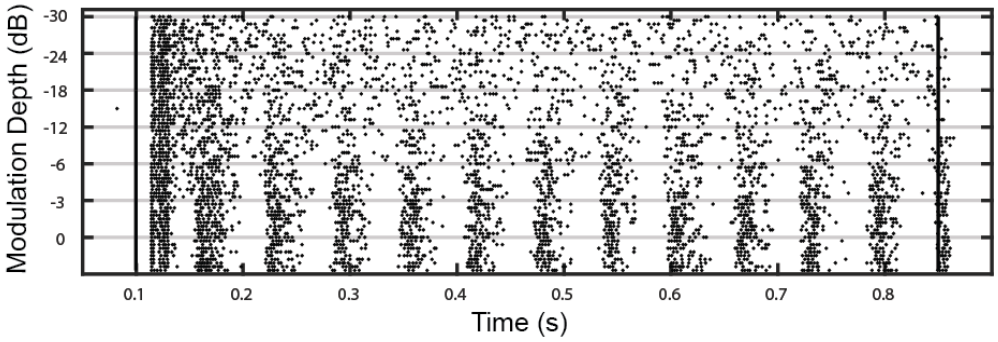

Figure 3.1. Raster plot of AM response of a typical single unit, MF=16Hz. 10 trials for each modulation depth are stacked along the Y-axis. Each black dot represents a spike.

The grand average and standard error of AM depth responses across all MFs, both nAM and tAM, are shown in Figure 3.2, with modulation frequency breakdown of Rayleigh and VS shown in supplementary figures (Figure A1 and A2). Both age groups exhibit a depth-dependent decrease in firing rate and synchrony, shown in total firing rate, as well as Rayleigh and VS. In the first three modulation depths (0dB, -2.5dB, -6dB), the aged nAM units have significantly lower firing rate (26.75±1.538Hz, 26.65±1.496 Hz, 23.58±1.423 Hz) than young nAM units (36.45±1.735 Hz, 36.47±1.766 Hz, 33.25±1.621 Hz), even using sound levels 10~20dB higher than those of young units to compensate for their higher hearing thresholds. However, in the first four depths (0~-12dB, Figure 3C), both aged nAM (VS=0.506±0.019, 0.511±0.018, 0.429±0.019, 0.306±0.015) and aged tAM (VS=0.566±0.024, 0.571±0.024, 0.498±0.024, 0.337±0.020) units show higher synchronicity than their younger counterparts (young nAM VS=0.423±0.017, 0.424±0.017, 0.345±0.016, 0.257±0.014; young tAM VS=0.402±0.021, 0.416±0.022, 0.316±0.021, 0.231±0.017) with higher VS, with the differences in tAM units being larger. The Rayleigh statistics of nAM and tAM units (Figure 3.2B) reflect the combined effect of the two trends in rate and temporal coding.

To illustrate the modulation depth-dependent changes of temporal parameters in young and aged units, we calculated the differences of Rayleigh (dRay) vector strength (dVS) between two adjacent depths for each unit. In nAM units, young and aged units experience similar trends of depth-dependent changes in VS (Figure 3.2C), with the biggest change between -6 to -12dB. In tAM units, dVS (Figure 3.2C) peaks at -3 to -6dB for young, -6 to -12dB for aged. This difference indicates that young units exhibit higher sensitivity toward decreasing AM depth than that of aged units.

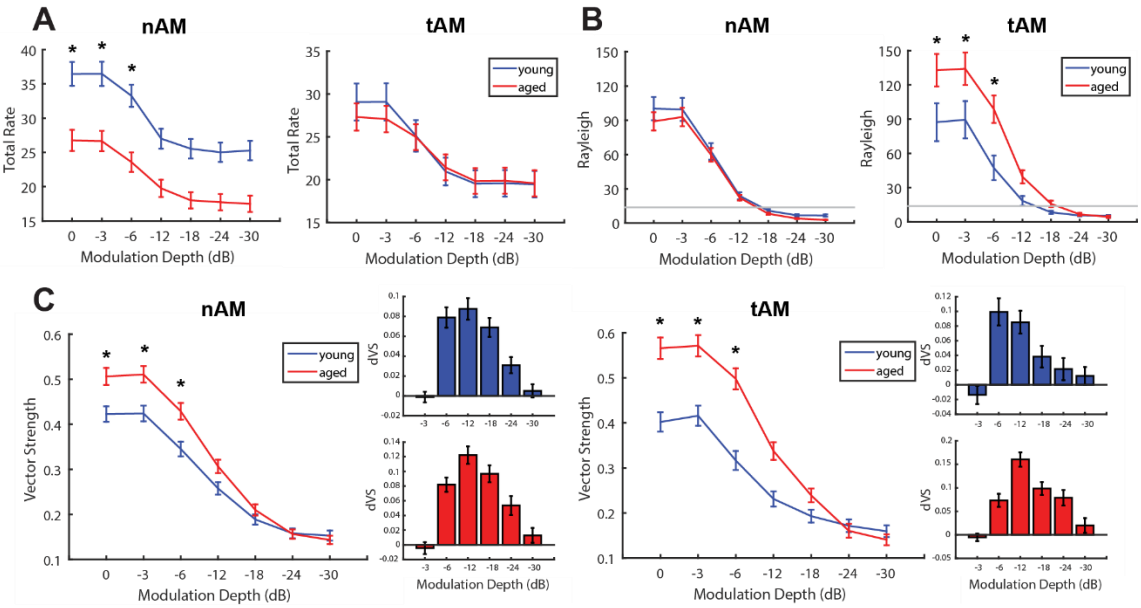

Figure 3.2. The grand average and standard error of AM depth responses across all MFs. Asterisks (*) indicate significant differences between age groups. Both young (blue) and aged (red) exhibit depth-related decrease of firing rate (A), Rayleigh (B) and vector strength (C). A) Firing rate of aged nAM units was significantly lower than young nAM for the first 3 depths (0dB, -3dB, -6dB, left panel) b) Rayleigh statistics of aged tAM units was significantly higher than young tAM for the first 3 depths. C) VSs of both nAM and tAM of aged units were significantly higher than young unit for the first 4 depths (0dB, -3dB, -6dB, -12dB). Depth-dependent changes in VSs for nAM (left panel) and tAM (right panel) are displayed in bar graphs for each panel, respectively.

In this study, we analyzed units from the same site but with different MFs as independent instances. However, to rule out any significant difference caused by multiple sampling on one site, we compared the Rayleigh and VS of all units with that from the units with the highest Rayleigh from each site. The trends are similar to those shown in Fig. 3.2, with the main change in the average 0dB VS of young units raised to 0.528 ± 0.023 and 0.491 ± 0.030 for nAM and tAM, respectively.

Figure 3.3A shows the differences in rate and temporal parameters between nAM and tAM in both age groups. Young nAM units have significantly higher total and sustained rates than young tAM and aged units with either carrier. Though VS was significantly lower in young units than aged units regardless of stimuli type, no significant difference in VS has been observed between nAM and tAM units of the same age group. Differences in depth-dependent synchrony thresholds for age and stimuli carrier types are shown in Figure 3.3B as the distribution of thresholds at which the linearly interpolated Rayleigh statistic falls below 13.8. Consistent with Figure 3.3A, the distributions of synchrony threshold between nAM groups were closely similar, while young tAM had drastically lower synchrony (peaks at -6dB) threshold than aged tAM.

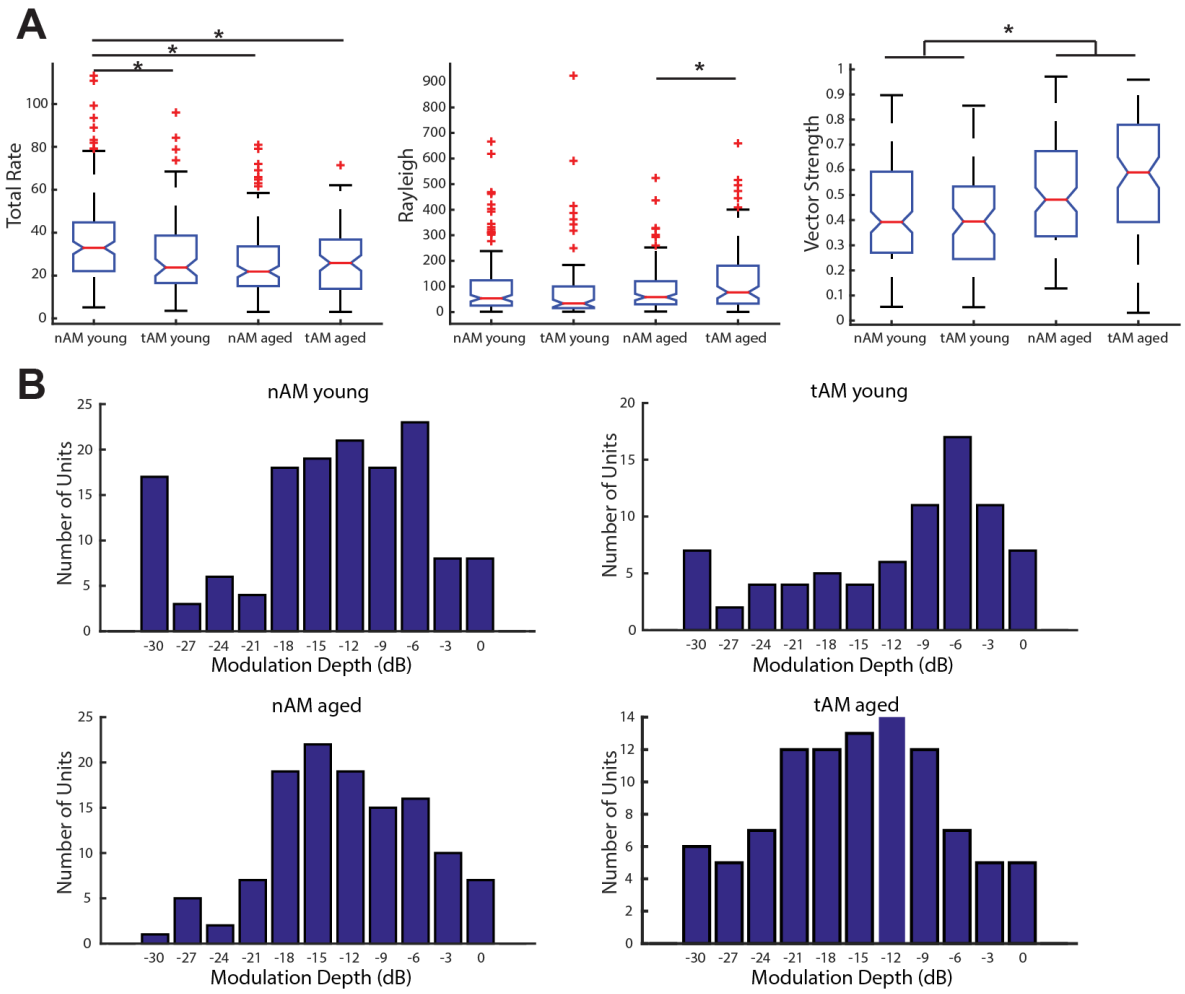

Figure 3.3. Comparison of rate and temporal coding parameters of nAM and tAM in young and aged single units. A) Total rate, Rayleigh and vector strength of young and aged single units at 100% modulation depth. Asterisks (*) indicate significant differences between groups. Young groups showed a lower VS than aged groups regardless of stimulus type. B) Depth-dependent synchrony threshold of young and aged nAM and tAM units.

3.3.2 Period histograms showed wider distribution of spiking in young units and greater discrepancies in peak phase between aged units

Traditionally, we have been looking at the phase-locking properties of IC units on an individual level, in which synchronicity is represented by the value of vector strength from each unit. In this method, information regarding the peak phase, the shape of spike distribution and the sum performance of multiple units has been largely ignored. As multiple units project from the IC to converge on neurons in the auditory thalamus, if the peak phases of multiple units do not align, it would affect the information relayed to the auditory thalamus. In such cases, the disruption of temporal information would only be represented as a decline in output auditory thalamic vector strength, without understanding how synchronized inputs convert to non-synchronized outputs. Thus, it is worthwhile to look at the spike distribution from multiple

units using circular analysis methods. Since nAM units are more robustly sampled (Table 3.1), we focus our discussion on the result of nAM units.

We utilized populational Period Histograms to illustrate the sum performance of units tested for the same modulation frequencies. The period histogram, which is essentially a peristimulus time histogram (PSTH) of units with a certain MF wrapped around their modulation cycle, was described by Rose et al. in the auditory nerve (Rose et al. 1971). Since then, this method has been frequently utilized under auditory context (Krishna and Semple 2000; Ter-Mikaelian et al. 2007; Henry and Heinz 2012; Herrmann et al. 2017). Here, spike distribution curves and combined peaks of five AM depth attenuations (-0dB, -6dB, -12dB, -18dB, and -30dB as baseline) are shown in Figure 3.4A, 3.4B and Figure 3.5. For the convenience of display, the combined vectors are shown in 1/10 length. The difference in distribution shape was clearly illustrated in units with low MFs (8Hz and 16Hz). Young units displayed a wider firing window than aged units, which was consistent with their lower vector strength than that of aged. Such spike distribution shapes could also imply that the ability to represent modulation shape was stronger in young, as we see a distinct shape change in spike distribution curve from -6dB (green) to -12dB (cyan).

As modulation frequency goes up above 32 Hz, where a cycle is equal or shorter than the scale of IC neurons' recovery time (Sayegh et al. 2012), refractoriness starts to limit the ability of a neuron to code temporally (Gaumond et al. 1982; Garcia-Lazaro et al. 2013). A neuron could only fire once or twice in each cycle, making modulation width coding difficult. In these faster MF units, the spike distribution curve exhibits strong irregularities (Figure 3.4) and even dual peaks, a result likely due to the combination of few spikes per cycle or having different units prefer the rising or falling phase preferentially. Interestingly, we observed that the "duo-peak" phenomenon most strongly in 32 Hz for both age groups, but in 64Hz young it completely disappeared, while 64Hz aged still show widened distribution similar to the shape of 32Hz. We speculate that in these "in-between" MFs, the cycle is long enough for the units to fire twice or more per cycle, but not long enough for neurons to fire synchronized as in slow MF, therefore making a portion of their spikes out of synch, resulting in lower VS in these MFs. The difference in MF where the "duo-peak" subsides for different age groups may be a result of reduced GABA level in aged units affecting its minimum recovery time, a phenomenon observed in bats (Zhou and Jen 2003).

We calculated the combined population vector strength of nAM units from each MFs, standardized by total spike number, and compared them with the absolute average VS value of the same population. If a population's peak phases highly agree with one another, this would

result in a small difference between absolute VS and PH VS; and if there is a greater variance between each neuron's peak phase, they will cancel each other out, resulting in a greater difference between absolute VS and PH VS. On the other hand, if a population has a negative difference between these two values, it means there are units with robust but out-of-synch firing among the population that level out the vector contribution of other spikes, another rare but underrepresented condition shown by simply averaging VS from every unit. In most MFs and depths, the difference was positive, except for the weakly synchronized 8Hz nAM aged population under -18dB depth (Figure 3.4C). In all MFs except 32 Hz, we see the trend of young units having a smaller difference between Period Histogram VS than aged units (Figure 3.4C). This trend indicates that the peak phases for aged AM units are more varied among themselves than that of young units.

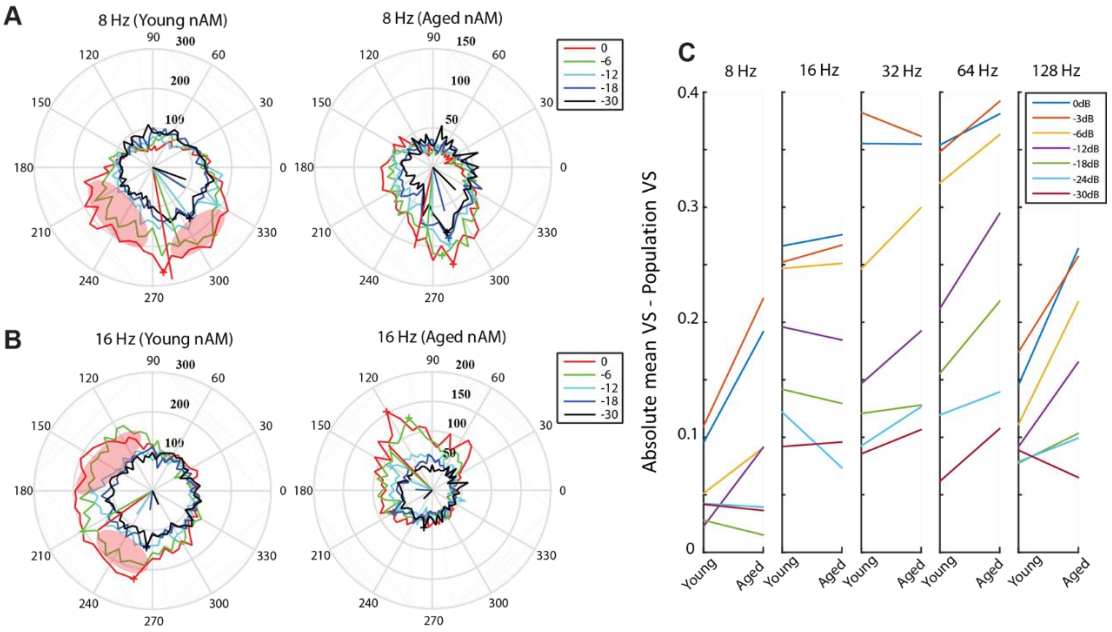

Figure 3.4. Period Histogram of young and aged nAM units, MF=8Hz (A) and 16 Hz (B). For the convenience of display, the combined vectors are shown in 1/10 length. Population peak firing phases are shown as small crosses (+). Population VS of young units showed a smaller difference to absolute mean VS than that of aged units in most MF and depth conditions (C), indicating that the peak phases of aged units were more varied.

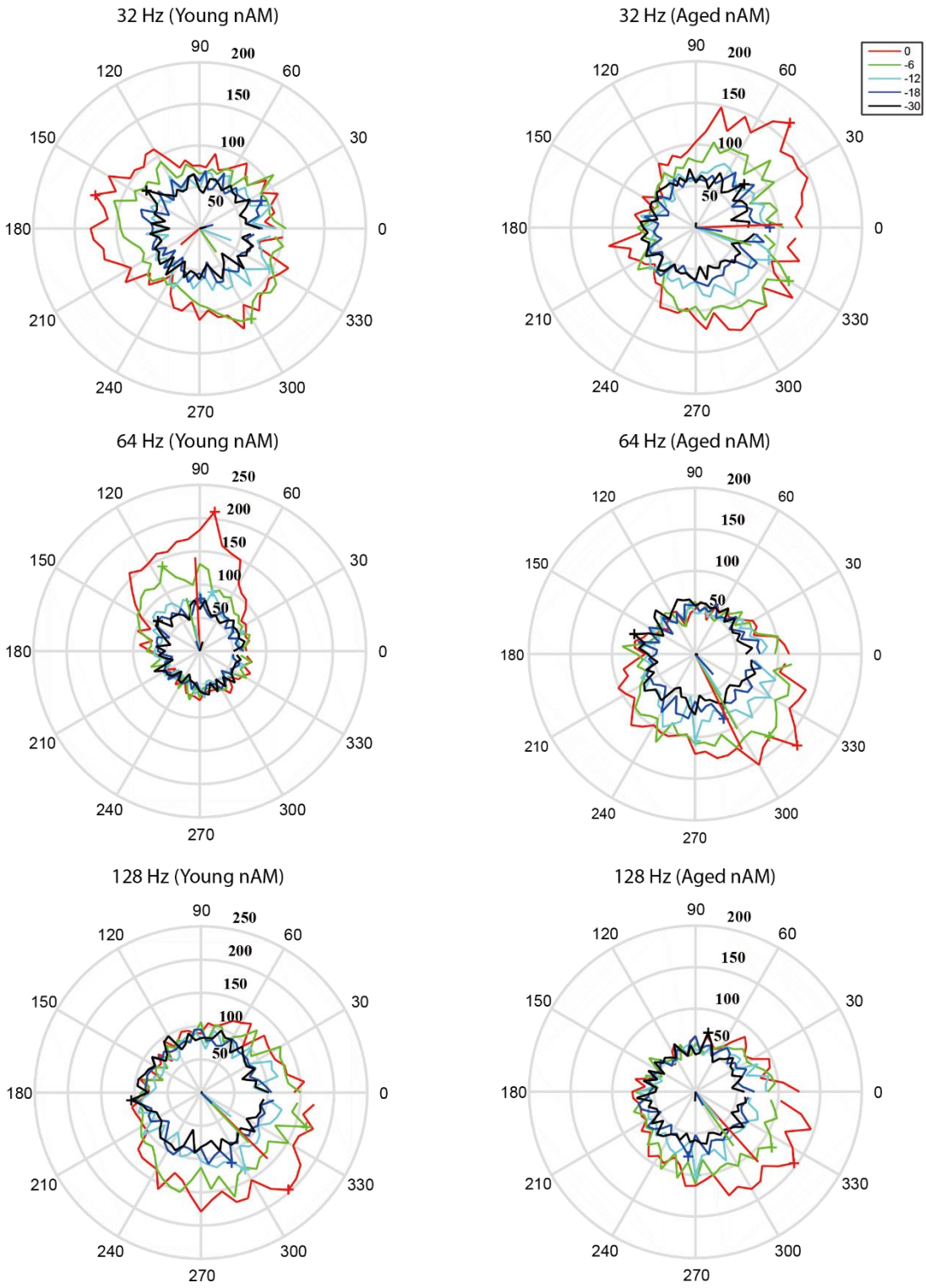

Figure 3.5. Period Histogram of young and aged nAM units at higher MFs (16Hz, 32Hz and 128Hz). For the convenience of display, the combined vectors are shown in 1/10 length. Combined peak firing phases are shown as small crosses (+).

3.3.3 Circstat jitter analysis showed wider firing distribution in young units, but no significant, consistent difference in unit peak phase between age groups

The Period Histogram method shows a combined effect of performance from multiple units. Here, with circular statistics tools, we want to investigate how the peak phase distribution difference of individual units and spike distribution difference within single units contribute to the differential performance in both VS and Period Histogram. To illustrate them, we calculated the circular standard deviation of all peak phases (in radians) as "phase jitter", and the circular standard deviation of spikes within one unit/one depth as "spike jitter" (Fig. 3.6A). Phase jitter represents the variation of peak phase among all units of the same MF, and spike jitter represents the phase variation of spikes within one unit.

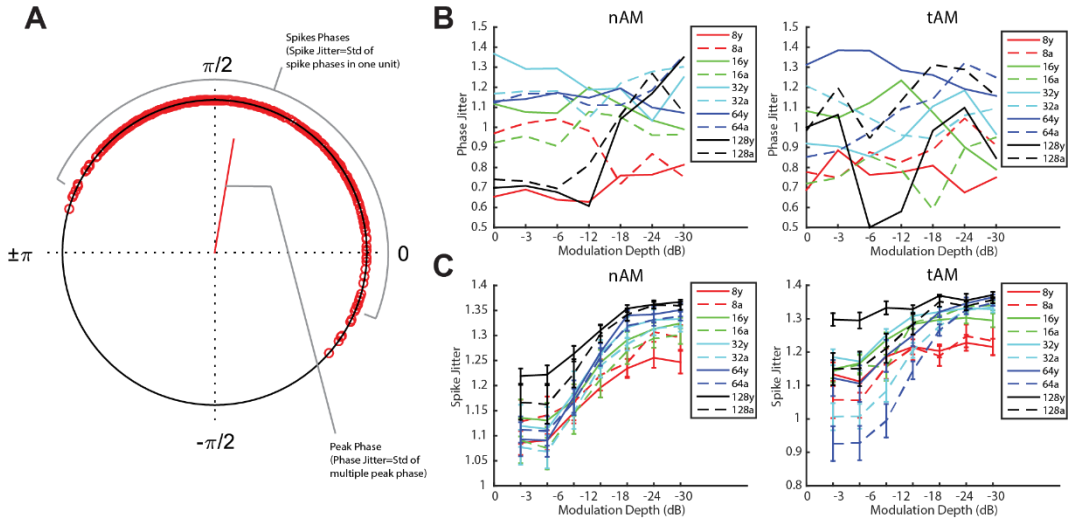

Figure 3.6. A) Schematic of CircStat (Berens 2009) circular statistics for an AM unit as laid out on a polar plot. B) Phase jitter of nAM and sAM depth units. Phase jitter of aged nAM units was higher than young units only at 8 Hz MF. C) Spike jitter was higher for young units in most MFs for both nAM and tAM, showing a wider distribution of spikes around AM phase.

Aged nAM units differ in peak phase more than young units under 8Hz AM with modulation depth from 0dB to -12dB (Figure 3.6B), in line with their difference in absolute VS and Period Histogram VS (Figure 5C). Correspondingly, among 16Hz and 32 Hz AM units where young units show widened distribution of spikes or "duo-peak" in Period Histogram and have lower VS, phase jitter values are larger. The larger value in peak phase standard deviation for 16Hz nAM young units was not in line with the lower difference in absolute VS and Period Histogram VS, precisely because the differences concentrate, almost symmetrically, around a stable window around the collective peak, as seen in their Period Histogram (Figure 3.4A and B). Not much difference can be seen in 64Hz and 128Hz. No significant trend can be observed

from tAM units, as the difference in peak phase distribution changes shows no correlation to depth or MF. In all, the circular standard distributions of peak phases for young and aged units were consistent with the observations in Period Histogram, but few consistent trends can be observed with significance.

In nAM units, spike jitter was higher in young than aged in all MFs except 8Hz, expectedly showing similar trends with VS (Figure 3.6C and 3.2C), but the difference was not significant for all frequencies (Figure 3.7). In tAM units, young units had higher spike jitter for all high MFs, though these differences are only significant in 32Hz (Young, 0~-12dB: 1.185 ± 0.024, 1.172 ± 0.026, 1.251 ± 0.018, 1.308 ± 0.011; Aged, 0~-12dB: 1.007 ± 0.040, 1.008 ± 0.037, 1.084 ± 0.033, 1.205 ± 0.022) and 64Hz (Young, 0~-12dB: 1.122 ± 0.054, 1.106 ± 0.055, 1.189 ± 0.048, 1.250 ± 0.032; Aged, 0~-12dB: 0.926 ± 0.052, 0.928 ± 0.051, 0.994 ± 0.050, 1.146 ± 0.027) for the first 4 depths (Figure 3.8). The differences in spike distributions were greater between aged groups in tAM than in nAM. This was likely due to the fact that tAM inherits from only a small population of frequency-specific inputs, thus more vulnerable to age-related synaptopathy and loss of excitation. The spikes of aged units become more sparse, and through the loss of inhibitory neurotransmission, are likely to concentrate on the peak phase of input, as postulated by Herrmann et al. (2017), resulting in far greater VS and far smaller spike jitter than young units.

From the above analysis, we can conclude that peak phase difference is a contributor to the difference between the phase-locking performances of age groups only in nAM 8Hz, 16Hz and 32Hz. In other conditions, spike distribution difference was predominantly correlated with phase-locking performance. tAM units have a more complicated relationship between peak phase difference, spike distribution and age, a result likely due to interference between the coding of spectral and temporal information in IC units (Rodríguez et al. 2010; Chen et al. 2012), but our data from tAM units are not sufficient to illustrate such interference in detail.

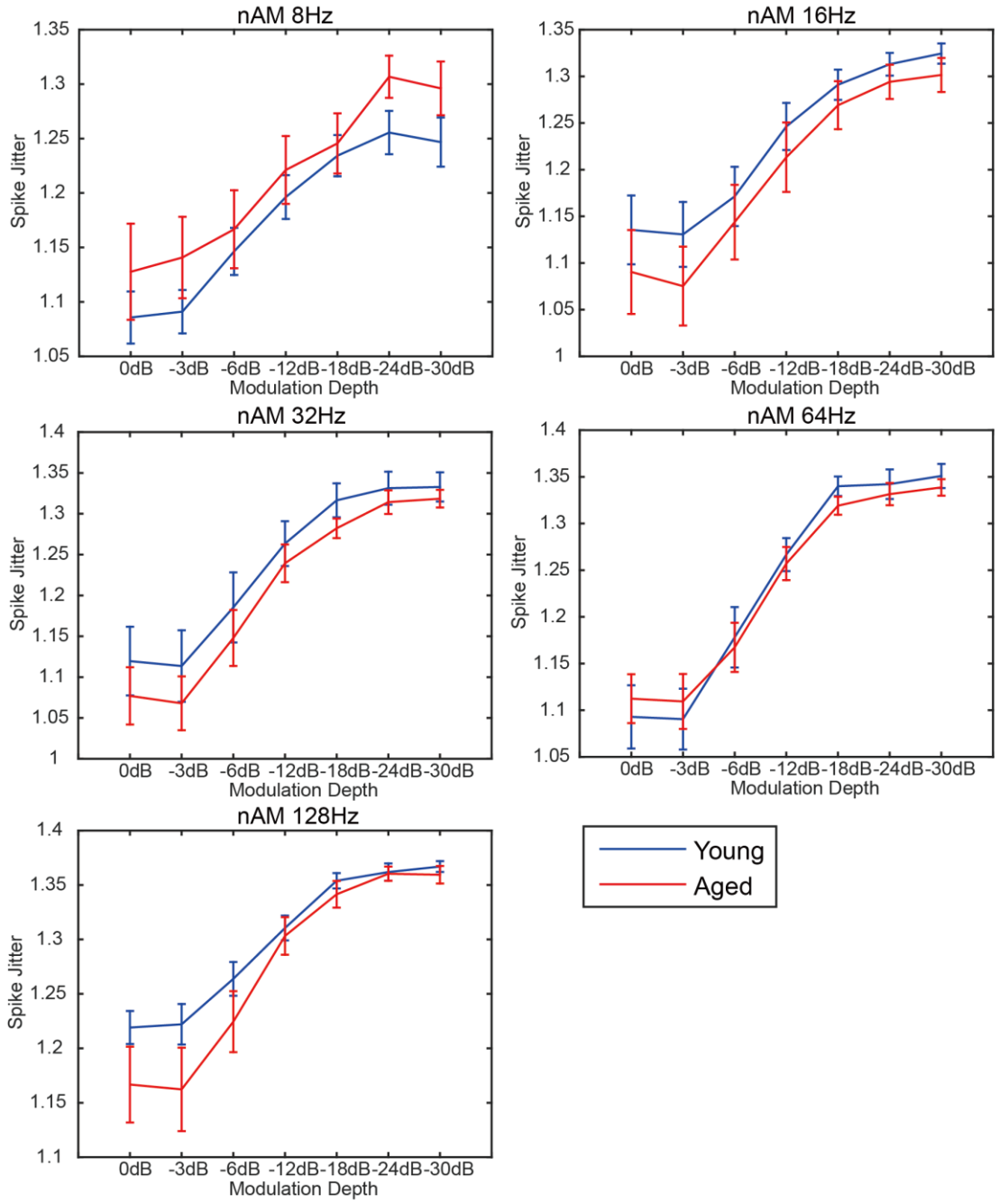

Figure 3.7. Circular statistics spike jitter of young and aged nAM units, broken down by MF.

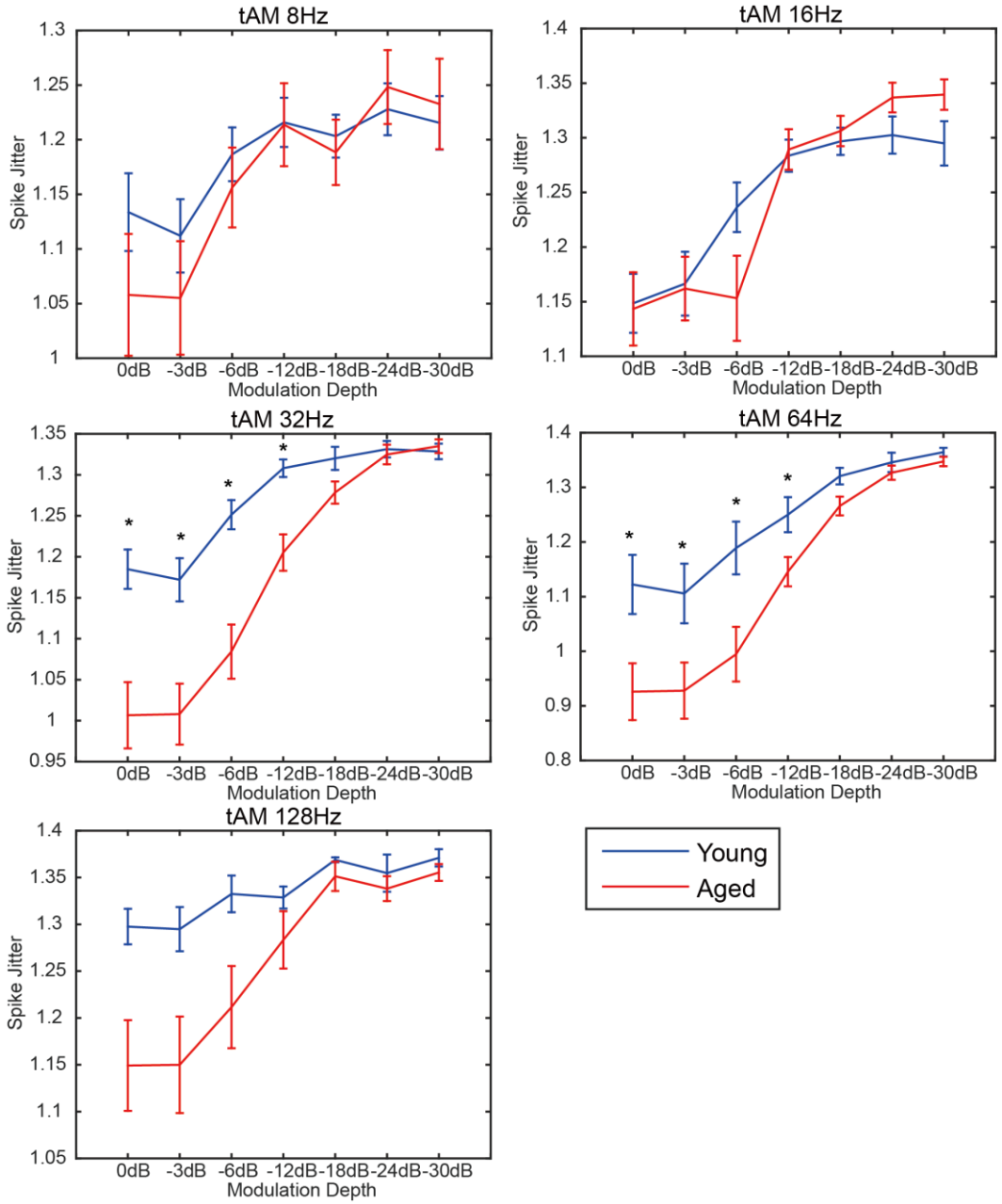

Figure 3.8. Circular statistics spike jitter of young and aged tAM units, broken down by MF. Asterisks (*) indicate significant differences between groups.

3.3.4 Aged AM depth units were lower in LFP response amplitude but higher in FFT ratio

Consistent with the more robust firing rate (Figure 3.2A and 3.2B) and FFR amplitude (Parthasarathy et al. 2014) in young phase-locking IC units, we observed larger absolute peak LFP amplitudes in all three major peaks (N_1, P_a and P_b) in young units than aged units (Figure 3.9A). Peak FFT was also higher for young units (Figure 3.9B), similar in the scale of the difference of sustained firing rates (Figure 3.2B). These are thought to reflect a higher level of presynaptic activities in young IC units, especially in the anesthetized preparation where

sensory inputs to IC predominate (Bullock 1997; Buzsáki et al. 2012). FFT ratio of LFP also showed a depth-dependent decline similar to that of VS (Figure 3.2C), following depth attenuation (Figure 3.9C). Interestingly, aged units show a higher FFT ratio in LFP than young units, with significant differences from -6dB to -18dB ($p<0.05$), but not at 0dB to -3dB attenuation. LFP responses recorded from sites where non-synchronized rBMF units were recorded, though exhibiting similar depth-related coding, showed no significant difference between young and aged (not shown).

When we break down the peak FFT ratio data of nAM units by MF, we see different trends between low MF units and high MF units: namely, higher for young for low MFs <32 Hz, similar between age groups at 32Hz, and higher for aged at higher MFs >32 Hz, though only significant for 64Hz (Figure 3.9D). Similar trends are observed in tAM units with reduced significance (not shown).

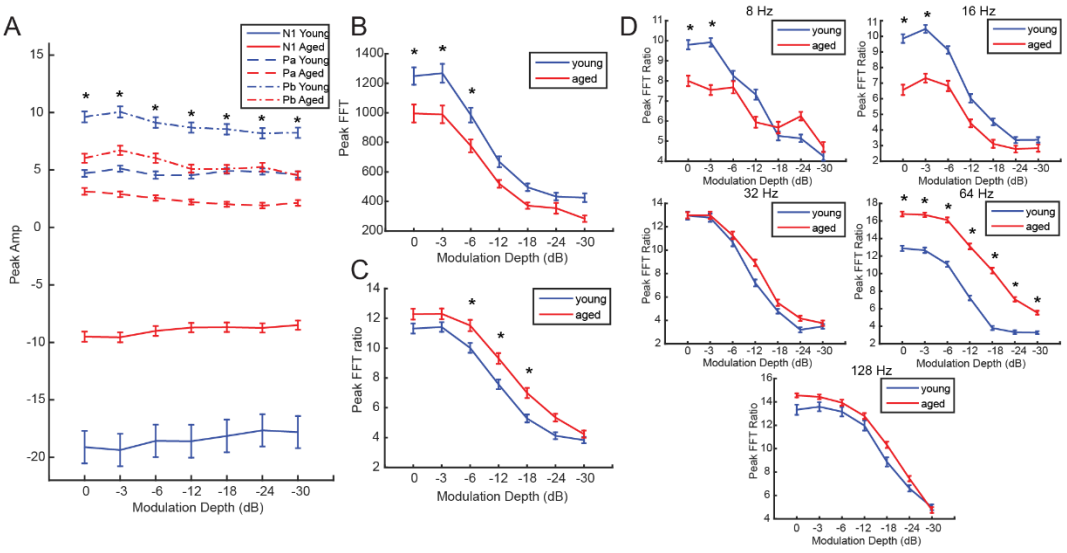

Figure 3.9. LFP statistics of young and aged AM depth units. A) Absolute peak LFP amplitudes were larger for young units than aged units at all modulation depths. B) Peak FFT amplitude of LFPs. C) Peak FFT ratio of LFPs. D) Peak FFT ratio of LFPs of nAM units, broken down by MF. Asterisks (*) indicate significant differences between groups.

When looking at the distribution of FFT and FFT ratio of the LFPs of aged and young units, we see that young units have a slightly more even distribution in both peak FFT value as well as FFT ratio in both nAM and tAM units (Figure 3.10A, blue), indicating more robust presynaptic activities and diverse temporal responsiveness. Aged units, however, though having a few high FFT outliers, show a low level of presynaptic activities achieving high VS in general (Figure 3.10A, red).

Low FFT ratio (<5) – high VS (>0.6) units are predominantly seen in aged tAM, and more mid-high FFT ratio (>10) – low VS (<0.4) units are seen in young than aged (Figure 3.10B). Aged tAM units show a more linear relationship between FFT ratio, an indicator of the temporal property of local input, and VS than that of young tAM units (Corrcoef: Aged: 0.36, Young: 0.13), indicating a slightly simpler, more relay-like processing of presynaptic inputs.

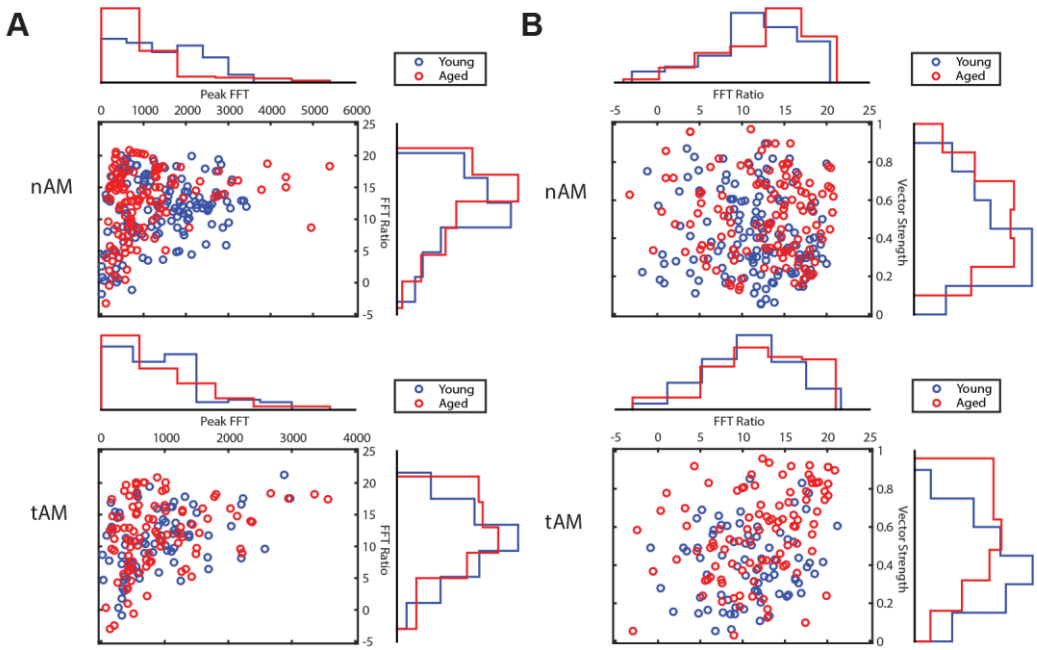

Figure 3.10. A) Correlation between peak FFT and FFT ratio, nAM and tAM, at 100% depth; B) Correlation between FFT ratio and VS, nAM and tAM, at 100% depth.

3.3.5 Wide Variance and Relative Independence of Rate and Temporal Coding in the IC

A recent study on AM response in the auditory cortex shows a positive correlation between rate and temporal coding in young animals but not in aged (Overton and Recanzone 2016). In our study, we look for this correlation between sustained rate and VS in our AM depth data from aged and young IC. Although slightly more linear (Corrcoef=0.34) in young tAM, there was no significant positive correlation between rate coding and temporal coding in IC neurons in response to AM (Figure 3.11. Corrcoef: aged nAM=-0.28, young nAM=-0.06; aged tAM=0.04), unlike in auditory cortex. Similar to the observation of low LFP FFT/FFT ratio, low VS units in aged tAM population, there was a group of low rate (<40/s), high VS (>0.6) units consisting of predominantly aged tAM units. Maximum and minimum VSs did not differ by much, although quantile analysis showed that aged tAM units were overwhelmingly

distributed towards higher VS, with a quarter of synchronized aged tAM units having a VS higher than 0.7, while the same quantile of young tAM units fell at 0.571 (Table 3.2).

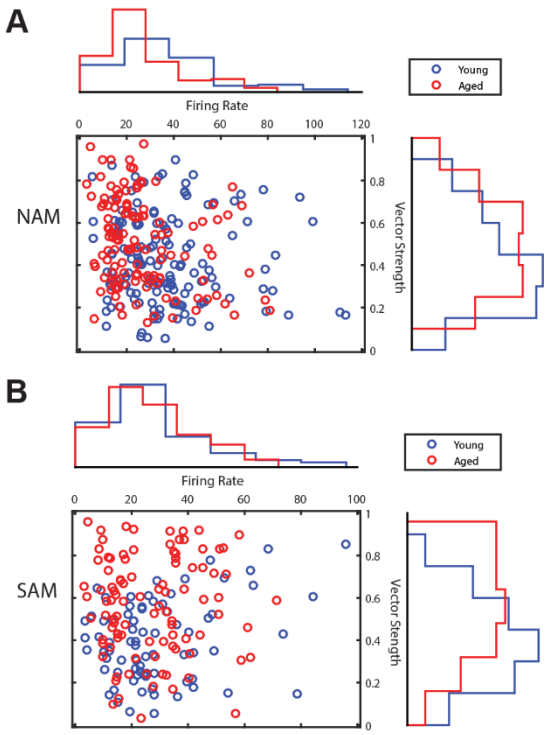

Figure 3.11. Correlation between sustained rate and VS, nAM and tAM, at 100% depth.

Table 3.2 Quantile analysis of VS distribution of young and aged tAM units, at 100% depth

	Min	0.25	0.5	0.75	Max
Young	0.054	0.351	0.536	0.701	0.897
Aged	0.031	0.253	0.394	0.571	0.971

3.4 Discussion

Our study aims to test whether there is a systematic difference in the single-unit coding of Amplitude Modulation depth between young and aged Inferior Colliculus. We mainly looked at depth-dependent changes in rate and temporal coding (as Vector Strength and the Rayleigh statistic) and focused our analysis on temporally synchronized units. We also included the observation of units that are not temporally synchronized but exhibit significant depth-related rate coding. These data confirm that IC neurons code AM depth with both rate and temporal coding, as exemplified by depth-dependent total rate and VS, and both exhibited

similar slopes in their measures with respect to modulation depth, decreasing with the attenuation of depth.

Our analysis of rate and VS across age groups (Figure 3.2 and 3.3) confirmed that young IC units are significantly more robust in rate coding of AMd stimuli, in line with previous observations that young IC neurons have a more robust cycle-by-cycle coding than aged neurons in response to low frequency 100% AM (Walton et al. 2002). However, young IC units exhibited lower VS than their aged counterparts. Not only was the VS of young AM depth units smaller, but young tAMd units also more sensitive to depth decrease than their aged counterparts in this dataset (Figure 3.2C and 3.3B). Because our analysis used the Rayleigh criterion to identify "synchronized" units, there may be an uneven inclusion of high-rate, low-VS young units in the dataset using the Rayleigh criterion – since young units have higher firing rate, units with lower VS are more likely to be selected as "synchronized." However, as carrier frequency selectivity is partly inherited from auditory brainstem structures, including the cochlear nucleus, superior olivary complex and lateral lemniscus, this could also be interpreted as the combined effect of age-related change in both the CN (Schatteman et al. 2008) and compensation of receptor sensitivity in the IC in response to age-related loss of GABAergic input (Milbrandt et al. 1996). Notably, studies have suggested changes in the composition of not only GABA receptor subunits but also glutamate and glycine receptor subunits in the IC as a result of peripheral hearing loss (Holt et al. 2005), which could lead to the overall decrease of rate coding intensity reported above. We observed no significant difference in depth sensitivity of rate coding between young and aged IC units, either in temporally synchronized units and rate-only units (Figure 3.2A and C; Figure 3.3A).

Specifically, we utilized circular statistics tools to analyze the phase-locking ability of these IC units (Figure 3.4 – 3.8). Since neurons may have different latencies or show peak firing in various phases of a modulation cycle, their individual temporal coding may cancel out each other when their firings are relayed towards higher nuclei in the auditory pathway. This effect was not evident in VS statistics, so we used the period histogram method to show it. When aligned together to their AM cycles, young units show better preservation of synchronicity collectively (Figure 3.4C), as observed in period histograms, especially in lower MFs (8~16Hz, Figure 3.4A and 3.4B). Individual aged neurons may phase-lock just well, as shown in their higher VS than young units, but there was a wider distribution of peak phases among units. Such variability may be underrepresented when analyzing clustered responses (Harris et al. 2012; Herrmann et al. 2016), but resulting in a reduction of response amplitudes. This observation may explain why population response measures such as AMFR are worse

with aged animals, as seen in previous EFR and EEG studies (Parthasarathy and Bartlett 2012; Harris and Dubno 2017). This degradation of neural synchrony may come from a few sources such as age-related cochlear synaptopathy, demyelination and loss of AN activities (Schmiedt et al. 1996; Lang et al. 2010; Xing et al. 2012), further exacerbated by an age-related disruption of inhibitory neurotransmission in the auditory system (Caspary et al. 2008).

Our result of young units having poorer VS at first seems contrary to our previous observation in AMFR (Parthasarathy and Bartlett 2011), in which aged units exhibit lower AMFR response when the saliency of the AM stimuli was reduced by the presence of noise or decreased modulation depth. However, when looking at the result from the period histogram method, as well as rate coding and LFP amplitude, we could see how collectively, young units yields a more robust response towards AM stimuli, even with decreased modulation depth, and thus contribute to more reliable processing in auditory thalamus and the cortex. Young units also showed a broader coding of phase, both individually (as evident through spike jitter, Figure 3.6) and collectively (as evident through PH, Figure 3.4), showing more spikes in phase areas surrounding the peak firing phase, while spikes from aged units are concentrated. These "slope" areas, while containing auditory information, naturally reduce stimuli VS. The reduced VS of young units, rather than showing worse synchrony, may be evidence of more robust tuning of AM shape. Because spikes of aged units were highly concentrated in a narrow phase, showing little detection of the "slope" areas, thus VSs of aged single units were less affected by the reduction of depth. Young units may pick up differences in AM shape better through coding of these "slope" areas in stimuli, and this, in turn, is consistent with previous findings (Parthasarathy and Bartlett 2011; Herrmann et al. 2017; Parthasarathy et al. 2019b), where young animals showed higher fidelity in AM shape EFR and high, single-unit spike correlation with AM shape, especially with gentle, ramped onset.

Rate coding and temporal coding remain relatively independent of each other in IC neurons (Figure 3.11), showing less correlation of spectral and temporal coding, contrary to that observed in the auditory cortex (Overton and Recanzone 2016; Thomas et al. 2019). However, the active transformation of presynaptic temporal information into the firing patterns of neurons attuned to different AM features may have already started in small, local circuits of young IC neurons (Chen et al. 2012; Schnupp et al. 2015), whereas aged neurons lose some of their response heterogeneity (Khouri et al. 2011) and show slightly simpler, relay-like processing (Figure 3.10). Herrmann et al. (2017) postulated that these changes may be a result of both excitatory and inhibitory imbalance, as indicated by several studies (Le Beau et al. 1996;

Holt et al. 2005) and is consistent with our speculation from computational modeling (Rabang et al. 2012).

Overton and Recanzone (2016) also reported decreased proportion of AM synchronized units in the aged primary auditory cortex. Because the limited dataset drew only from confirmed AM synchronized units, we have little ways to confirm a similar decrease in the proportion of synchronized neurons in the IC in a study primarily focusing on the effect of AM depth. However, we did observe that aged, rate-coding units with a clear rBMF were significantly less than their young counterparts. Nonetheless, this remains a potential contributing factor to the observed extremely high synchrony in aged tAM depth units. It is possible that a large part of mediocrely synchronized neurons has been lost in aged IC, and only the very explicitly synchronized units remain. On the other hand, healthy young IC has more diversity in the spectrotemporal coding preference among the neurons, many exhibiting a trade-off between spectral and temporal resolution (Rodríguez et al. 2010; Khouri et al. 2011; Morrison et al. 2014). Adding up that higher firing rates allow many young units with mediocre synchrony to be drawn into the dataset, these relatively poorly synchronized neurons contribute to the significantly worse performance of young tAM units in our dataset.

The relative independence between rate and temporal coding, as well as wildly varied circular statistics in units with pure tone carriers, echoes with existing studies on the IC's anatomical heterogeneity. Ito and colleagues described two types of GABAergic neurons in the IC: large GABAergic neurons with VGLUT2 axonal terminals, and small GABAergic neurons without such terminal (Ito et al. 2009). Glutamate terminals found in the IC are traced to different origins - specifically, VGLUT2 terminals exclusive to large GABAergic neurons are traced to laminal lemniscus, dorsal cochlear nucleus, superior olive and the IC itself (Ito and Oliver 2010), indicating potential coding mechanisms happen only in certain IC neuron. However, age-related physiological differences in different subtypes of IC neurons corresponding to their differential circuit properties have yet to be found. Our methods limited the capacity of linking IC neurons' physiological performance to their individual anatomical characteristics, and we have been traditionally treating IC neurons as a homogenous group. However, since recent studies have observed similar response properties shared by GABAergic and glutamatergic neurons in the rodent IC (Ono et al. 2017), this presupposition was likely not a significant limiting factor of the current study's impact.

3.5 Conclusion

Through utilizing circular statistics, we demonstrated potential mechanisms of age-related changes in temporal coding in the IC, manifested as a decrease of overall activity, a loss of modulation "slope" coding and a disagreement of synchronization phase at a population level. Central gain compensation in the IC was evident as an increased sensitivity towards LFP input and amplification of VS in post-synaptic activity, but the compensation was not enough to make up for the decrease of activity and came at the cost of nuanced temporal coding. Our study reinforced the findings of previous studies such as Parthasarathy et al. (2019b) and provided further insights into understanding the mechanisms of age-related temporal processing degradation in speech and complex sound perception.

CHAPTER 4. LONGITUDINAL AUDITORY PATHOPHYSIOLOGY FOLLOWING MILD BLAST INDUCED TRAUMA

This chapter is currently under revision to be published in the Journal of Neurophysiology. A preprint version is available on BioRxiv as Han et al. (2020).

4.1 Introduction

Hearing loss stands out as one of the most commonly reported consequences following blast injuries and can last for months or even years without significant external injury (Cohen et al. 2002; Cave et al. 2007; Ritenour et al. 2008; Saunders et al. 2015). Hearing difficulties have been hypothesized to contribute to many behavioral complaints associated with mild blast traumatic brain injury (Gallun et al. 2012b; Vander Werff 2012). Most studies regarding blast-induced hearing loss have focused on damage in different parts of the peripheral auditory system (PAS) (Kerr 1980; DePalma et al. 2005). However, significant hearing difficulties can occur in the absence of peripheral diagnostic indicators such as eardrum rupture or clinical threshold shifts (hearing loss >25 dB), indicating potential disruptions further upstream (Remenschneider et al. 2014; Saunders et al. 2015; Van Haesendonck et al. 2018). Increasing clinical (Berger et al. 1997; Cohen et al. 2002; Cave et al. 2007; Ritenour et al. 2008; Lew et al. 2009; Gallun et al. 2012a) and laboratory (Patterson and Hamernik 1997; Ewert et al. 2012; Cho et al. 2013b; Du et al. 2013; Masri et al. 2018) evidence suggest that both peripheral and central auditory system (CAS) are important blast-susceptible structures, where CAS includes the brainstem, midbrain, thalamus, and cortex.

Subcortical CAS such as the auditory brainstem may be particularly vulnerable to blast injury, including hemorrhages, intracranial deformation and blood-brain barrier (BBB) permeability, glutamate excitotoxicity, elevated calcium, as well as elevated markers of oxidative stress and neuroinflammation from near short-term (1-7 days) up to 2 weeks (Knudsen and Øen 2003; Leung et al. 2008; Säljö et al. 2011; Cho et al. 2013a; Song et al. 2015; Walls et al. 2016). Functional changes, such as spontaneous hyperactivity in the auditory brainstem (Luo et al. 2014a, 2014b), as well as structural changes in OHC loss (Ewert et al. 2012), axonal integrity, white matter changes in the inferior colliculus (IC) and auditory thalamus (Mao et al. 2012a), have been shown post-blast at various time points, from 24 hours, 7 days up to 2-3 weeks. Most of these previous studies only assessed one or two time points post-blast. Given the likelihood of multiple phases of primary and secondary blast-induced damage and their corresponding anatomical and electrophysiological changes, understanding

the trajectory of post-blast recovery can help to identify critical time points and to direct therapies that are matched to the recovery mechanisms at those time points.

Clinical reports have suspected “hidden hearing loss” in blast-exposed veterans due to deficits in suprathreshold auditory processing with minimal changes in auditory thresholds (Gallun et al. 2012a; Saunders et al. 2015; Bressler et al. 2017). This occurs in age-related or noise-induced sensorineural hearing loss and encompasses putative changes resulting from hair cell or auditory nerve/synapse damage (Hickox and Liberman 2014; Plack et al. 2014; Bharadwaj et al. 2015; Kujawa and Liberman 2015; Viana et al. 2015; Liberman 2017). One consequence could be CAS adaptations in response to peripheral deafferentation (Caspary et al. 2005, 2008; Wang et al. 2009b), which has been speculated to impair temporal processing (Walton 2010; Parthasarathy and Bartlett 2011, 2012; Rabang et al. 2012). Blast studies on human subjects often used speech and complex temporally modulated stimuli to pin down “hidden” temporal processing losses that were not apparent with simple audiological measures (Gallun et al. 2012b; Saunders et al. 2015; Bressler et al. 2017; Kubli et al. 2018). However, blast studies in animals rarely go beyond simple auditory stimuli such as clicks, tones and AM modulation in a quiet background (Ewert et al. 2012; Race et al. 2017; Masri et al. 2018).

Using the same rat model as our previous publication (Race et al. 2017), our study documents a detailed time course of blast-induced hearing loss recovery in the subcortical CAS using auditory evoked potentials (AEPs). We specifically chose Iterated Rippled Noise (IRN) with pitch sweep alongside Amplitude Modulation (AM) stimuli in quiet and in modulated noise as temporally complex stimuli in assessing the processing of temporal attributes. IRN was used in neurophysiological and behavioral studies in both human (Krishnan et al. 2014, 2015; Peter et al. 2014; Thompson and Marozeau 2014; Wagner et al. 2017) and animal models (Bendor and Wang 2005; Alsindi et al. 2018), creating “pseudo-pitch” pitch contours with broadband carriers. IRN bypasses limitations posed by animal frequency range as well as permitting easily adjustable pitch intelligibility by altering the number of noise iterations and thus, the strength of temporal regularity and pitch salience (Patterson et al. 1996).

4.2 Materials and Methods

4.2.1 Subject

Male Sprague-Dawley rats (3-4 months) were assigned into Sham group and Blast group randomly. A total of 11 Sham animals and 13 blast animals were used in this study. All

animals were kept and raised in relatively quiet and standard laboratory animal housing conditions. All protocols were approved by the Purdue Animals Care and Use Committee (PACUC #1111000280).

4.2.2 Blast Exposure

Animals were anesthetized through intraperitoneal injection of a ketamine/xylazine cocktail (80 mg/kg and 10 mg/kg, respectively). The absence of eye-blink and paw-withdrawal reflexes was ensured prior to proceeding. Anesthetized animals were then placed on a platform beneath an open-ended shock tube to be exposed to the blast event, as described in our prior publications (Song et al. 2015; Walls et al. 2016; Race et al. 2017).

For the Blast group, each rat's head was positioned beneath the open end of the shock tube such that the dorsum of the skull was the incident surface exposed to a composite blast (shock wave + blast wind). A custom plexiglass housing was temporarily placed over the animal's torso for body protection to avoid cardiac or pulmonary effects of blast and to simulate the protective effects of military body armor (Rafaels et al. 2011). The head was fixed with a stereotaxic head frame with bite bar and ear bars (Kopf Instruments) to prevent blast wind-induced head acceleration. The blast exposure exhibited a recorded pressure profile with a rise to peak pressure within 0.3 msec, followed by overpressure and underpressure periods as follows: side-on (static) 150 kPa maximum overpressure, 1.25 msec overpressure duration, and 20 kPa minimum underpressure; face on (dynamic) 160 kPa maximum overpressure, 1.75 msec overpressure duration, and 5 kPa minimum underpressure. These conditions were the same as reported in our prior publications (Song et al. 2015; Walls et al. 2016; Race et al. 2017). All but one blast animal survived the exposure without displaying any external deficit during each animal's longitudinal follow-up period.

Sham animals were placed equidistant from the blast source, but out of the path of the shockwave, therefore only exposed to the blast noise. Tympanic membrane integrity was verified for all Blast and Sham animals after injury using a surgical microscope.

4.2.3 Auditory Evoked Potential Recordings

The animals underwent two-channel Auditory Evoked Potential (AEP) recordings at the following time points: pre-exposure (baseline), 1 day, 4 days, 7 days, 10 days, 14 days, 1 month, and 2 months. While the animals were under 1.8-2% isoflurane anesthesia, subdermal needle electrodes (Ambu) were inserted in the following locations (Fig. 4.1A): Channel 1

positive electrode was placed along the midline of the head (mid-sagittal) oriented Fz to Cz. Channel 2 positive electrode was positioned C3 to C4 along the interaural line. The negative/inverting electrode (used with positive electrodes for both channels 1 and 2) was placed under the mastoid of the right ear ipsilateral to the speaker. A ground electrode was placed in the back of the animal. These configurations were consistent with prior publications from our laboratory (Parthasarathy and Bartlett 2011, 2012; Parthasarathy et al. 2014; Lai and Bartlett 2015; Lai et al. 2017). Electrode impedances were confirmed to be less than 1 kΩ using a low impedance amplifier (RA4LI, TDT). After electrode placement, we subsequently sedated the animals by intramuscular injection of 0.2-0.3 mg/kg dexmedetomidine (Dexdomitor). AEP recordings were performed 10-15 min after removal from isoflurane to avoid anesthetic effects. The animals could respond to pain and acoustic stimuli but tend sit calmly under dexmedetomidine sedation, allowing about 3 hours of recording time.

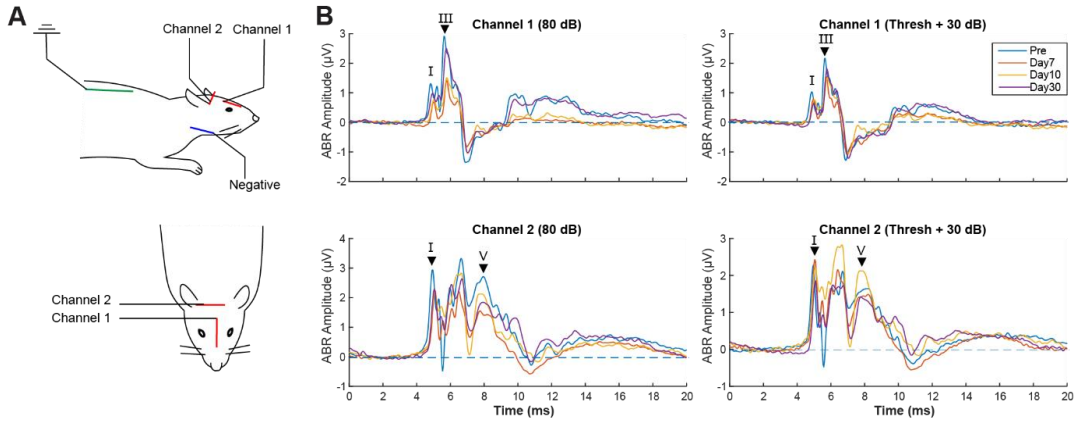

Figure 4.1. Auditory evoked potential experiment setup and examples of ABR waveforms. A) Electrode placement and channel configuration of the study's auditory evoked potential experiment. B) Examples of ABR waveforms at 80 dB SPL and 30 dB SL, with relevant wave peaks labeled. The waves for which amplitudes were measured are labeled with a black triangle.

Acoustic stimuli were presented free-field to the right ear (90^0 azimuth) of animals, with directly in front of the animals' face as the reference for 0^0 azimuth, using a calibrated speaker (Bowers and Wilkins) at a distance of 115 cm directly facing the right ear. The measurements used in this study included auditory brainstem responses (ABRs), middle-latency responses (MLRs), envelop-following responses (EFRs) using AM in noise stimuli, and IRNs.

ABR and MLR

6 Sham animals and 10 Blast animals were used in ABR analysis. For ABR, rectangular clicks (0.1 msec duration) and tone-pips (2 msec duration, 0.5 msec $\cos^2$ rise-fall time) with frequencies of 8 kHz and 16kHz were used. 8 kHz and 16 kHz were chosen based on previous findings: with 6-16 kHz being the most sensitive hearing region of rats, 8 kHz near the most sensitive region of normal rat audiogram (Parthasarathy et al. 2014) and hearing of frequencies higher than 8 kHz being most vulnerable to blast injury (Race et al. 2017). The sound levels of clicks and pips ranged from 90 to 10 dB peak SPL in 5-dB steps. All stimuli were presented in alternating polarity at 26.6 per second with 1500 repetitions (750 at each polarity). A 20 msec acquisition window (0-20 msec) was used.

Data were processed with a 30 Hz high-pass (HP) filter and a 3000 Hz low-pass (LP) filter prior to analysis. The ABR threshold was visually determined as the minimum sound level that produced a distinct ABR waveform, with confirmation from two other researchers. The ABR amplitudes of waves I and V from channel 2 were estimated as the differences of each wave's amplitude, as seen in BioSigRP (TDT) and the baseline amplitude (measured as an average of 2 msec waveform prior to the cochlear microphonic).

6 Sham animals and 8 Blast animals were used in MLR analysis. For MLR, similar rectangular clicks and 8 kHz tone pips of alternating polarity as in ABR were used but were presented at a slower rate (3.33/sec vs. 26.6/sec in ABRs) and with a recording window of longer duration (100 msec vs. 20 msec in ABRs). This time window provides enough time to capture the stimulus-evoked "middle-latency" neural responses from the auditory midbrain, thalamus and cortex (Barth and Shi Di 1991; McGee et al. 1991; Di and Barth 1992; McGee and Kraus 1996; Phillips et al. 2011; Šuta et al. 2011) alongside ABR. Stimuli were presented at 80 dB sound pressure level (SPL) and 30 dB sensation level (SL, 30 dB above corresponding ABR thresholds), as determined in the previous ABR recordings. 1500 repetitions were collected over an acquisition time window of 100 msec to obtain an average response. Only one animal exhibited hearing threshold higher than 80 dB SPL at only one time point, for which MLR recording has been excluded for that point.

Data were processed with HP (fc = 10 Hz) and LP (fc = 300 Hz) filters prior to analysis.

EFRs

EFRs were recorded during the same recording session following ABRs and MLRs using the same electrode configurations with similar techniques to Lai and Bartlett (2018) and

Lai (Lai et al. 2017). The two channels were sensitive to a complementary range of amplitude modulation frequencies (AMFs) (Parthasarathy and Bartlett 2012), with channel 1 (mid-sagittal) being more sensitive to higher AMFs (90-2048 Hz) while channel 2 (interaural) is more sensitive to lower AMFs (8-90 Hz). The AM stimuli used for EFRs were sinusoidally amplitude-modulated (AM) sounds, with Gaussian noise, 8 kHz tone, or 16 kHz tone as carriers, and under 100% and 50% modulation depth with a stimulus duration of 200 msec. The AMFs selected for this study are 10 Hz, 45 Hz, and 256 Hz, based on the findings in Race at al. (Race et al. 2017), which found significant differences, particularly at the lower AMFs. The acquisition window was 300 msec long, and each response was an average of 200 repetitions. The stimuli were presented at 30 dB SL. For animals that had a hearing threshold above 70 dB SPL, which usually happens on day 1 post-exposure, EFR was not collected at the time point due to the limitation of the speaker and BiosigRP.

For AM in Noise stimuli, the same EFRs were used alongside a 71 Hz sinusoidally AM masker of the same length and onset, with Gaussian noise as the carrier, similar to Lai and Bartlett (Lai and Bartlett 2018). Noise AM maskers were presented at sound levels of 20dB SNR and 0SNR to the sound level of target AM. Prior to EFR amplitude analysis, data were passed through an LP filter of 3000 Hz and a high-pass filter that was either slightly below the AMF for AMFs <90 Hz, or 80 Hz for AMFs $\geqslant$ 90 Hz.

IRNs

For 6 Sham animals and 8 Blast animals, IRNs were recorded during the same recording session following the previous stimuli using the same electrode configurations. The sound level of presentation was 30 dB SL (above click hearing threshold). Data for animals with a hearing threshold above 70 dB SPL were not collected at the time point.

IRN tone stimuli were created by sequential delay and add operations. Time-varying pitch curves were created by applying polynomial equations to create delays constructed from the fundamental frequencies of Chinese tone 2 and tone 4, delaying Gaussian noise (80 Hz-40 kHz) by the inversion of pitch and adding it back on itself in a recursive manner (Yost 1996a). The core MATLAB program used for generating IRN was modified from Krishnan et al. (Krishnan et al. 2014, 2015) This would generate dynamic, curvilinear pitch patterns (Swaminathan et al. 2008) that preserves variations in pitch using a broadband carrier. The number of iteration steps for these stimuli was 32, beyond which there is little or no change in pitch salience (Yost 1996b).

IRN iteration (ite) stimuli were created with the same polynomial equations used for tone 2, but with different iterations to create an array of IRN stimuli with different pitch salience. The numbers of iteration steps were 32, 16, 8, 4, and 2.

All IRN stimuli consisted of pairs of waveforms in original and inversed polarities to compensate for envelope or fine structure response under different calculations and cancel any microphonics. The stimulus duration was 250 msec, and the acquisition window was 300 msec long. Each response was an average of 200 repetitions.

4.2.4 Statistics

Statistics were performed with statistics software JASP (Version 0.11, JASP Team, 2019). All statistics for ABR and EFR utilized 2-way repeated measures ANOVA test (α = 0.05) to check the significance of each main effect and interaction, undergoing Greenhouse-Geisser sphericity corrections (Greenhouse and Geisser 1959) and Tukey Post Hoc corrections (Tukey 1949). For ABR statistics, Wave I (channel 2), III (channel 1) and V (channel 2) were measured at each time point (Fig. 4.1B), corresponding to the auditory nerve (Wave I), cochlear nucleus (Wave III), and rostral brainstem/IC sources (Wave V) (Parthasarathy and Bartlett 2012; Simpson and Prendergast 2013). For EFR statistics, responses were analyzed from channel 2 for 10 Hz and 45 Hz, and from channel 1 for 256 Hz (Parthasarathy and Bartlett 2012). Prior to statistical tests, EFR amplitudes at signal frequencies were acquired through Fast Fourier Transformation (FFT) in MATLAB (MathWorks) similar to (Lai and Bartlett 2018).

For MLR statistics, P1, N1, P2, and N2 (Fig. 5A) peaks were measured at each time point, corresponding to subcortical (P1), thalamocortical (N1) and cortical sources (P2, N2) (Simpson and Prendergast 2013). Peak amplitudes were normalized to the pre-blast exposure baseline measurements for display in Fig. 5C, D. The peak amplitudes at each time point were compared to the pre-stimulus baseline using a paired sign-rank test, with a 0.05 significance criterion.

For IRN statistics, we performed moving-window autocorrelations in 25 msec moving windows (5 msec steps) on each response waveform to simulate physiological tracking of temporal periodicity. Peak autocorrelation frequency was defined by the inverse of the time lag where peak autocorrelation value occurs in each window. This process yielded a total of 51 peak frequencies that reflect the frequency representation of the IRN auditory response. Of those, 45 occurred during the stimulus. The peak frequencies were then compared to the

"pseudopitches" of the IRN stimuli on corresponding time points. A value within 5 Hz of absolute difference to corresponding "pseudopitch" was considered "tracked." We used this number of "tracked" peak frequencies, or "pitch-tracking score," as a quantification for IRN performance. The significance of each main effect (time, blast condition, and IRN iterations) and interaction was assessed using similar 2-way repeated measures ANOVA test as ABR statistics ($\alpha = 0.05$). For response-to-response correlation (Fig. 8D), the cross-correlation was measured between the response to the IRN stimuli pre-exposure and the response to the same stimulus post-exposure. Blast versus sham group was tested using the paired sign-rank test for this measure ($\alpha = 0.05$).

4.3 Results

4.3.1 ABR and MLR

ABR Thresholds

Click ABR recordings captured distinctive courses of threshold changes over the two months post-exposure for blast and sham animals (Fig. 4.2). A large, >30dB SPL maximum threshold increase was observed in post-blast-exposure animals (Fig. 4.2, red lines). Adjacent animals exposed only to blast noise (Sham) did not undergo significant threshold shifts (Fig. 4.2, blue lines). Thresholds for blast group animals showed clear recovery during the first two weeks, with the largest changes occurring between 4 days – 10 days. Thresholds for blast-exposed animals remained significantly elevated (worse) than those of sham animals throughout the two months post-exposure that were measured ($F=12.727$, $p=0.003$). Significant main effects of both Group ($F=61.943$, $p=<0.001$, $\eta^2_p=0.816$) and Time Point ($F=41.932$, $p<0.001$, $\eta^2_p=0.750$), as well as a significant Group*Time Point interaction effect ($F=23.503$, $p<0.001$, $\eta^2_p=0.627$), were observed.

Similar trends were observed with tone ABR recordings of 8 kHz and 16 kHz (Fig. 4.2), with a significant ($p\leq0.001$) >30 dB increase in threshold within 48 hours post-blast-exposure and most prominent recovery between 4 days – 10 days. 8 kHz threshold differences between blast conditions became non-significant ($F=3.151$, $p=0.098$) at 10 days post-blast. At two weeks post-exposure, 16 kHz thresholds remained significantly elevated ($F=16.527$, $p<0.001$), after which point the thresholds for the two chosen tone frequencies were no longer significantly different between Blast and Sham. Our rmANOVA analysis using Group and

Time Points as factors showed significant main effects of Group (8 kHz: F=10.847, p=0.005, η^2p=0.437; 16 kHz: F=19.697, p<0.001, η^2p=0.585), Time (8 kHz: F=25.837, p<0.001, η^2p=0.649; 16 kHz: F=20.181, p<0.001, η^2p=0.590) and Group*Time Point interaction (8 kHz: F=13.490, p<0.001, η^2p=0.491; 16 kHz: F=15.860, p<0.001, η^2p=0.531) for 8 kHz and 16 kHz threshold respectively. These results demonstrate that broadband click thresholds remain significantly elevated over the 60 days measurement window. 8 kHz thresholds largely returned to baseline (Day 30: 8 dB difference, p=0.118; day 60: 4 dB difference, p=0.965) after two weeks, and 16 kHz thresholds remained significantly elevated compared to pre-blast baseline according to post hoc analysis (Day 30: 15.5 dB difference, p<0.001; day 60: 14.5 dB difference, p<0.001), although the difference between blast and Sham was not significant at these time points.

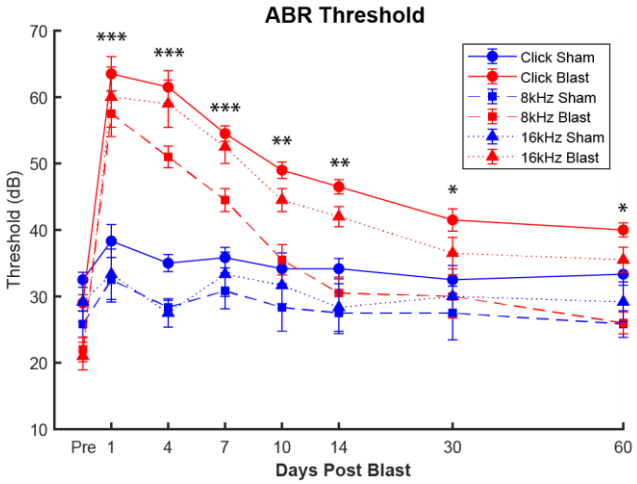

Figure 4.2. ABR threshold changes of Blast (N=10) and Sham (N=6) rats during the first two months post-exposure. Blast animals demonstrated drastic increases (worse) of Click, 8 kHz, and 16 kHz thresholds (red lines) post-exposure as opposed to Sham animals (blue lines). Significant main effects (p≤0.001) of Groups and Group*Time interactions were observed in all carriers. Significant Simple Main Effect of single time points observed in various carriers throughout the two months.

***Blast threshold significantly higher than Sham in Click, 8kHz, and 16kHz, p<0.05;
**Blast threshold significantly higher only in Click and 16 kHz;
*Blast threshold significantly higher only in Click.

ABR Thresholds

For our ABR and MLR measurements, we used two sound levels: 80 dB SPL was chosen because it is commonly used in auditory evoked potential studies in rat and human studies (Simpson et al. 1985; Alvarado et al. 2012; Race et al. 2017), and it elicits clear ABR responses in all except the most extreme cases of blast-exposure. In order to compensate for changes in threshold induced by blast exposure, we also measured ABR amplitudes at 30 dB

SL above threshold (sensation level, or SL). This enabled us to separate changes in ABR amplitudes due to audibility (threshold) versus those due to threshold-independent changes in subcortical auditory signaling. Note that we did not attempt to compare later ABR waves with equivalent wave I amplitudes, as in Lai et al. (2017).

ABR wave amplitudes were assessed for wave I (putative auditory nerve), III (putative cochlear nuclei), and V (putative rostral brainstem and inferior colliculus) in response to click stimuli at 80 dB SPL (Fig. 4.3) and 30 dB SL (Fig. 4.4). Repeated measures statistics for 80 dB SPL and 30dB SL are shown in Tables 4.1-4.4.

Wave I: Wave I amplitudes at 80 dB SPL for all ABR carriers at 80 dB SPL exhibited significant main effects of Group, Time, and Group*Time interaction (Table 4.1). Compared to pre-exposure responses, wave I amplitudes were significantly smaller at all time points tested in blast animals for clicks, 8 kHz tones, and 16 kHz tones, indicating lasting cochlear/auditory nerve damage (Table 4.4). No significant changes in wave I amplitudes were observed in Sham exposed animals at any time point.

Wave III: Wave III amplitudes at 80 dB SPL for all ABR carriers at 80 dB SPL exhibited significant main effects of Group, Time, and Group*Time interaction (Table 4.1), with Group effects lasting for 14 days for Click and 16 kHz tones and 10 days for 8 kHz tones. Compared to pre-exposure responses, wave III amplitudes were significantly smaller at all time points tested in blast animals for clicks and 16 kHz tones and up to 30 days for 8 kHz tones, indicating lasting declines in cochlear nucleus excitation (Table 4.4). No significant changes in wave III amplitudes were observed in Sham exposed animals at any time point.

Wave V: Wave V amplitudes at 80 dB SPL for all ABR carriers at 80 dB SPL exhibited significant main effects of Group, Time, and Group*Time interaction (Table 4.1), with Group effects lasting for 14 days for Click and 16 kHz tones and 7 days for 8 kHz tones. Compared to pre-exposure responses, wave V amplitudes were significantly smaller at all time points tested in blast animals for clicks, indicating lasting declines in rostral brainstem/IC excitation for brief, broadband clicks (Table 4.4). However, decreases in wave V amplitudes persisted for only 7 days for 8 kHz tones and 14 days for 16 kHz tones, suggesting that despite decreases in cochlear nucleus excitation (as represented by wave III amplitude), rostral brainstem/IC responses compensated and restored their responses. No significant changes in wave V amplitudes were observed in Sham exposed animals at any time point except for a small decline for 16 kHz responses 60 days post Sham exposure (Table 4.4).

The effects on ABR waves were greatly diminished when responses to 30 dB SL sounds were measured, as shown in Table 4.2 and Table 4.3. For Wave I, significant main effects of

Time (Click: F=2.554, p=0.043, η^2_p=0.154; 8 kHz: F=3.146, p=0.018, η^2_p=0.183; 16kHz: F=2.325, p=0.031, η^2_p=0.142) but not Group (Click: F=3.637, p=0.077, η^2_p=0.206; 8 kHz: F<0.001, p=0.994, η^2_p<0.001; 16kHz: F=1.046, p=0.324, η^2_p=0.070) were observed for click, 8 kHz, and 16 kHz. Additionally, significant Group*Time interaction effects were only observed for Click (F=2.630, p=0.039, η^2_p=0.158) and 16 kHz (F=2.381, p=0.027, η^2_p=0.145). Simple main effects of Group were only observed in Click (Table 4.3).

Compared to pre-exposure responses, wave I and V responses to clicks were significantly reduced 1 day post-blast and wave III responses were significantly reduced days 1-4. Otherwise, there were no significant declines in wave amplitudes in the Blast group, and there were no significant amplitude changes in the Sham group.

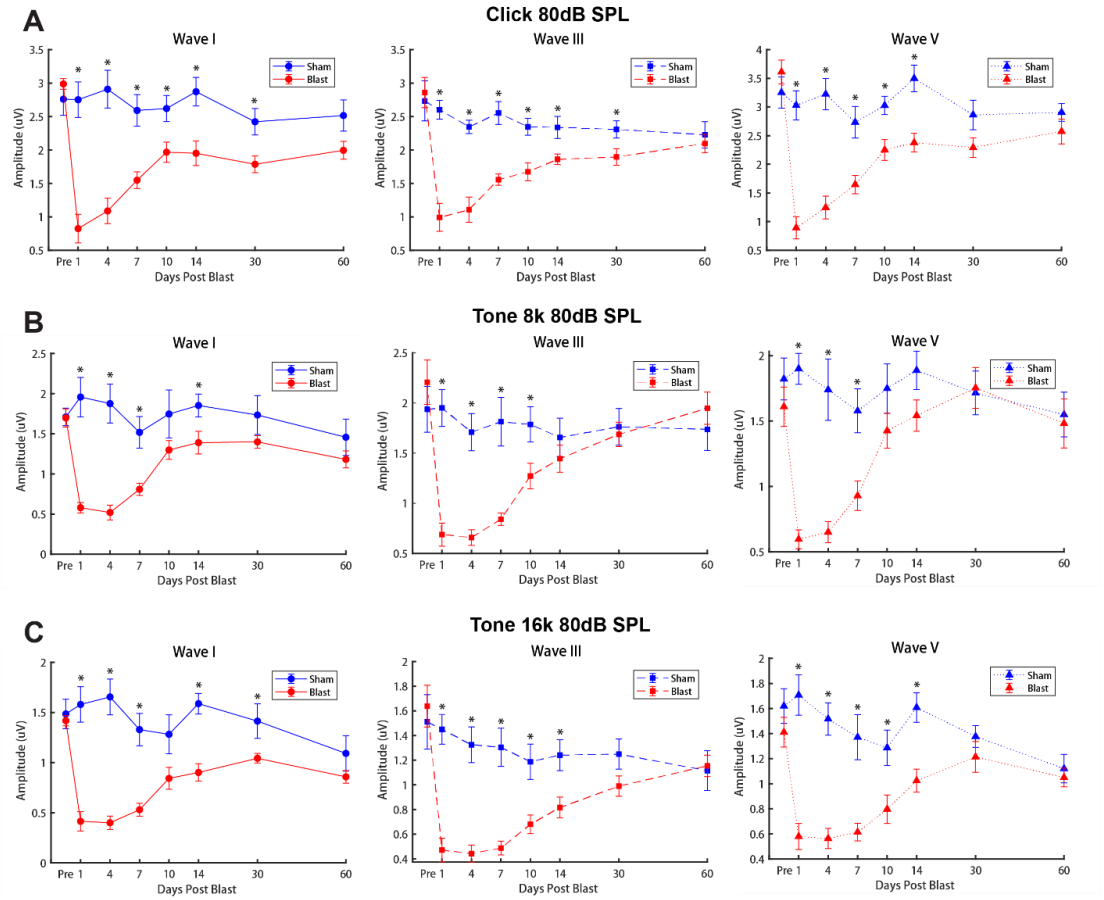

Figure 4.3. ABR wave I, III, and V amplitudes of Blast (N=10) and Sham (N=6) rats during the first two months post-exposure expose persistent blast-induced differences at 80 dB SPL. Significant main Group*Time interaction effects ($p \leq 0.001$) observed in waves I (left column), III (center column), and V (right column) for all carriers: A) Click ABR; B) 8 kHz ABR; C) 16 kHz ABR. Click ABR revealed blast-induced reduction of ABR wave amplitudes to a greater degree than both tone ABRs. Later waves (Wave III and V) showed earlier recovery in Blast animals.

*Significant Simple Main Effect of Group in ABR Wave Amplitudes, $p<0.05$.

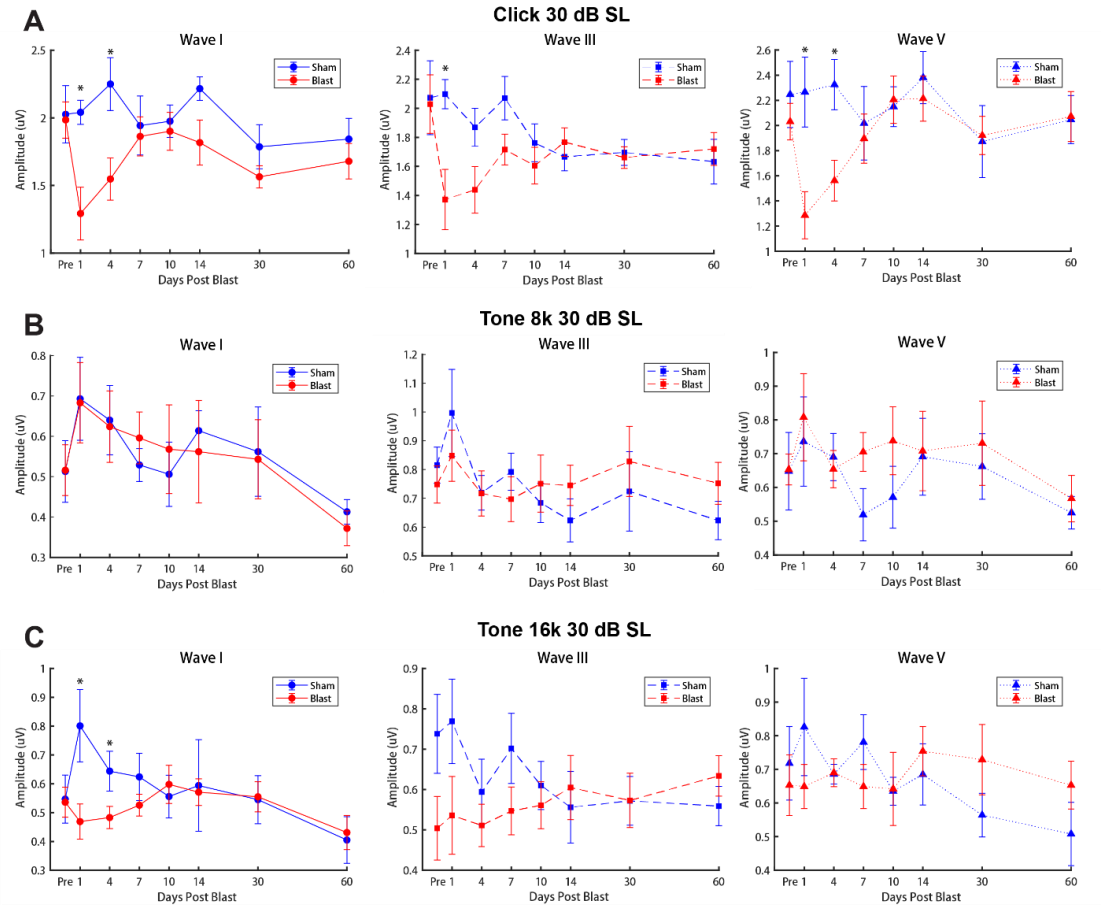

Figure 4.4. ABR wave I, III, and V amplitudes of Blast (N=10) and Sham (N=6) rats during the first two months post-exposure at 30 dB SL. Similar format to Fig. 3. Significant main Group*Time interaction effects only observed with Click ABR waves (Wave I: p=0.016; Wave III: p=0.04; Wave V: p=0.003) A) Click ABR; B) 8 kHz ABR; C) 16 kHz ABR.

*Significant Simple Main Effect of Group in ABR Wave Amplitudes, p<0.05.

Table 4.1. Summary of 80 dB SPL ABR Wave I, III and V repeated measure ABR statistics.

80dB ABR			**F**	**p**	**η^2_p**
Click	Wave I	Time	9.980	< **.001**	0.416
		Group	23.080	< **.001**	0.622
		Time * Group	11.685	< **.001**	0.455
	Wave III	Time	11.065	< **.001**	0.441
		Group	17.207	< **.001**	0.551
		Time * Group	8.871	< **.001**	0.388
	Wave V	Time	14.134	< **.001**	0.502
		Group	23.203	< **.001**	0.624
		Time * Group	10.990	< **.001**	0.440
8 kHz	Wave I	Time	8.102	< **.001**	0.367
		Group	14.409	**0.002**	0.507
		Time * Group	11.760	< **.001**	0.457
	Wave III	Time	14.084	< **.001**	0.501
		Group	6.266	**0.025**	0.309
		Time * Group	13.826	< **.001**	0.497
	Wave V	Time	8.545	< **.001**	0.379
		Group	9.859	**0.007**	0.413
		Time * Group	9.346	< **.001**	0.400
16 kHz	Wave I	Time	9.845	< **.001**	0.413
		Group	27.486	< **.001**	0.663
		Time * Group	14.328	< **.001**	0.506
	Wave III	Time	9.845	< **.001**	0.413
		Group	13.048	**0.003**	0.482
		Time * Group	14.328	< **.001**	0.506
	Wave V	Time	8.838	< **.001**	0.387
		Group	20.528	< **.001**	0.595
		Time * Group	10.066	< **.001**	0.418

Table 4.2. Summary of 30 dB SL ABR Wave I, III and V repeated measure ABR statistics.

30dB SL ABR			**F**	**p**	**η^2_p**
Click	Wave I	Time	2.554	**0.019**	0.154
		Group	3.637	0.077	0.206
		Time * Group	2.630	**0.016**	0.158
	Wave III	Time	2.544	0.052	0.154
		Group	1.811	0.200	0.115
		Time * Group	2.720	0.040	0.163
	Wave V	Time	2.568	**0.018**	0.155
		Group	1.479	0.244	0.096
		Time * Group	3.429	**0.003**	0.197
8 kHz	Wave I	Time	3.146	**0.018**	0.183
		Group	6.852e -5	0.994	0.000
		Time * Group	0.200	0.945	0.014
	Wave III	Time	2.432	0.069	0.148
		Group	0.020	0.889	0.001
		Time * Group	1.184	0.328	0.078
	Wave V	Time	1.837	0.136	0.116
		Group	0.361	0.558	0.025
		Time * Group	0.618	0.648	0.042
16 kHz	Wave I	Time	2.325	**0.031**	0.142
		Group	1.046	0.324	0.070
		Time * Group	2.381	**0.027**	0.145
	Wave III	Time	0.562	0.651	0.039
		Group	1.149	0.302	0.076
		Time * Group	1.930	0.136	0.121
	Wave V	Time	1.160	0.338	0.077
		Group	4.905e -4	0.983	0.000
		Time * Group	1.646	0.161	0.105

Table 4.3. Summary of 30 dB SL ABR Wave I, III and V repeated measure ABR statistics.

Simple Main Effects			**80 dB SPL**			**30dB SL**		
		Time	Mean square	F	p	Mean Square	F	p
Click	Wave I	day1	13.942	31.329	**< .001**	2.097	8.019	**0.013**
		day4	12.438	30.917	**< .001**	1.843	7.730	**0.015**
		day7	4.081	18.418	**< .001**	0.024	0.102	0.754
		day10	1.601	7.023	**0.019**	0.020	0.127	0.726
		day14	3.180	10.008	**0.007**	0.596	3.044	0.103
		day30	1.517	8.285	**0.012**	0.184	1.829	0.198
		day60	1.013	4.393	0.055	0.102	0.632	0.440
	Wave III	day1	9.708	30.148	**< .001**	1.977	6.629	**0.022**
		day4	5.754	23.070	**< .001**	0.692	3.416	0.086
		day7	3.725	33.967	**< .001**	0.470	3.917	0.068
		day10	1.690	11.712	**0.004**	0.093	0.665	0.429
		day14	0.854	8.587	**0.011**	0.039	0.474	0.502
		day30	0.634	4.714	**0.048**	0.005	0.088	0.771
		day60	0.064	0.315	0.584	0.029	0.219	0.647
	Wave V	day1	17.134	45.066	**< .001**	3.596	9.213	**0.009**
		day4	14.672	35.376	**< .001**	2.178	8.580	**0.011**
		day7	4.419	13.382	**0.003**	0.056	0.132	0.722
		day10	2.264	8.415	**0.012**	0.012	0.043	0.839
		day14	4.709	16.223	**0.001**	0.104	0.347	0.565
		day30	1.214	3.651	0.077	0.009	0.028	0.870
		day60	0.414	1.155	0.301	0.002	0.007	0.934
8 kHz	Wave I	day1	7.136	45.959	**< .001**	0.000	0.004	0.948
		day4	6.915	37.954	**< .001**	0.001	0.014	0.909
		day7	1.892	15.704	**0.001**	0.017	0.551	0.470
		day10	0.754	2.693	0.123	0.014	0.159	0.696
		day14	0.803	4.657	**0.049**	0.010	0.096	0.762
		day30	0.421	2.532	0.134	0.001	0.015	0.904
		day60	0.285	1.562	0.232	0.006	0.450	0.513
	Wave III	day1	5.977	37.898	**< .001**	0.084	0.838	0.375
		day4	4.139	36.832	**< .001**	0.000	0.000	0.984
		day7	3.544	23.802	**< .001**	0.034	0.703	0.416
		day10	0.990	5.847	**0.030**	0.017	0.232	0.637
		day14	0.167	0.851	0.372	0.055	1.274	0.278
		day30	0.022	0.131	0.722	0.041	0.301	0.592
		day60	0.167	0.640	0.437	0.062	1.420	0.253
	Wave V	day1	6.374	100.269	**< .001**	0.020	0.135	0.719
		day4	4.459	28.229	**< .001**	0.005	0.165	0.691
		day7	1.580	11.078	**0.005**	0.129	3.798	0.072
		day10	0.392	2.043	0.175	0.104	1.256	0.281
		day14	0.449	3.269	0.092	0.001	0.010	0.924
		day30	0.006	0.026	0.875	0.018	0.149	0.705

Table 4.3 continued

		day60	**0.017**	**0.060**	**0.811**	**0.007**	**0.187**	**0.672**
16 kHz	Wave I	day1	5.090	40.130	**< .001**	0.205	2.470	0.138
		day4	5.910	61.374	**< .001**	0.026	0.827	0.378
		day7	2.397	29.278	**< .001**	0.090	2.321	0.150
		day10	0.723	4.602	0.050	0.009	0.305	0.590
		day14	1.766	24.888	**< .001**	0.009	0.153	0.701
		day30	0.515	6.551	**0.023**	0.000	0.000	0.992
		day60	0.205	2.242	0.156	0.022	1.009	0.332
	Wave III	day1	3.592	39.592	**< .001**	0.205	2.470	0.138
		day4	2.919	38.728	**< .001**	0.026	0.827	0.378
		day7	2.507	35.072	**< .001**	0.090	2.321	0.150
		day10	0.965	11.997	**0.004**	0.009	0.305	0.590
		day14	0.676	8.374	**0.012**	0.009	0.153	0.701
		day30	0.253	3.337	0.089	0.000	0.000	0.992
		day60	0.006	0.056	0.816	0.022	1.009	0.332
	Wave V	day1	4.772	37.802	**< .001**	0.118	1.617	0.224
		day4	3.414	44.163	**< .001**	0.000	0.005	0.945
		day7	2.150	21.095	**< .001**	0.066	1.575	0.230
		day10	0.902	7.214	**0.018**	0.000	0.002	0.961
		day14	1.283	15.210	**0.002**	0.017	0.336	0.571
		day30	0.100	0.888	0.362	0.103	1.301	0.273
		day60	0.019	0.293	0.597	0.079	1.541	0.235

Post-blast ABR amplitudes of Blast (N=10) and Sham (N=6) groups are compared using rmANOVA at each time point recorded. A $p<0.05$ showed significant simple main effect of Group at that time point.

Table 4.4. Summary of 30 dB SL ABR Wave I, III and V repeated measure ABR statistics. Post-blast ABR amplitudes of Blast (N=10) and Sham (N=6) were compared against pre-blast amplitudes of the same group to show blast impact and recovery.

			80dB SPL							**30dB SL**						
			day1	**day4**	**day7**	**day10**	**day14**	**day30**	**day60**	**day1**	**day4**	**day7**	**day10**	**day14**	**day30**	**day60**
Click	I	Blast	**<0.001**	**<0.001**	**<0.001**	**<0.001**	**<0.001**	**<0.001**	**<0.001**	**0.001**	0.244	1.000	1.000	1.000	0.300	0.808
		Sham	1.000	1.000	1.000	1.000	1.000	0.984	0.999	1.000	1.000	1.000	1.000	1.000	0.997	1.000
	III	Blast	**<0.001**	**<0.001**	**<0.001**	**<0.001**	**<0.001**	**<0.001**	**0.002**	**0.003**	**0.015**	0.780	0.285	0.934	0.528	0.797
		Sham	1.000	0.916	1.000	0.915	0.902	0.838	0.600	1.000	1.000	1.000	0.966	0.767	0.854	0.652
	V	Blast	**<0.001**	**<0.001**	**<0.001**	**<0.001**	**<0.001**	**<0.001**	**<0.001**	**0.009**	0.440	1.000	1.000	1.000	1.000	1.000
		Sham	1.000	1.000	1.000	1.000	1.000	0.990	0.997	1.000	1.000	1.000	1.000	1.000	0.967	1.000
8 kHz	I	Blast	**<0.001**	**<0.001**	**<0.001**	**0.129**	**0.525**	**0.575**	**0.008**	0.840	0.996	1.000	1.000	1.000	1.000	0.943
		Sham	0.978	1.000	0.998	1.000	1.000	1.000	0.972	0.957	0.999	1.000	1.000	1.000	1.000	1.000
	III	Blast	**<0.001**	**<0.001**	**<0.001**	**<0.001**	**<0.001**	**<0.023**	0.878	0.998	1.000	1.000	1.000	1.000	1.000	1.000
		Sham	1.000	0.996	1.000	1.000	0.968	1.000	0.999	0.995	1.000	1.000	0.998	0.932	1.000	0.932
	V	Blast	**<0.001**	**<0.001**	**<0.001**	0.993	0.994	1.000	1.000	0.902	1.000	1.000	1.000	1.000	1.000	1.000
		Sham	1.000	1.000	0.991	1.000	1.000	1.000	0.974	1.000	1.000	0.998	1.000	1.000	1.000	0.999
16 kHz	I	Blast	**<0.001**	**<0.001**	**<0.001**	**<0.001**	0.050	**0.020**	**<0.001**	1.000	1.000	1.000	1.000	1.000	1.000	0.999
		Sham	1.000	0.993	0.997	0.965	1.000	1.000	0.149	0.296	0.999	1.000	1.000	1.000	1.000	0.973
	III	Blast	**<0.001**	**<0.001**	**<0.001**	**<0.001**	**<0.001**	**<0.001**	**<0.001**	1.000	1.000	1.000	1.000	0.993	1.000	0.930
		Sham	1.000	0.990	0.973	0.534	0.805	0.838	0.203	1.000	0.982	1.000	0.994	0.880	0.938	0.890
	V	Blast	**<0.001**	**<0.001**	**<0.001**	**<0.001**	**0.031**	0.879	0.063	1.000	1.000	1.000	1.000	0.998	1.000	1.000
		Sham	1.000	1.000	0.899	0.520	1.000	0.915	**0.031**	1.000	1.000	1.000	1.000	1.000	0.986	0.843

4.3.2 MLR

In order to observe thalamocortical and cortical neural transmission in response to acoustic transients, we recorded middle-latency auditory responses to click and 8 kHz tone stimuli. These stimuli were identical to those used for ABR, but the presentation rate was much slower, and the analysis window and filters were different (see Methods). Measurements were made for the first four main peaks of the MLR. Here, P1 corresponds to subcortical activity, largely encompassing the ABR. N1 corresponds to thalamocortical transmission, while P2 and N2 are thought to correspond to primarily cortical activity (Deiber et al. 1988; Liégeois-Chauvel et al. 1994; Tichko and Skoe 2017; Musiek and Nagle 2018).

80 dB SPL responses

In blast animals, all waves were decreased relative to pre-blast baseline for days 1-7 post-blast ($p<0.05$, sign-rank test) in response to 80 dB SPL click stimuli. Grand average traces are shown for MLR responses in this time window in Fig. 4.5A, relative to the pre-blast waveform (thick blue line in Fig. 4.5A-D). Even after the blast, the morphology and timing of the MLR waveform remained relatively intact, but the amplitudes were significantly diminished. In Fig. 4.5E-H, wave amplitudes were normalized to the pre-blast waves and measured. Between 7 and 10 days, the early P1 wave recovers to within 10-15% of its baseline amplitude, whereas the later waves recovered more slowly (Fig. 4.5E). In particular, the N1 wave, thought to reflect thalamocortical transmission (Barth and Shi Di 1991; McGee et al. 1991, 1992; Di and Barth 1992; Brett et al. 1996; McGee and Kraus 1996; Phillips et al. 2011; Šuta et al. 2011), remained significantly lower in blast animals even 60 days post-blast ($p<0.05$, sign-rank test, Fig. 4.5E). By contrast, the MLR waves in sham animals were largely stable across the measurement time (Fig. 4.5F). Although there was some decline in the later waves for the last time window, this was not statistically significant (Fig. 4.5B, D, F).

MLR responses to 8 kHz, 80 dB SPL tone pips largely mirrored the results to clicks, with significant decreases for all waves for post-blast days 1-7 and a lasting decline in N1 for the duration of measurements ($p<0.05$, sign-rank test, traces not shown). Sham responses did not show any significant changes in MLR waves in response to the 80 dB SPL tone pips.

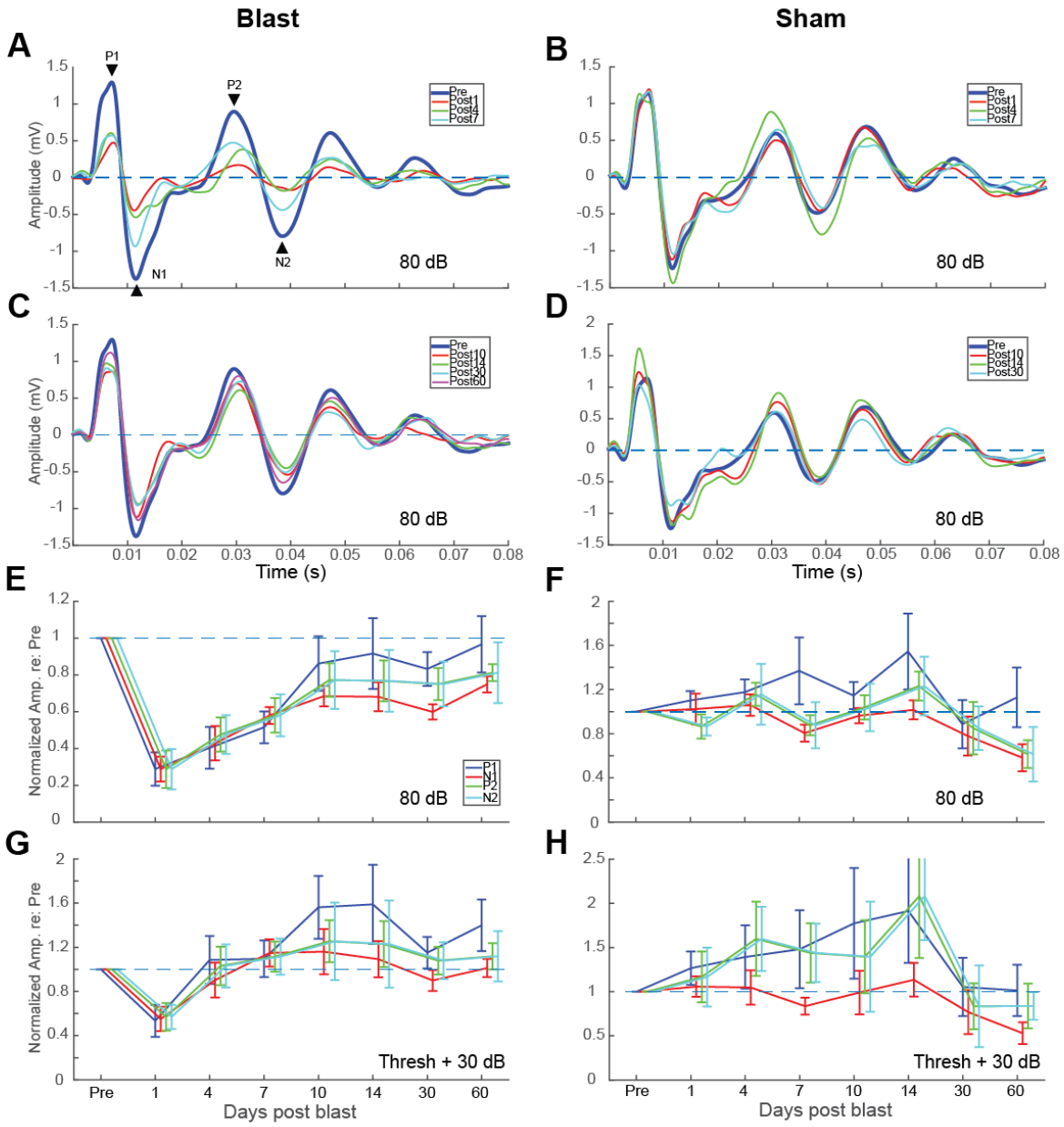

Figure 4.5. MLR waveforms and peak amplitudes of Blast (N=8) and Sham (N=6) rats during the first two months post-exposure at 80 dB SPL and at 30 dB SL (Thresh + 30 dB). Grand average traces of Click MLR waveforms at 80 dB SPL: A) Blast, pre-blast to day 7. Arrowheads indicate measured peaks in E-H; B) Sham, pre-blast to day 7; C) Blast, day 10 to day 60; D) Sham, day 10 to day 60. Normalized Click MLR wave amplitudes over time: E) Blast, 80 dB SPL; F) Sham, 80 dB SPL; G) Blast, 30 dB SL; H) Blast, 30 dB SL.

30 dB SL

MLR responses to clicks at 30 dB SL were reduced in Blast animals 1 day after the blast but recovered to baseline levels afterwards. There was a tendency towards elevated P1 amplitudes, but this was not significant (Fig. 5G). Sham animals did not show any significant changes, though there was a tendency towards an increase in wave amplitude (Fig. 5H). Similar results were found for responses to tones at 30 dB SL (not shown).

4.3.3 EFR and EFR in noise

Given the different time courses and extents of ABR threshold change for clicks and tones, we measured the corresponding EFRs in response to Gaussian broadband noise (NAM), 8 kHz, and 16 kHz sinusoidal tone carriers. Considering that slow AM (<50 Hz) and faster AM (>50 Hz) are differentially represented throughout cortical and subcortical auditory nuclei (Joris et al. 2004; Wang et al. 2008), three representative AMFs (10, 45, and 256 Hz) were selected from previous publications (Parthasarathy et al. 2010, 2014; Parthasarathy and Bartlett 2011, 2012; Race et al. 2017) and tested in quiet at 100% and 50% modulation depth (Fig. 4.6A). AM stimuli were also presented at 30 dB SL with a 71 Hz sinusoidally AM masker of the same length and onset, with Gaussian noise as the carrier, at 20dB SNR and 0 SNR relative to the sound level of target AM (Fig. 4.7A). For each carrier, simple main effects of all conditions were analyzed.

EFRs in quiet: For all three carriers in quiet, EFR amplitudes were similar at 10 and 256 Hz across time points and AM modulation depths (Fig. 4.6). Overall, the NAM FFT amplitudes were reduced in the Blast group in quiet ($F=9.629$, $p=0.0018$, $\eta^2_p=0.426$), with 45 Hz being the most affected. Interestingly, in contrast to the lower FFT Amplitude found in Blast AM at 80 dB SPL (Race et al. 2017), when the hearing threshold has been compensated, FFT amplitude of 45 Hz NAM was higher in Blast than in Sham animals. This difference was most salient on day 7 for 45 Hz NAM ($p=0.006$). For 8 kHz SAM and 16 kHz SAM, the slight elevation of AM FFT Amplitude in Blast animals was not significant. Surprisingly, time did not have a significant interaction across repeated measures for AM response with any carrier either.

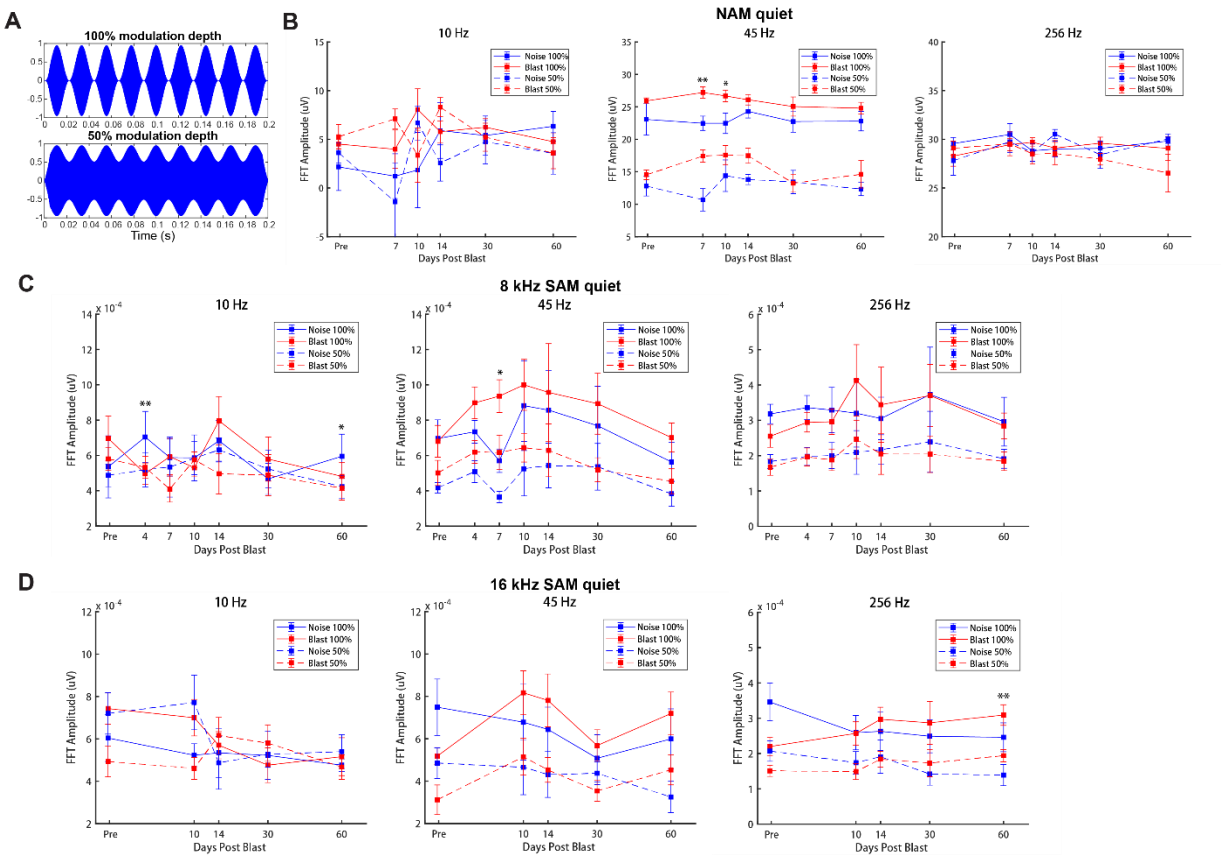

Figure 4.6. AM depth stimuli and EFR responses from Blast (N=10) and Sham (N=6) rats during the first two months post-exposure at 30 dB above threshold, in quiet. A) AM depth stimulus waveforms at 100% and 50% modulation depths; B) NAM FFT amplitudes at 10 Hz (left), 45 Hz (center), and 256 Hz (right). Significant Group effect at 45Hz (p=0.007); Similar format in C and D. C) SAM 8 kHz FFT amplitudes at 45 Hz show a steady yet insignificant increase in later short-term (day 7-14); D) SAM 16k FFT amplitudes found no significant Group effect.

**Significant Simple Main Effect of Group in FFT Amplitudes in both 100% depth and 50% depth
* Significant Simple Main Effect of Group in FFT Amplitudes only in 100% depth

EFR in noise: Not surprisingly, Noise level and Modulation Depth both had a significant repeated measures effect on NAM (Noise level: $F=263.217$, $p<0.001$, $\eta^2_p=0.953$; Depth: $F=455.655$, $p<0.001$, $\eta^2_p=0.972$), 8 kHz SAM (Noise level: $F=19.308$, $p<0.001$, $\eta^2_p=0.580$; Depth: $F=72.031$, $p<0.001$, $\eta^2_p=0.837$) and 16 kHz SAM (Noise level: $F=16.691$, $p<0.001$, $\eta^2_p=0.544$; Depth: $F=49.742$, $p<0.001$, $\eta^2_p=0.780$). Noise level and Depth also have a significant interaction effect with Blast Groups for NAM overall (Noise level: $F=10.295$, $p<0.001$, $\eta^2_p=0.442$; Depth: $F=6.057$, $p=0.029$, $\eta^2_p=0.318$), showing blast NAM responses as less affected 20 SNR noise, but more sensitive amplitude declines for lower modulation depth (Fig. 4.7B). Noise level also affects

8 kHz SAM differently between Groups ($F=5.696$, $p=0.008$, $\eta^2_p=0.289$). These conditions do not have significant interaction effects with Blast Group on 16 kHz SAM. Noise level had significant interaction effects with both Blast Group ($F=6.130$, $p=0.011$, $\eta^2_p=0.320$) and Depth ($F=19.438$, $p<0.001$, $\eta^2_p=0.599$) for NAM 45 Hz, while the effect of Time or Depth between Groups was not significantly different for any modulation frequency.

For 8 kHz SAM, the effects of Noise level were applied differently between Blast Groups, as significant interaction effects were observed between Noise and Group for 10 Hz ($F=12.795$, $p=0.001$, $\eta^2_p=0.477$) and 45 Hz ($F=4.878$, $p=0.015$, $\eta^2_p=0.258$) modulation frequencies, though not for 256 Hz. Modulation Depth affects FFT amplitude without regard to blast condition, with no significant interaction effects with Group observed. For 16 kHz SAM, none of the parameters tested had significantly different effects between Groups at 30 dB SL (not shown).

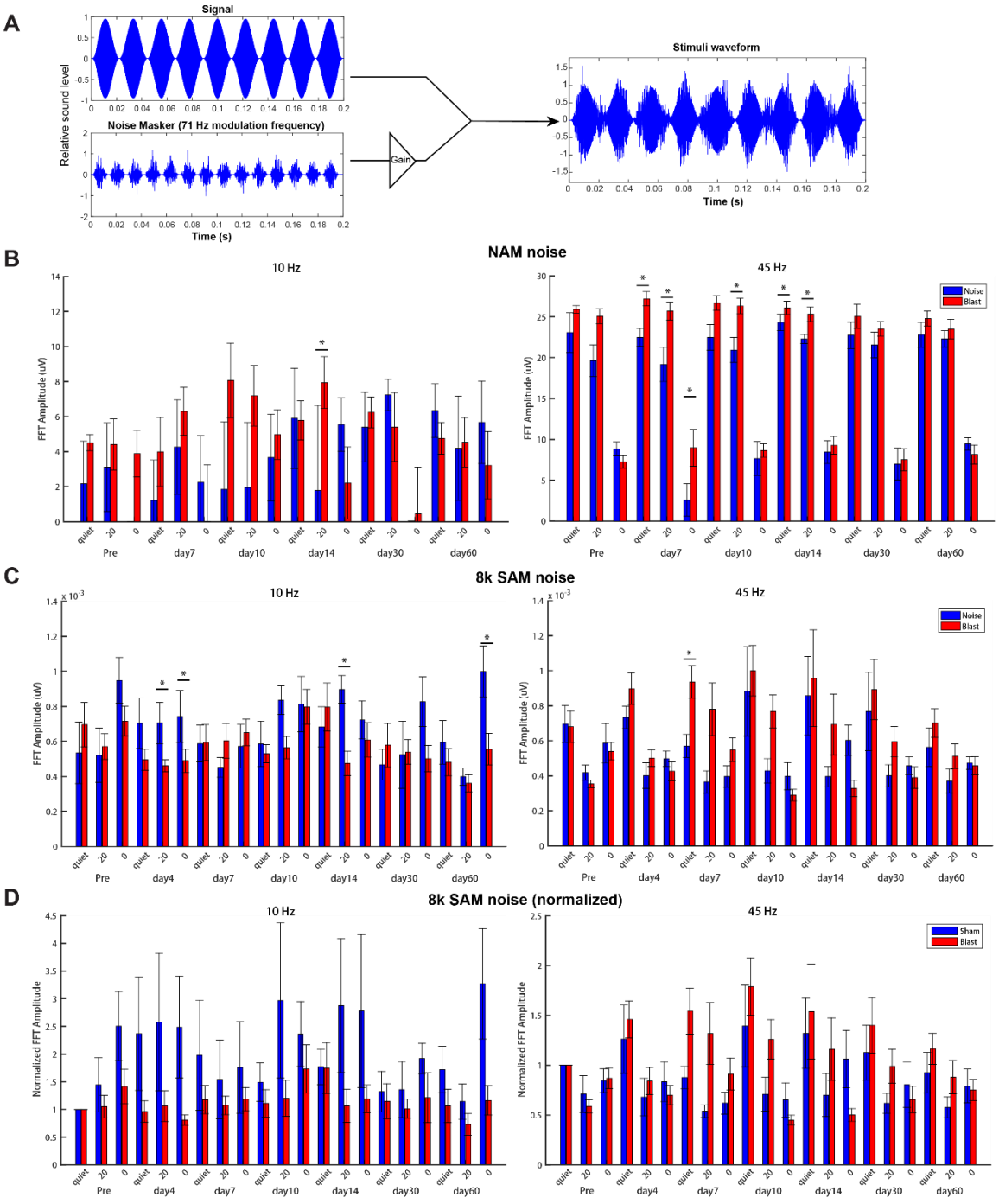

Figure 4.7. AM noise stimuli and EFR responses from Blast (N=10) and Sham (N=6) rats during the first two months post-exposure at 30 dB above threshold. A) AM noise stimulus composition and waveform. B) Amplitude modulated noise carrier. FFT amplitudes at signal modulation frequency in quiet and with 71 Hz AM noise masker level of 20SNR or 0SNR (equal) show significant Noise * Group effect for: B) NAM noise at 45 Hz (p=0.011) modulation frequency; C) SAM 8 kHz noise at 10 Hz (p=0.001) and 45 Hz (p=0.015) modulation frequency.

* Significant Simple Main Effect of Group

4.3.4 IRN

Time-varying IRN stimuli were used to elicit frequency-following response (FFR) mimicking Mandarin tone 2 (T2, rising) and tone 4 (T4, falling) pitch contours to measure pitch-tracking ability using a broadband speech-like carrier at 30 dB SL (4.7A), similar to what has been measured in human studies of auditory learning and hearing loss (Anderson et al. 2010, 2013b; Skoe and Kraus 2010). We used autocorrelation interval contours that simulated pitches similar to the forms of rising (T2) and falling (T4) pitch contours of the Mandarin Chinese vowel /yi/ (Krishnan et al. 2014, 2015, 2017a, 2017b). IRN responses were evaluated based on the pitch-tracking score, which measures the number of windows where the dominant autocorrelation frequency of the response matches that of the IRN stimulus autocorrelation frequency (see Methods). In general, we observed a loss of pitch-tracking fidelity in Blast animals over the two months post-exposure. Even for the most salient pitch (32 Iterations), blast exposure had a significant Group effect on pitch-tracking scores in both Tone 2 ($F=6.495$, $p=0.026$, $\eta^2_p=0.351$) and Tone 4 ($F=6.115$, $p=0.029$, $\eta^2_p=0.338$), with the largest mean differences on day 7-10. The interaction effect between Time and Group was not significant.

Blast exposure significantly changed the neural response's morphology to IRN at 30 dB SL ($p=0.016$, paired sign-rank test, Fig. 4.8D), such that the cross-correlation between the pre-exposure response and the post-exposure response was much lower in the Blast group up to 30 days post-blast.

IRN iterations: As expected, reduced pitch salience, controlled by reducing iteration number, affected pitch-tracking responses in animals ($F=41.697$, $p<0.001$, $\eta^2_p=0.777$), also showing a significant interaction effect with Time post-exposure ($F=1.722$, $p=0.031$, $\eta^2_p=0.125$). Specifically, pitch-tracking performances to 32 iterations and 16 iterations worsened significantly up to 7-10 days post-exposure, with various degrees of recovery over the following time course. Both the Blast and Sham group exhibited worse pitch tracking with reduced iterations (salience) and to a similar degree. No significant interaction effects with Group were observed for Time and Iterations (Fig 4.9).

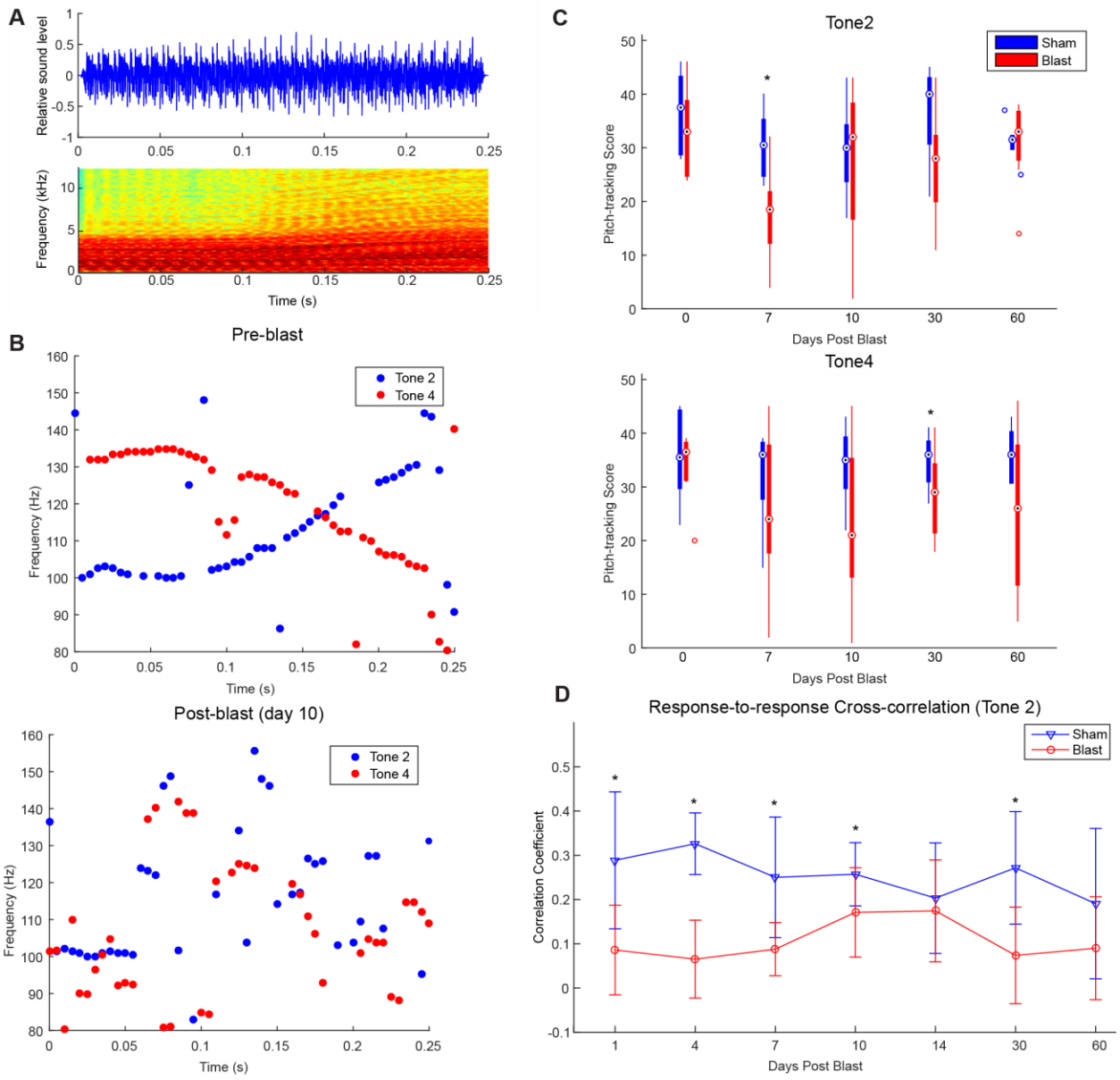

Figure 4.8. IRN Chinese Tone stimuli and responses from Blast (N=8) and Sham (N=6) rats during the first two months post-exposure at 30 dB above threshold A) Example waveform and spectrogram of IRN Tone 2 stimulus; B) Examples of Peak Frequency of IRN Evoked Potential in Pre-blast and Post-blast Brain (day 10 post-blast) from an individual animal; C) Significant effect of Group (*) was seen in IRN Tone 2 (top, p=0.026) and Tone 4 (bottom, p=0.029) pitch-tracking score, though Simple Main Effect of was limited for individual time points; D) Cross-correlation of post-blast IRN responses to corresponding pre-blast responses. Significant differences (*) in correlation coefficients to pre-blast responses between Blast and Sham were observed in two waves: day 1-10, and day 30 ($p<0.05$, paired sign-rank).

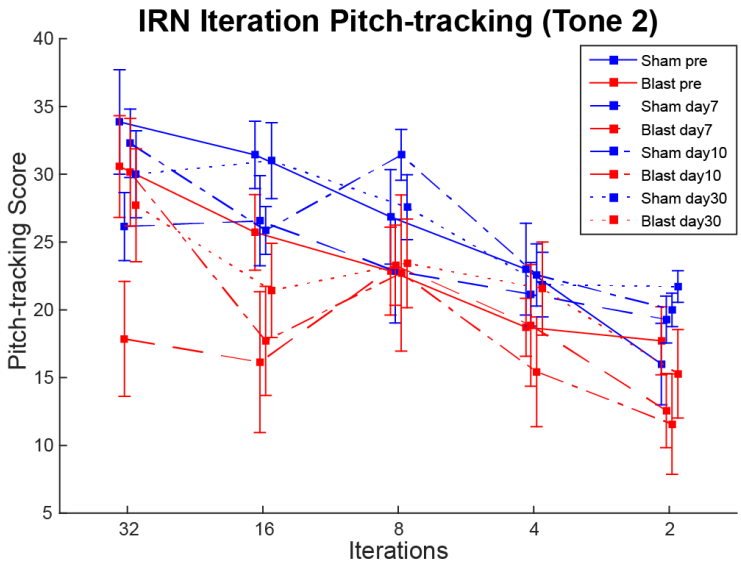

Figure 4.9. Pitch tracking scores of responses to IRN Tone 2 stimuli with pitch salience controlled by altering iteration number at different time points, at 30 dB above threshold. Though the effect of Iterations on pitch-tracking score was significant ($p<0.001$), no significant Iteration * Group interaction was observed.

4.4 Discussion

The purpose of this study was to examine the time course of recovery from a single mild blast injury using simple and complex auditory stimuli longitudinally over a two-month period. Our study demonstrated drastic changes in high-frequency and click hearing thresholds from ABR recordings and reductions in putative subcortical and thalamocortical transmission from ABR and MLR recordings throughout the first two weeks post-exposure. At 30-60 days post-blast, significant increases in click threshold, decreases in wave I amplitude, decreases in MLR N1 amplitude, and declines in pitch-tracking of speech-like IRN pitch trajectories were observed. Compensating for threshold shift and using 30 dB sensation level for AM stimuli, we found that responses to sinusoidal AM stimuli in quiet or noise recovered within 14 days. The 7-14 day window was particularly rapid in the recovery of many auditory parameters, suggesting this as a therapeutic time period when important changes take place.

4.4.1 ABR

We documented the rapid increase of threshold and slow recovery after trauma from blast-exposure. Most notably, a >30 dB peak increase in threshold was observed for click, 8 kHz, and

16 kHz (Fig. 4.2) during the first 4 days. This was consistent with the description of IHC and OHC disturbances across a wide range of frequencies due to blast overpressure as stated in multiple previous publications (Patterson and Hamernik 1997; Ewert et al. 2012; Race et al. 2017). Cho et al. (2013b) reported that ABRs exhibit the least recovery at the highest and lowest frequencies. This broadband threshold shift extended to the last time point at 60 days, though the ~10 dB difference would not be considered clinically relevant.

Over the two-month observation, rapid improvements in ABR threshold and wave amplitudes were observed in the 7-10 days recovery period for waves I, wave III, and wave V (Fig. 4.3). Such rapid recovery could be explained by neuroplastic remodeling within central auditory ABR generator regions (Mulders and Robertson 2009, 2011, 2013; Mulders et al. 2011; Manzoor et al. 2013; Robertson et al. 2013) and recovery of hearing thresholds. Notably, wave V amplitude recovered earlier than wave I, possibly indicating the role of compensation in auditory midbrain as one of the post-blast recovery mechanisms.

We hypothesized that the recovery of ABR threshold and wave I amplitude were the results of a two-fold process, with persistent changes contributing to degraded speech perception (Holmes and Griffiths 2019; Yeend et al. 2019). These parameters showed two waves of post-blast changes: one between 1-10 days post-exposure, and one 10-30 days, as evidenced by Figs. 4.2 and 4.3. We hypothesize that these two waves of deficits indicated the distinction of primary, physical impacts to multiple loci in PAS and CAS (Garman et al. 2011; Ewert et al. 2012; Cho et al. 2013b; Song et al. 2015; Walls et al. 2016) and a series of secondary, biochemical impacts surrounding CAS (Laplaca et al. 1997; Knudsen and Øen 2003; Hamann et al. 2008a; Garman et al. 2011; Säljö et al. 2011; Luo et al. 2014a, 2014b; Song et al. 2015; Walls et al. 2016). Our observations of blast recovery were mostly consistent with this hypothesis.

4.4.2 MLR

At 80 dB SPL, we found persistent deficits in thalamocortical and cortical transmission based on the N1, P2 and N2 peaks (Fig. 4.5A vs. B, C vs. D), which were affected at 30 and 60 days, even after the early P1 response had fully recovered (Fig 5E). These deficits were not present at 30 dB SL, suggesting that effects were at least partially due to shifts in auditory thresholds (Fig. 4.5G), but the moderate, subclinical threshold shifts observed are probably highly relevant functionally. In veterans and the general population with lifetime noise exposure, MLR responses

were shown to be smaller even when subjects had clinically normal audiograms, and there was some evidence of increased cortical gain (Valderrama et al. 2018; Bramhall et al. 2020). In another study with blast-exposed veterans, most of the changes in auditory-evoked potentials were correlated with hearing loss (Meehan et al. 2019). Together, these results suggest that hearing loss may be the main contributor to MLR changes leading to declines in suprathreshold responses. However, more work needs to be done for sustained sounds post-blast to examine the relationships between early evoked potentials, representing subcortical neural activities, and later potentials, representing cortical activities, since studies in aging and noise exposure have suggested enhanced cortical responses (Syka and Rybalko 2000; Sun et al. 2012; Bidelman et al. 2014; Herrmann et al. 2019). These results also suggest that there may be more pronounced hearing deficits from intense combined auditory and mechanical trauma such as blast, compared to medium to intense level of auditory exposure alone, such as recreational or occupational noise (Fulbright et al. 2017; Grinn et al. 2017; Guest et al. 2018).

4.4.3 Amplitude Modulation EFRs

The current study extended an earlier study (Race et al. 2017) to include EFR responses to more challenging auditory stimuli, including lower modulation depth (Fig 6) and in the presence of modulated noise (Fig 7). The Race et al. (Race et al. 2017) study revealed differences in AM processing at 80 dB SPL between Blast and Sham animals, such that blast animals had lower AM FFR amplitudes, especially at lower modulation frequencies in the 20-50 Hz range. However, when the hearing threshold has been compensated, the differences in AM FFR amplitude diminished and even changed sign (Fig. 4.6), suggesting that both changes in audibility and changes in the gain of subcortical auditory system are critical contributors to AM FFR deficits in the blast-exposed auditory system. There are complicated interactions between the AM FFR amplitudes, blast exposure, and the presence of noise, evident as a persistent Group*Noise Level interaction effect in both NAM and 8 kHz SAM. AM responses consist of contributions from multiple generators along the auditory neuraxis, with cortical generators contributing mainly to lower AMFs <50 Hz, and higher frequency AM responses limited to nuclei lower in the auditory neuraxis. The lack of blast-induced differences at higher AMFs distinguishes the blast-induced damage from age-related changes, which are most prominent at higher modulation frequencies (Parthasarathy et al. 2010, Parthasarathy and Bartlett 2012, Lai et al. 2017).

The differences in low-middle AMFs were manifested in opposed directions under slow (10 Hz) and middle (45 Hz) AMFs: notably, normalized FFT amplitudes of 8 kHz SAM in noise was lower for Blast at 10 Hz modulation frequency, but higher for Blast at 45 Hz (Fig 4.7D). This dichotomy is ripe for further study since the 10 Hz and 45 Hz modulations represent different temporal processing regimes and components of speech (Rosen 1992). In studies on age-related auditory nerve deficit models and AM-in-noise responses in aged animals, decreased sensitivities to lower SNRs in AM-in-noise in damaged auditory systems have been observed (Parthasarathy et al. 2016; Lai et al. 2017; Lai and Bartlett 2018). This phenomenon could partly explain the changes seen in 45 Hz AMF. It should be noted that the variance in AM responses post-blast exposure could also be a result of post-blast increases in spontaneous activity for DCN and IC units sensitive to tone versus noise carriers (Luo et al. 2014a, 2014b), which could either desynchronize responses or strengthen AM response simply by heightened excitability.

Taken together, our results suggested that: 1) CAS neuroplasticity partially compensates for hearing loss after blast exposure; and 2) surprisingly, at least for a single mild blast with small lasting threshold shifts, our results suggest that sinusoidal AM processing in quiet and noise largely recovers.

4.4.4 IRN EFRs

Bressler et al. (2017) have noted that perceptual and behavioral deficits persist in blast-exposed veterans in the absence of major clinical threshold or ABR abnormalities. Simple auditory tests such as ABRs and AM EFRs in a quiet background are limited indicators of auditory challenges that blast-exposed individuals would face in daily life. The present study investigated how noise affects responses post-blast as well as using IRN stimuli that simulate the pitch trajectories and sound like simple speech sounds. These stimuli may capture the more complex hearing deficits reported by humans who have experienced blast injuries (Gallun et al. 2012a; Saunders et al. 2015; Kubli et al. 2018).

Complex temporal periodicity between 50 Hz and 500 Hz carries important speech information such as voicing, stress and intonation (Rosen 1992). The present study provided insights into blast-induced sound processing deficits through the use of an IRN stimulus that simulates Chinese intonations and whose pitch and salience can be reliably controlled, showing that IRN can be a useful diagnostic tool for neurotrauma. We found out that even when click ABR

thresholds have returned to subclinical threshold shifts, the deficits in pitch-tracking response to IRN tone stimuli, lingered at least 30 days post-exposure (Figs. 4.8D).

Decreased salience (fewer iterations), showed an overall reduction in pitch tracking in Blast animals (Fig. 4.9), particularly for higher iterations which should be most salient, but they were not differentially affected by the number of iterations. It is worth noting that a previous study showed that increased IRN iterations improved auditory stream segregation in normal hearing veterans more than hearing-impaired veterans (Thompson and Marozeau 2014). Our IRN data (Figs. 4.8-9) suggest that more dynamic and speech-like modulation changes do not recover quickly or completely from even a single mild blast exposure.

4.4.5 Limitations and Future Directions

This study has examined injuries elicited by a single dorsal blast exposure with body shielding that did not result in tympanic membrane ruptures. Therefore, the deficits observed may not be as drastic as that documented by some previous studies in which the injuries were caused by more intense or multiple exposures (Cho et al. 2013b; Du et al. 2013; Luo et al. 2014a, 2014b; Mahmood et al. 2014), often resulting in death or tympanic membrane rupture. The distribution of injuries also differed from models in which blast exposure comes from different orientations, as predicted in animals (Chavko et al. 2011; Dal Cengio Leonardi et al. 2012) and computational studies (Hua et al. 2017; Unnikrishnan et al. 2019). These differences in pressure wave amplitude, duration, and propagation patterns would affect both the distribution and severity of damage across the brain. Although these could change the potential mechanisms of recovery and compensation, it is likely that all blast exposures undergo a multi-stage recovery process similar to that observed in the present study. Our model utilized a top-down mild blast model as described by Song et al. (2015), which exerts a blast impact from the top of the skull. The overpressure blast wave passes through the entire rat brain, such that TBI can be observed throughout the brain, including the frontal cortex and in multiple thalamic regions (Walls et al. 2016), and it results in increased ventral BBB membrane permeation and inflammation, encompassing many subcortical auditory nuclei and axonal tracts. While overlapping loci of vulnerability were described in anatomical studies of animal exposed to blast impacts of different or unknown orientations (Knudsen and Øen 2003; Säljö et al. 2011; Mao et al. 2012b), additional injury mechanisms of different loci and nature may be expected from blast impacts from a different angle. Moreover, non-invasive physiological

measurements of the auditory thalamus and cortex may be indicators of more widespread blast damage in auditory and non-auditory brain regions.

4.5 Conclusion

Based on our chronic longitudinal AEP measurements over a two-month period, this study documented the significant changes in auditory pathophysiology and a potential multi-stage recovery process in animals exposed to a single mild blast trauma. We found that hearing thresholds largely recovered except for broadband stimuli, and some aspects of lasting deficits could be explained by threshold shifts. Recovery of temporal processing of AM sounds was confined to lower modulation frequencies (<50 Hz), with responses dependent on time point, sound level, noise masking, and AMF. More complex, speech-like stimuli (IRN) demonstrated lasting deficits, pointing towards more effective stimuli for elucidating the behavioral difficulties in human and animal listeners.

CHAPTER 5. DYNAMIC, INTERDEPENDENT PATTERNS OF GABA NEUROTRANSMISSION AND ALTERED AUDITORY EVOKED POTENTIALS IN BLAST-EXPOSED CENTRAL AUDITORY SYSTEM

5.1 Introduction

Blast-induced neurotrauma (BINT) is a type of diffuse injury encompassing multiple loci across the human brain. Among the sensory functions impacted, hearing deficits are perhaps the most apparent, leaving a profound impact on the survivor's quality of life (Gallun et al. 2012b; Vander Werff 2012; Saunders et al. 2015). The development of blast-induced hearing deficits is a complicated process, combining elements of mechanical trauma to the eardrum and the inner ear, noise-induced hearing loss, as well as metabolic hearing loss. Depending on the intensity, blast exposure is known to leave significant lesions on the tympanic membrane and the organ of Corti, disrupting the structural integrity of huge swaths of outer hair cells (OHCs), inner hair cells (IHCs) as well as supporting cells (Patterson and Hamernik 1997; Ewert et al. 2012); concurrently, a cascade of anatomical and biochemical changes across central auditory pathway occurs at various time points post-blast, such as gene expression regulation in the inner ear (Wang et al. 2020), changes in axonal integrity, white matter changes in the inferior colliculus (IC) and auditory thalamus (Mao et al. 2012a), elevated oxidative stress and neuroinflammation (Hamann et al. 2008a; Cho et al. 2013a; Walls et al. 2016; Frati et al. 2017). These changes affect multiple subcortical auditory nuclei interdependently, making the understanding of blast-induced central auditory processing changes a complicated process.

Central auditory processing involves intricate excitatory and inhibitory neuronal activities in order to preserve precision and stability in complex environmental conditions. Inhibitory input is especially known to shape the response to amplitude modulation (Burger and Pollak 1998; Koch and Grothe 1998; Caspary et al. 2002) and complex spectral stimuli (Barbour and Wang 2003; Razak and Fuzessery 2009; Rodríguez et al. 2010). The disruption of excitatory/inhibitory balance could therefore induce changes in central auditory processing, contributing to hearing deficits. Studies in noise-induced hearing loss (Milbrandt et al. 2000; Sturm et al. 2017; Schrode et al. 2018; Deng et al. 2020) and age-related hearing loss (Milbrandt et al. 1996; Caspary et al. 2005; Ling et al. 2005; Tadros et al. 2007; Burianova et al. 2009; Wang et al. 2009b; Richardson et al. 2013) have long-established the role of excitatory/inhibitory imbalance and reorganization in hearing

deficits, especially inhibitory loss as represented by loss of GABA inhibitory transmission (Caspary et al. 1999, 2008, 2013). Therefore, it is reasonable to hypothesize that excitatory/inhibitory imbalances in multiple auditory nuclei along the auditory pathway would also be key contributors to the mechanisms of blast-induced hearing deficits as well. The understanding of these excitatory/inhibitory imbalances is further complicated by the fact that blast injury development is a multilocal and everchanging process, with a series of pathological and protective/compensatory mechanisms interacting at different time stages. The time-dependent nature of blast injury development indicates that the scale of excitatory/inhibitory balance could tip to different sides at acute and chronic stages: while acute changes may favor inhibition as a neuroprotective response to the initial impact, similar to the inhibitory upregulation observed in noise impact (Abbott et al. 1999) and non-blast TBI models (Cantu et al. 2015; Guerriero et al. 2015); later-term changes may favor an increase of excitability in order to mitigate the structural and biochemical changes that settle in more slowly post-blast.

Studies on blast neurotrauma have long been aware of excitatory/inhibitory imbalance in the post-blast central auditory system. Spontaneous hyperactivity in cortical and subcortical auditory structures is known to contribute to threshold change, tinnitus and other auditory impairments, both blast-induced (Luo et al. 2014a, 2014b, 2017) and non-blast-induced (Bauer et al. 2008; Mulders et al. 2011; Boyen et al. 2014). In the inner ear, regulations in gene expression related to immune responses, cellular signaling, synaptic transmission, structural maintenance and other biological processes showed different trends in immediate short-term (1-day post-exposure) and long-term (Wang et al. 2020). Not limited to the auditory neuroaxis, previous work has found glutamate excitotoxicity and elevated calcium level post-blast in rat cortex, hippocampus and nucleus accumbens (Cho et al. 2013a; Sajja et al. 2013; Guerriero et al. 2015). Unlike in noise trauma, in which excitotoxicity is primarily observed in the cochlea and auditory nerve (AN) (Puel et al. 1998; Pujol and Puel 1999), the diffuse nature of excitotoxicity in blast injury could mean an exacerbation of hearing loss beyond the impact of blast noise. Glutamate excitotoxicity has been proposed to be a contributing factor of blast-induced hearing loss (Choi 2012), and the treatment to it may contribute to the amelioration of blast-induced damage in the cochlea, dorsal cochlear nucleus and medial geniculate body (Ewert et al. 2012; Du et al. 2013). These studies, while isolated, all suggest a complicated and interdependent web of excitatory/inhibitory imbalances and regulations closely linked to post-blast auditory performance. The different time courses during

which these imbalances take place and the interference between auditory brain structures could further complicate our understanding towards how blast-induced hearing deficits relate to excitatory and inhibitory neuronal activities and what diagnostic and preventative measures should be taken to combat them. Therefore, systematic observation of excitatory/inhibitory changes, especially inhibitory, and their relation to auditory electrophysiological metrics in multiple cortical and subcortical auditory nuclei is needed to devise a complete understanding.

Among blast-induced biochemical changes that have been suggested to lead to lasting, secondary impacts in the central auditory system, including shifts in excitatory/inhibitory balance, oxidative stress has been a prominent candidate. Acrolein-mediated oxidative stress has been observed to contribute to demyelination, synaptopathy and general neurodegeneration in spinal cord injury models (Hamann et al. 2008a; Zheng et al. 2013; Due et al. 2014). A transient elevation of acrolein level in the acute phase (from blast exposure to 4-5 days) has also been observed in a mild blast model (Walls et al. 2016). The extent of acrolein-mediated oxidative stress is yet unknown in the auditory system, but given the diffuse nature of blast injury, it is reasonable to suspect the role of acrolein in the subcortical auditory system. If the presence of acrolein in more peripheral auditory structures leads to neurodegeneration, this peripheral deafferentation could contribute to a later stage loss of inhibition in auditory structures upstream such as the IC and cortex, not dissimilar to that observed in cochlear ablation (Godfrey et al. 2014), noise-induced (Milbrandt et al. 2000; Schrode et al. 2018) and age-related hearing loss (Milbrandt et al. 1996; Helfert et al. 1999; Caspary et al. 2008).

One simple and non-invasive way to measure blast-induced hearing deficits is through auditory evoked potential (AEP) methods, such as auditory brainstem response (ABR) and middle latency response (MLR) tests. Click/tone pips generating ABR and MLR responses have been instrumental in studying hearing loss from traumatic impacts (Wang et al. 2009b; Gallun et al. 2012a; Luo et al. 2014a, 2014b; Bressler et al. 2017; Race et al. 2017; Han et al. 2020), revealing a multitude of potential deficits along the auditory neuroaxis. Gallun et al. (2012a) for example have looked extensively into the ABR wave amplitudes and latencies between waves of human veterans and found little differences between blast and non-blast groups despite behavioral complaints from the blast-exposed individuals. One difficulty in making conclusive observations in human studies on blast injury is the number of variables that cannot be controlled or eliminated, such as exposure intensity, time post-exposure, life experience, past auditory exposure as well as

individual differences in ABR measurements. However, unlike in most human studies, earlier ABR wave amplitudes can be reliably measured in rats (Plack et al. 2016), and the duration between AEP measurements and blast exposure can be controlled in animal studies. Specifically, the non-homogeneity in peripheral damage and threshold change can be controlled by analyzing the ratio of later wave amplitudes to wave I of ABR. Past studies on age-related hearing loss have utilized ABR wave ratio to isolate central gain in the inferior colliculus from peripheral changes (Parthasarathy and Kujawa 2018; Parthasarathy et al. 2019a). Although previously cited studies have documented blast-induced ABR wave amplitude changes at various time points post-blast, blast ratio has yet to be systemically investigated at more than two time points post-blast.

Taken together, the knowledge gaps in blast-induced hearing loss mechanisms as laid out, along with the limitations of previous ABR studies, necessitate the investigation of the extent and time course of blast-induced central excitatory/inhibitory changes with both electrophysiological and anatomical assessment. The likelihood of acrolein-mediated oxidative stress contributing to peripheral deafferentation also calls for anatomical investigation and study into potential treatment options. Notably, the FDA-approved antihypertensive drug Hydralazine (HZ) has also been proposed as a treatment that targets acrolein-mediated oxidative stress and has been proven effective *ex vivo* in non-blast TBI models (Hamann et al. 2008b; Hamann and Shi 2009). The current study aimed to provide insights into the mechanisms and acrolein-targeting treatment potentials through a longitudinal investigation of ABR and MLR wave ratios, which exemplify the transmission and gain in activities between major auditory nuclei along the auditory pathway. By comparing ABR and MLR ratios between peaks with corresponding immunohistochemistry profiles, we aim to uncover the interaction of excitatory/inhibitory interactions between different auditory nuclei after blast impact in a time-sensitive fashion.

5.2 Methods

5.2.1 Subject

All animals were kept and raised in relatively quiet and standard laboratory animal housing conditions. All protocols were approved by the Purdue Animals Care and Use Committee (PACUC #1111000280).

5.2.2 Blast Exposure

Male Sprague-Dawley rats (3-4 months) were assigned into Sham group and Blast group randomly. Animals were anesthetized through intraperitoneal injection of a ketamine/xylazine cocktail (80 mg/kg and 10 mg/kg, respectively). Blast animals were then placed on a platform beneath an open-ended shock tube to be exposed to a composite blast (shock wave + blast wind), as described by Song et al. (2015), while Sham animals were placed on another platform equidistant from the blast source, but out of the path of the shockwave, therefore only exposed to the blast noise.

The shock tube was perpendicular to the dorsum of Blast rat's skull. A custom plexiglass housing was temporarily placed over the animal's torso to avoid cardiac or pulmonary effects of blast and to simulate the protective effects of military body armor (Rafaels et al. 2011). A stereotaxic head frame with a bite bar and ear bars (Kopf Instruments) was used as head fixtures to prevent blast wind-induced head acceleration. The blast exposure exhibited a recorded pressure profile with a rise to peak pressure within 0.3 msec, followed by overpressure and underpressure periods as follows: side-on (static) 150 kPa maximum overpressure, 1.25 msec overpressure duration, and 20 kPa minimum underpressure; face on (dynamic) 160 kPa maximum overpressure, 1.75 msec overpressure duration, and 5 kPa minimum underpressure. After the blast event, tympanic membrane integrity, behavior and mobility were ensured for all Blast and Sham animals prior to electrophysiology.

5.2.3 Auditory Evoked Potential Recordings

The two-channel Auditory Evoked Potential (AEP) setup was similar to that described in our previous publications (Parthasarathy and Bartlett 2012; Race et al. 2017). Recordings were performed at the following time points: pre-exposure (baseline), 1 day, 0.5-week, 1 week, 1.5 weeks (10 days), 2 weeks and 1 month (30 days).

While the animals were under 1.8-2% isoflurane anesthesia, subdermal needle electrodes (Ambu) were inserted in locations described in Table 5.1. Electrode impedances were confirmed to be less than 1 kΩ using a low impedance amplifier (RA4LI, TDT). The animals were then sedated through intramuscular injection of 0.2-0.3 mg/kg dexmedetomidine (Dexdomitor),

allowing around 3 hours of recording time. AEP recordings were performed 10-15 min after removal from isoflurane to minimize the effect of anesthesia.

Acoustic stimuli were presented free-field to the right ear (90^0 azimuth) of animals, with directly in front of the animals' face as the reference for 0^0 azimuth, using a calibrated speaker (Bowers and Wilkins) at a distance of 115 cm directly facing the right ear.

Table 5.1. Electrode placement in two-channel auditory evoked potential recording.

Electrode	Placement
Channel 1 (positive)	Along the midline of the head (mid-sagittal), oriented fz to cz
Channel 2 (positive)	C3 to c4 along the interaural line
Negative (used with positive electrodes for both channels 1 and 2)	Under the mastoid of the right ear ipsilateral to the speaker
Ground	In the back of the animal

5.2.4 Auditory brainstem response

8 Sham animals and 10 Blast animals were used in ABR analysis. For ABR, rectangular clicks (0.1 msec duration) and 8 kHz pure tone tone-pips (2 msec duration, 0.5 msec cos2 rise-fall time) were used. 8 kHz was chosen based on previous findings: with 6-16 kHz being the most sensitive hearing region of rats, 8 kHz near the most sensitive region of normal rat audiogram (Parthasarathy et al., 2014) and hearing of frequencies higher than 8 kHz being most vulnerable to blast injury. The sound levels of clicks and pips range from 95 to 10 dB peak SPL in 5-dB steps. All stimuli were presented in alternating polarity at 26.6 per second with 1500 repetitions (750 at each polarity). A 20 msec acquisition window (0-20 msec) was used.

Data were processed with a 30 Hz high-pass (HP) filter and a 3000 Hz low-pass (LP) filter prior to analysis. The ABR threshold was defined as the minimum sound level that produced a distinct ABR waveform.

The ABR amplitudes and latencies of waves I and III from channel 1, and waves I and V from channel 2 were estimated as the differences of each wave's amplitude, as seen in BioSigRP (TDT) and the baseline amplitude. Wave III/Wave I ratios are calculated by waves III amplitude from channel 1 divided by corresponding wave I from channel 1. Wave V/Wave I ratios are

calculated by waves V amplitude from channel 2 divided by corresponding wave I from channel 2. The waves and channels were chosen based on previous studies of our lab (Parthasarathy and Bartlett 2012), with wave III most prominent on channel 1 and wave V most clear on channel 2. Between-waves latencies were calculated by the differences between target wave latencies and wave I latency measurements from the same channel.

5.2.5 MLR

8 Sham animals and 8 Blast animals were used in MLR analysis. For MLR, similar rectangular clicks and 8 kHz tone pips of alternating polarity as in ABR were used but were presented at a slower rate (3.33/sec vs. 26.6/sec in ABRs) and with a recording window of longer duration (100 msec vs. 20 msec in ABRs). This time window provides enough time to capture the stimulus-evoked "middle-latency" neural responses from the auditory midbrain, thalamus, and cortex (Barth and Shi Di, 1991; McGee et al., 1991; Di and Barth, 1992; McGee and Kraus, 1996; Phillips et al., 2011; Šuta et al., 2011) alongside ABR. Stimuli were presented at 80 dB and 30dB above corresponding ABR thresholds, as determined in the previous ABR recordings. 1500 repetitions were collected over an acquisition time window of 100 msec to obtain an average response.

Data were processed with HP (fc = 10 Hz) and LP (fc = 300 Hz) filters prior to analysis.

5.2.6 Hydralazine Treatment

To assess the effectiveness of acrolein inhibition in mitigating blast-induced auditory deficits, Hydralazine, an FDA-approved antihypertension drug with acrolein-scavenging effect (Burcham et al. 2000; Burcham and Pyke 2006; Hamann and Shi 2009), was used in a treatment sub-study. 6 treatment animals and 6 non-treatment (NT) animals were included in Hydralazine (HZ) treatment study. Animals are subjected to the same blast exposure that Blast animals underwent. After blast exposure, treatment animals received an intraperitoneal (IP) Hydralazine injection of 5mg HZ/kg body weight each day from day 0 of blast exposure to day 6 post-blast. NT animals received an IP injection of the same schedule as treatment animals, but with 5mg filtered 1x phosphate-buffered saline (PBS)/kg body weight.

Treatment and NT animals undergo the same AEP measurements as blast and sham animals.

5.2.7 Anatomical Analyses

Immunohistochemistry

5 Blast and 5 Sham rats were euthanized at each of the following time points: 2 days, 1 week, 2 weeks and 1-month post-blast. Rats were perfused with oxygenated Krebs solution prior to whole-brain extraction. One hemisphere from each rat was used for immunohistochemistry, the other for membrane permeability. Immediately following extraction, immunohistochemistry brain hemispheres were fixed in 4% paraformaldehyde at 4C in PBS overnight. Brain hemispheres were transferred to 30% sucrose and incubated for 24-48hrs at 4℃ for cryoprotection. Following incubation, brain hemispheres were embedded in Tissue-Tek OCT compound (VWR, Batavia, IL, USA), flash-frozen with liquid nitrogen and stored in -80℃ until sectioned.

To prepare for antibody staining, 25μm sections of the brain hemisphere were cut using a cryostat. Primary antibodies used were rabbit anti-GAD65+GAD67 (Abcam, ab183999, 1:2500) and rabbit anti-TNF alpha (Abcam, ab6671, 1:500). Sections were permeabilized with two washes of 0.1% PBS-triton, followed by 30 minutes in 3% PBS-triton. Sections were washed in PBS and incubated in 10% blocking solution for 2 hours. Next, sections were incubated in primary antibody overnight at 4℃. After primary antibody incubation, sections were washed three times with 0.1% PBST, followed by incubation at room temperature with secondary fluorescent antibodies, Donkey anti-mouse Alexa-594 and/or Donkey anti-rabbit Alexa 488 (1:500), for 2 hours (JacksonImmuno, West Grove, PA). Sections were counter-stained with DAPI and washed 3 times in PBS. Sections were then cover-slipped using Prolong Gold Antifade Mounting reagent (Invitrogen, Carlsbad, CA, USA). Sections were visualized on an Olympus Ix51 microscope. Fluorescence was quantified using Image J (NIH, Bethesda, MD, USA), and background-corrected intensity levels of five sections from each rat were randomly selected from regions of interest and averaged.

3,3'Diaminobenzidine (DAB) Assessment

For the assessment of acrolein oxidative marker, DAB substrate staining was used instead of immunofluorescence, similar to previously described methods (Hashimoto et al. 2001; Hovens et al. 2014). Primary antibodies used were: rabbit Anti-Myeloperoxidase antibody (Abcam, ab208670, 1:1000) and rabbit anti-Acrolein (Abcam, ab37110, 1:500). Sections were incubated

for 30 mins at room temperature in 3% peroxidase/H_2O and permeabilized in 3% PBS-triton for 20 mins after. Sections were incubated in 10% blocking solution for 2 hours at room temperature. Then, sections were incubated overnight at 4C in primary antibody. After three washes of 0.1% PBST, sections were incubated for 2 hours in secondary antibody, biotinylated goat anti-rabbit (Vector Labs BA-1000, 1:500). Sections were washed three times in 1% PBST and incubated in ABC reagent for 30 minutes (Vector Labs, SK-4100). After washing with 1% PBST, sections were developed with peroxidase substrate. Next, sections were rinsed in PBS and mounted on gelatin-coated slides. Slides were allowed to dry and were immediately dehydrated with incremental 50% Ethanol to 100% Ethanol 2-minute washes. Slides were briefly washed with Xylene and cover-slipped with Perma-Mount (Fischer Scientific, Hampton, NH). Sections were visualized on an Olympus Ix51 microscope. Staining intensity was quantified using Image J (NIH, Bethesda, MD, USA), and background-corrected intensity levels of five sections from each rat were randomly selected from regions of interest and averaged. The Paxinos and Watson Third Edition Rat Brain atlas (Paxinos and Watson 2007) was used to find appropriate regions of interest (ROIs) for the auditory thalamus, inferior colliculus, and superior olivary complex structures. Regions corresponding to approximately Bregma -5.20mm to -6.04mm were used for auditory thalamus (medial geniculate body), approximately Bregma -8.30 to -9.30mm for inferior colliculus, and approximately Bregma -8.80mm to -10.04mm for the superior olivary complex. ROIs were drawn according to the characteristic shape of each region and were, approximately, $1mm^2$ for the thalamus and SOC and $2mm^2$ for the IC (regions sizes varied slightly between rats).

Membrane permeability Assessment

The exclusion of the hydrophilic dye tetramethyl rhodamine dextran (TMR, MW 10kD, Invitrogen, Carlsbad, CA, USA) was used to measure membrane permeability (Hamann et al. 2008b). Rats were perfused with oxygenated Kreb's solution. Immediately following perfusion, brains were halved, and one hemisphere was immediately placed in 0.01% lysine fixable TMR and incubated for 1 hour in the dark. Following Incubation, TMR brain hemispheres were frozen and sectioned and as described in the Immunohistochemistry protocol above. Immediately following, sections were cover-slipped using Prolong Gold Antifade Mounting reagent (Invitrogen, Carlsbad, CA, USA. Sections were visualized on an Olympus Ix51 microscope. Fluorescence was quantified using Image J (NIH, Bethesda, MD, USA), and background-corrected intensity levels

of five sections from each rat were randomly selected from regions of interest and averaged. For analysis of individually stained cells, particle analysis was used according to ImageJ documentation, and the number of stained particles was counted for five sections and averaged.

5.2.8 Statistics

ABR statistics were performed with statistics software JASP (Version 0.14.1, JASP Team, 2020). All statistics for ABR ratio utilized 2-way repeated measures ANOVA test with Huynh-Feldt correction to check the significance of each main effect and interaction, with a 0.05 significance criterion. ABR latency statistics utilized a 2-way repeated measures ANOVA test with Huynh-Feldt correction, as well as correlation analyses, with a 0.05 significance criterion.

MLR statistics were performed with MATLAB (MathWorks, 2019). The peak ratios at each time point were compared to the pre-stimulus baseline using a paired sign-rank test, with a 0.05 significance criterion.

Statistics for anatomical analyses were performed with R (R Core Team, 2017). All statistics utilized a single factor ANOVA test, with a 0.05 significance criterion.

5.3 Results

5.3.1 ABR Ratio

ABR wave III-I ratios and V-I ratios are analyzed for 10 blast and 8 sham animals to assess blast-induced differences in central gain at the CN and IC level, respectively, as a function of time post-exposure (Fig. 5.1). Clicks and 8 kHz tones were tested at 80 dB SPL and 30 dB SL. Repeated measures ANOVA was conducted on the effect of time post-exposure (Time), as well as differences between blast vs. sham (Group). At 80 dB SPL, only 8 kHz wave III-I ratios exhibited a significant repeated measures effect of Time ($F=3.355$, $p=0.011$, $\eta^2_p=0.173$), as well as a significant Time*Group interaction effect ($F=3.403$, $p=0.010$, $\eta^2_p=0.175$). This difference in wave III-I trends was evident as an increased wave III-I ratio for blast animals in acute (day 1-4 post-blast) phase and day 7 post-blast, then a drastic reduction to similar or lower ranges on day 10 and after. Simple main effects showed that wave III-I ratio for blast was significantly higher than sham group on day 4 ($F=5.851$, $p=0.028$). The same trend could be observed in click wave III-I ratios, with blast wave III-I ratios higher at day 1-4 post-blast, then fell back to lower than sham ratio

after day 10 and after, with simple main effect of Group being significant on day 10 (F=5.330, p=0.035). The effect of Time, Group, or Time*Group interaction overall were not significant due to large variance in blast ABR, particularly at day 1 (standard error of mean=0.839, min=1.632, max=10.502) and day 4 (SEM=0.695, min=2.079, max=9.414), compared to sham ABR (day 1: SEM=0.186, min=1.872, max=3.328; day 4: SEM=0.184, min=2.147, max=3.805). It should be noted that the experimental setup allowed us to record ABR at 95 dB SPL max, therefore a few instances of equal SL ABR on day 1 could only reach 15~25 dB SL.

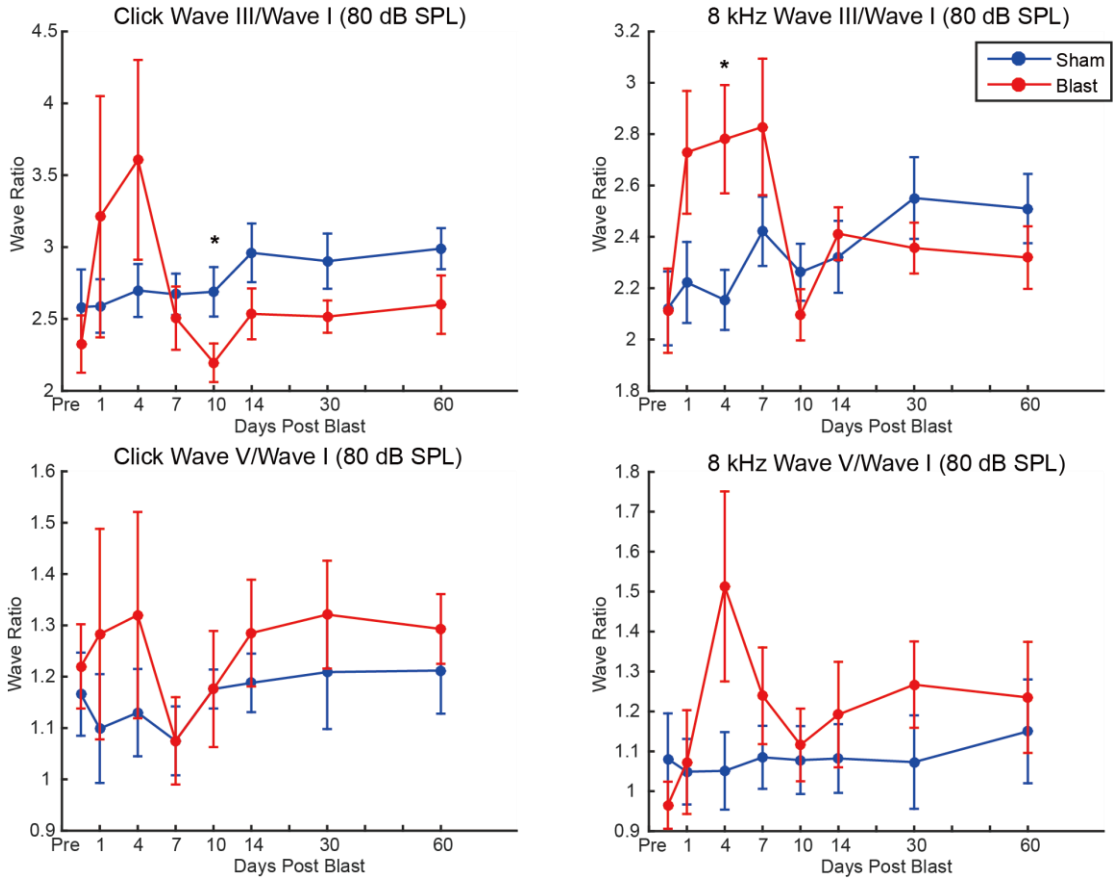

Figure 5.1. ABR wave III/I and V-I ratios of Blast (N=10) and Sham (N=8) rats during the first two months post-exposure at 80 dB SPL. Significant effect of Time (p=0.011) and Group*Time interaction effects (p=0.010) were observed in 8 kHz wave III/I (Top right).

*Significant Simple Main Effect of Group, p<0.05.

No significant effect of Time, Group or Time*Group interaction was found in ABR V-I ratios at 80 dB SPL. Both click and 8 kHz ABR V-I ratios showed elevation on day 1 and day 4 post-blast, mainly due to a greater reduction and variations in wave I. There was a second wave of

smaller elevation on day 14 and 1-month (30 days) post-blast, though no significant difference was found between groups at these time points.

Although ratio analysis should compensate for differences in peripheral activity due to blast-induced hearing threshold shift, it is useful to analyze wave ratios at a suprathreshold level that accounts for threshold shifts. Here, ABR wave III-I ratios and V-I ratios were also analyzed at 30 dB SL (Fig. 5.2). A significant repeated measures effect of Time was observed in click wave III-I ratio at 30 dB SL ($F=4.841$, $p<0.001$, $\eta^2_p=0.232$), demonstrating a wave of elevation from day 1 that ends around day 10, and another wave from day 14 onward. The trend was overlapping in both blast and sham groups, though. For click wave V, an elevation in wave V-I ratio was seen in blast beyond day 10, but no statistically significant difference was observed.

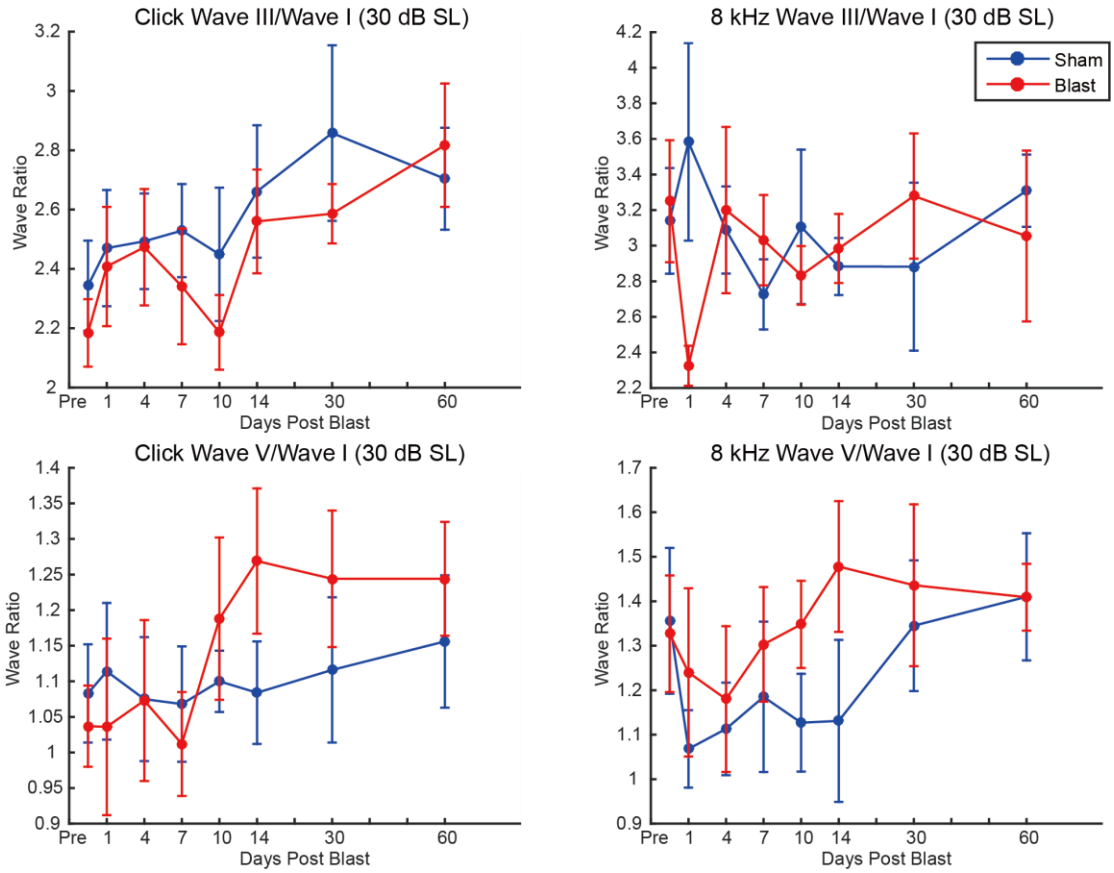

Figure 5.2. ABR wave III/I and V-I ratios of Blast (N=10) and Sham (N=8) rats during the first two months post-exposure at 30 dB SL. Significant effect of Time ($p<0.001$) was observed in click wave III-I ratio at 30 dB SL (Top left). No significant effect of Group was observed.

5.3.2 ABR Wave Latency

Shifts in ABR wave latency has been used in various studies as a hallmark of hearing deficits (Henry et al. 2011; Gallun et al. 2012a; Mehraei et al. 2016). We analyzed wave I, wave I-III, as well as wave I-V latencies of click and 8 kHz ABR at 80 dB SPL and 30 dB SL. Significant effects of Time ($F=12.569$, $p<0.001$, $\eta^2_p=0.440$), Group ($F=5.606$, $p=0.031$, $\eta^2_p=0.259$) as well as Time*Group interaction ($F=8.171$, $p<0.001$, $\eta^2_p=0.338$) were observed in click wave I latency at 80 dB SPL, showing significantly longer latencies for blast in the acute phase (day 1-7) than sham (Fig. 5.3A, left panel). A simple main effect of Group was significant up to day 7 post-blast ($F=8.515$, $p=0.010$). The significance of Time ($F=4.405$, $p=0.004$, $\eta^2_p=0.216$) and Time*Group interaction ($F=3.556$, $p=0.013$, $\eta^2_p=0.182$) effects were reduced, but still remains even after click thresholds have been compensated for in 30 dB SL measurements (Fig. 5.3A, right panel). A simple main effect of Group was significant on day 4 post-blast ($F=6.979$, $p=0.018$), and was consistent with the trend for days 1-7 (day 1: $F=4.295$, $p=0.055$; day 7: $F=4.426$, $p=0.052$). Post hoc tests showed that wave I latencies of blast animals were significantly longer compared to pre-blast measurements up to day 4 post-blast ($t=-5.438$, $p<0.001$, Tukey correction). The trend in click wave I latency, even with threshold compensated, was highly linked with click threshold (Fig. 5.3B). Click wave I latencies at 80 dB SPL (blast: Pearson's $r=0.752$, $p<0.001$; sham: $r=0.437$, $p<0.001$) and 30 dB SL (blast: $r=0.604$, $p<0.001$; sham: $r=0.375$, $p=0.002$) were positively correlated with click threshold for both blast and sham animals (Fig. 3C and D). High click threshold may be linked with cochlear synaptopathy disconnecting high center frequency (CF), low latency auditory nerve fibers (ANFs), creating longer latency even when sensation levels have been accounted for.

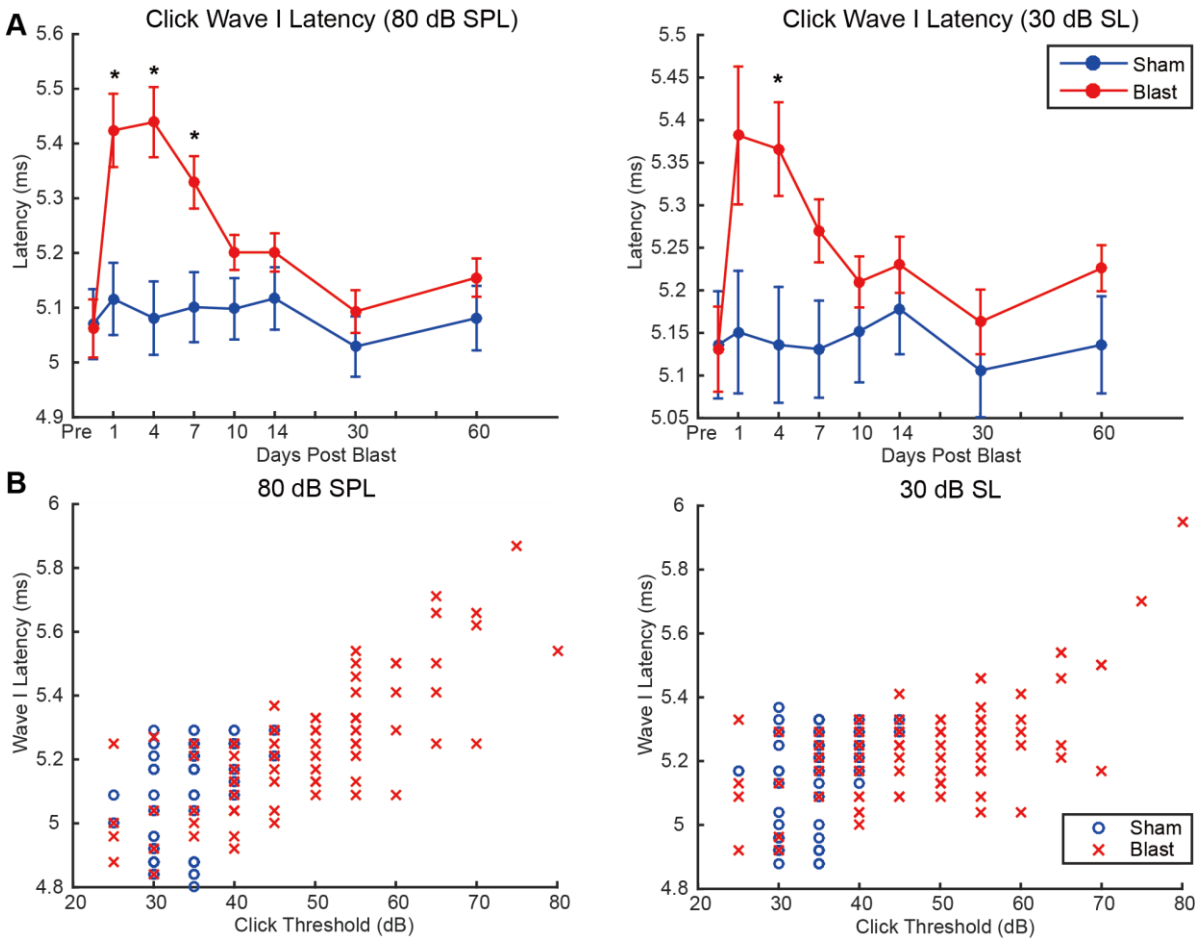

Figure 5.3. Click ABR wave I latencies of Blast (N=10) and Sham (N=8) rats during the first two months post-exposure at 80 dB SPL. A) Significantly longer latencies were observed in blast click wave I measurements, at 80 dB SPL from day 1-7 post-exposure and at 30 dB on day 4. B) Click wave I latencies at 80 dB SPL (blast: r=0.752, p<0.001; sham: r=0.437, p<0.001) and 30 dB SL (blast: r=0.604, p<0.001; sham: r=0.375, p=0.002) were positively correlated with click threshold for both blast and sham animals.

*Significant Simple Main Effect of Group, p<0.05.

Effects of Time (F=8.696, p<0.001, η^2_p=0.352) and Time*Group interaction (F=6.283, p<0.001, η^2_p=0.282) are also significant for 8 kHz wave I latency at 80 dB SPL, although the effect of Group was not significant. Blast 8 kHz wave I showed significantly prolonged latency compared to sham on day 1 and day 4, similar to the trend of Click latency (Fig. 5.4A). Only the Time effect (F=2.414, p=0.031, η^2_p=0.131) remained significant for 8 kHz wave I latency at 30 dB SL. 8 kHz wave I latencies at 80 dB SPL (blast: r=0.759, p<0.001; sham: r=0.662, p<0.001) were positively correlated with 8 kHz threshold (Fig. 5.4B), but 30 dB SL latencies were only positively correlated with threshold for sham (r=0.337, p=0.006) and not for blast (r=-0.004, p=0.976) group. This

observation suggested that blast-specific trauma disrupted the correlation between threshold and hair cell transduction efficacy of 8 kHz regions in the cochlea. Specifically, the positive correlation of threshold and latency at equal sensation level was gone for blast at 8 kHz region, despite blast and sham sharing similar 8 kHz wave I latency ranges at equal sensation level. Since pathological hair cells are known to maintain a negative correlation between latency and SPL similar to normal hair cells (Wang and Dallos 1972), and that ANF recruitment has been partially accounted for through equal sensation level, this disruption strongly indicates frequency-specific changes in the temporal properties of auditory nerve fibers or in the transduction process.

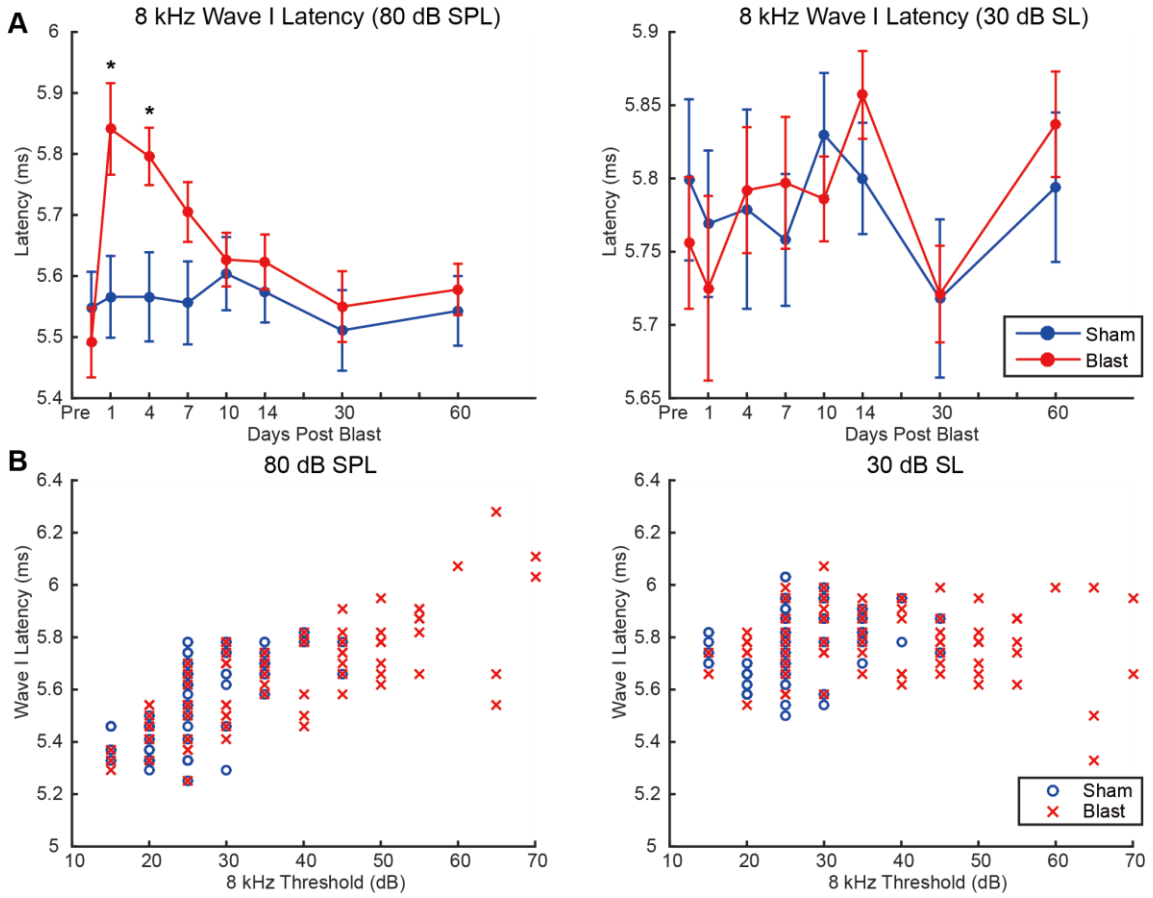

Figure 5.4. 8 kHz ABR wave I latencies of Blast (N=10) and Sham (N=8) rats during the first two months post-exposure at 80 dB SPL. A) Significantly longer latencies were observed in blast click wave I measurements, at 80 dB SPL from day 1-4 post-exposure, but not for 30 dB SL. B) 8 kHz wave I latencies of both groups at 80 dB SPL were correlated with 8 kHz threshold (blast: $r=0.759$, $p<0.001$; sham: $r=0.662$, $p<0.001$), but 30 dB SL latencies were only correlated with threshold for sham ($r=0.337$, $p=0.006$) and not for blast ($r=-0.004$, $p=0.976$) group.

*Significant Simple Main Effect of Group, $p<0.05$.

Click and 8 kHz latencies were positively correlated for both blast and sham in individual animals, at 80 dB SPL (blast: r=0.880, p<0.001; sham: r=0.919, p<0.001) and 30 dB SL (blast: r=0.642, p<0.001; sham: r=0.827, p<0.001) (Figure 5.5). Linear regression was performed for click - 8 kHz latencies correlation of all groups and sound level conditions. For both 80 dB SPL and 30 dB SL, the slopes of blast (80 dB SPL: 0.871; 30dB SL: 0.524) were smaller than that of sham group (80 dB SPL: 0.941; 30 dB SL: 0.707). This difference was consistent with our previous observation that broadband stimuli reveal blast-induced hearing deficits more robustly (Han et al. 2020). Click ABR recruits the activity of a broader range of frequency regions, including high-frequency regions of the cochlea and AN that were known to be disproportionally more affected by blast exposure (Race et al. 2017; Hickman et al. 2018). Therefore, click wave I latency reflects the combined hair cell damage, cochlear synaptopathy and ANF injuries of a broader frequency range, resulting in a larger increase than 8 kHz latency under the same degree of injury.

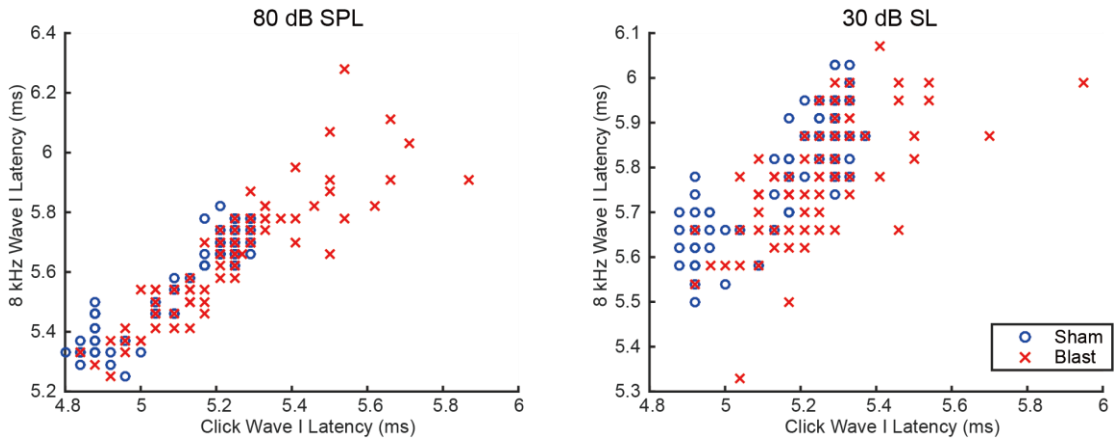

Figure 5.5. Click and 8 kHz latencies were positively correlated for both blast and sham in individual animals, at 80 dB SPL (blast: r=0.880, p<0.001; sham: r=0.919, p<0.001) and 30 dB SL (blast: r=0.642, p<0.001; sham: r=0.827, p<0.001).

Because of the drastic shifts in wave I latencies, wave I-III latencies and wave I-V latencies are calculated and analyzed to assess changes in central transmission efficacy to the CN and the IC, respectively, isolated from peripheral influence. No significant effect of Time, Group or Time*Group in wave I-III latency or wave I-V latency was found in either sound level, indicating that any potential change in synaptic and axonal transmission due to a single mild blast exposure was not enough to alter the transmission time of simple auditory cues from the AN to the auditory brainstem and midbrain.

5.3.3 MLR normalized peaks

MLR responses were collected using click or 8 kHz tone pips at 80 dB SPL and 30 dB SL at a lower rate to allow the capture of response waves in the auditory thalamus and auditory cortex. A grand average of blast click MLRs at different time points compared to pre-blast responses is shown in Figure 6A. In this study, aside from the absolute amplitudes of P1, N1, P2 and N2, we specifically analyzed the difference between P1-N1 and N1-P2, which is less dependent on the MLR baseline.

Because of the big variance in electrophysiological peaks observed in the previous chapter (Han et al. 2020) and previous sections of this chapter, as well as the dependence of post-exposure MLR peaks to pre-exposure levels (Popelar et al. 2008), we compared MLR peaks of later time points by normalizing each peak amplitude to the corresponding pre-blast amplitude of the same animal, using the Wilcoxon rank-sum test ($p<0.05$) to determine significance. For 80 dB (Figure 6B, left panel), MLR waves showed two periods of significant differences: wave P1 and N2 were significantly smaller post 1-7, and 30, N1, P1-N1 difference, and N1-P2 difference were significantly smaller days 1-60, and P2 was smaller days 1-7 and 30-60. As P1 can be seen as a rough representation of ABR responses, N1 represents thalamic and thalamocortical activation (Barth and Shi Di 1991; Di and Barth 1992; Popelar et al. 2008; Race et al. 2017), which experienced two waves of decreased ratio at day 1-7 and day 30 post-blast. P2 was significantly lower than pre-blast throughout the two months post-exposure, showing a compromised thalamocortical transmission. N2 and subsequent oscillations represent cortical activation, which was shown to be compromised at day 1-7 and day 30. This is consistent with previous observations (Race et al. 2017; Han et al. 2020). For 30 dB SL (Figure 6B, right panel), however, the differences in N1, P2, P1-N1 and N1-P2 as compared to pre-blast were reduced to only being significant at day 1, and no significant difference in P1 and N2 was observed. A wave of increase compared to pre-exposure levels was observed in both P1-N1 and N1-P2, from day 7 to day 14, but distributions were not significantly altered from baseline.

In addition to normalized wave amplitude analysis, we also conducted cross-correlation of the first 80ms of MLR response waves between pre-exposure and post-exposure time points. Interestingly, consistently reduced correlations to pre-exposure waveform were observed in both 80 SPL and 30 SL, from day 1 to day 7, and in 30 SL, on day 30 as well (Figure 6C). Taken

together, these results demonstrated that even a mild blast exposure could result in lasting alterations in thalamocortical auditory evoked activities.

No significant difference in MLR peaks and ratios compared to pre-blast was observed in sham animals. The result is similar to that of Race et al. (2017), with an even less significant difference observed for sham.

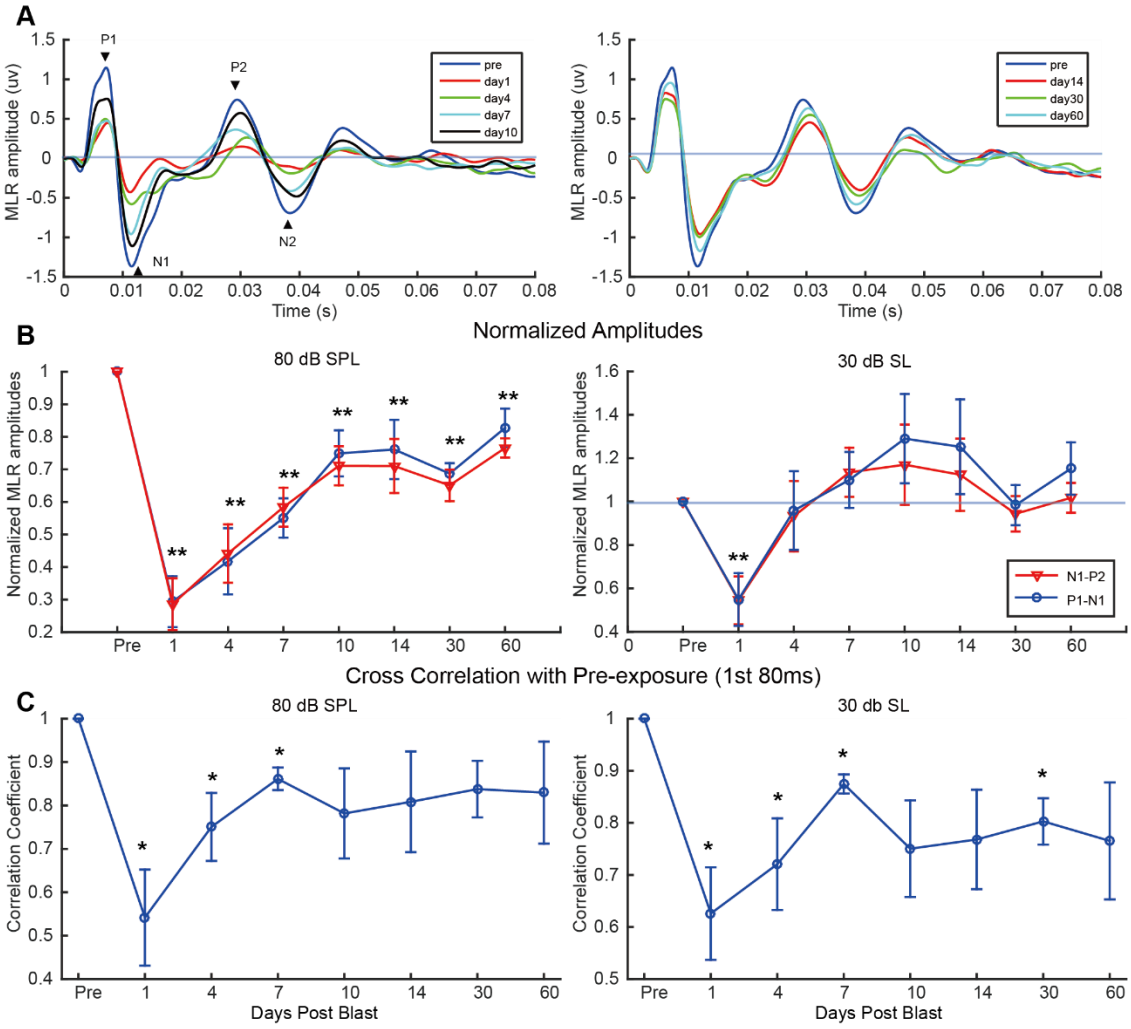

Figure 5.6. Middle latency response of Blast (N=8) rats during the first two months post-exposure. A) Grand average traces of Click MLR waveforms at 80 dB SPL. B) Normalized click P1-N1 and N1-P2 amplitudes showed a significant blast-induced reduction from day 1-60 at 80dB SPL. Reduction was only significant on day 1 at 30 dB SL. C) Cross-correlation with pre-exposure responses (1st 80ms) showed significant alteration in both 80 dB SPL and 30 dB SL.

**Significant difference in normalized P1-N1 and N1-P2 compared to pre-exposure, $p<0.05$.
*Significant difference in response correlation coefficient with pre-exposure, $p<0.05$.

5.3.4 Immunohistochemistry

GAD65+GAD67 immunofluorescent staining, TMR staining, and DAB assessment were conducted on the auditory thalamus, the IC, and the auditory brainstem with a focus on SOC and ventral axon tracks. Mean intensity was calculated for GAD and acrolein, and particle number (N) was calculated for TMR. At 2 days post-exposure, a drastic, but not statistically significant decrease of GAD (Blast: Intensity=12.210; Sham: Intensity=22.025. p=0.101) and increase of TMR (Blast: N=97.222; Sham: N=40.500. p=0.089) were observed in the SOC (Figure 5.7 and 5.8). The extent of membrane damage was diffuse, permeating the entirety of the ventral brainstem (Figure 5.8), showing significant elevation in ventral axon tracks (Blast: N=26.739; Sham: N=17.679. p=0.012) and may extend to regions adjacent to the ventral nucleus of the CN. Increased acrolein was also observed in the SOC at 2 days post-exposure. A significant decrease of GAD (Blast: Intensity=15.166; Sham: Intensity =30.468. p=0.032) was observed in the thalamus (Figure 5.7). Conversely, the IC exhibited a significant elevation of GAD (Blast: Intensity=46.739; Sham: Intensity =39.516. p=0.017). No significant TMR or acrolein difference was observed in the IC or the thalamus.

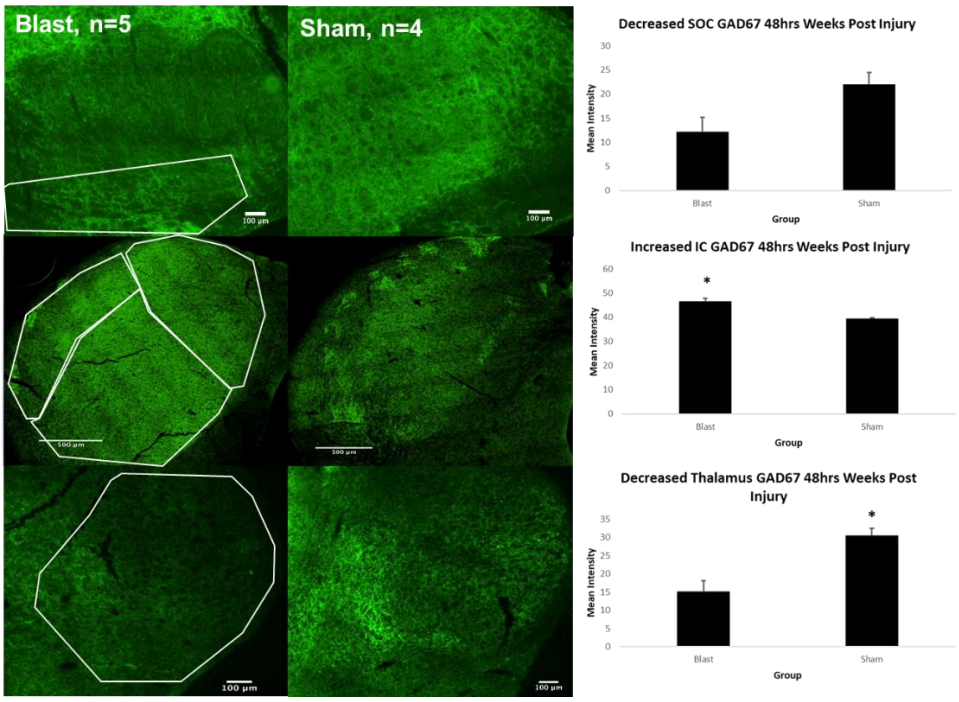

Figure 5.7. Altered GAD levels in the SOC (decrease), IC (increase) and auditory thalamus (decrease) in blast-exposed animals compared to sham, 48 hours post-exposure. Areas of interest were outlined with white lines.

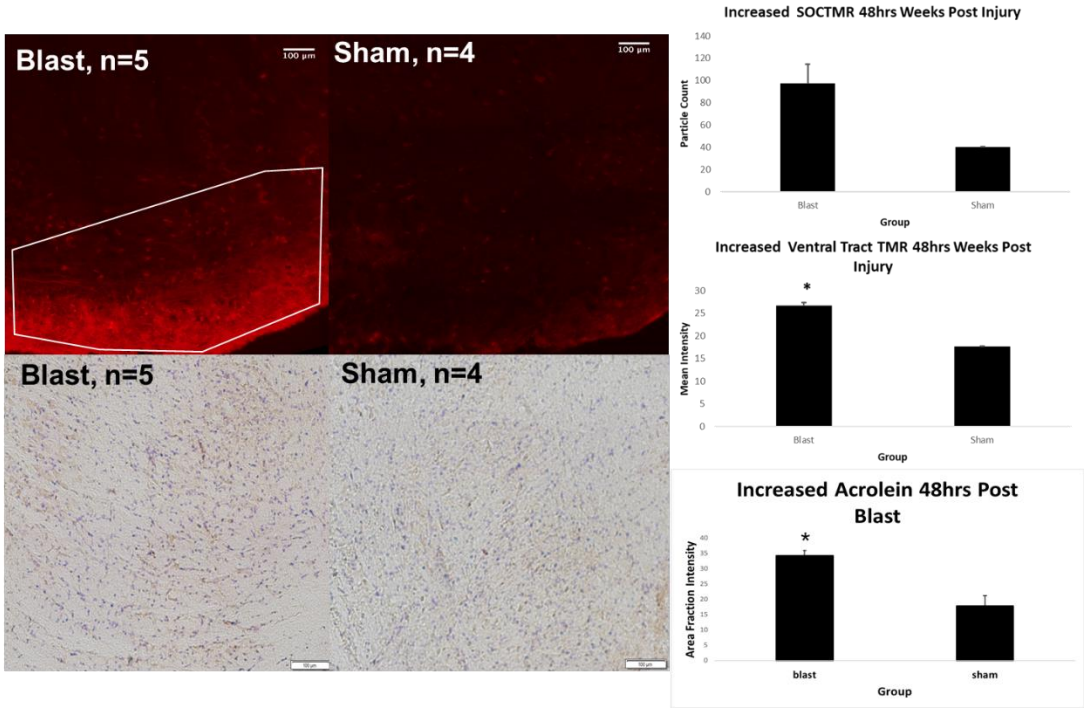

Figure 5.8. Increased TMR particles (red) indicated increased membrane damage in blast-exposed SOC and ventral axon tracts compared to sham, 48 hours post-exposure. Areas of interest were outlined with white lines. Increased acrolein (lower panel, colored dots) observed in blast-exposed SOC indicated oxidative stress.

At 7 days post-exposure, the elevation of TMR (Blast: N=186.375; Sham: N=85.833. p=0.021) persisted in the SOC and diffused regions of the brainstem, though the acute membrane damage in ventral axon tracks disappeared (Fig. 5.9). Significant decrease of GAD mostly disappeared in the SOC (Blast: Intensity=11.318; Sham: Intensity =17.656. p=0.055) but persisted in the thalamus (Fig. 5.10, Blast: Intensity =13.344; Sham: Intensity =17.724. p=0.019), but the increase of GAD disappeared in the IC (Blast: Intensity =1.023, Sham: Intensity =1.059. p=0.964). Notably, though the overall GAD levels were similar, blast and sham animals exhibit different GAD patterns in the IC. GAD appeared to concentrate in the ventral parts of the central nucleus of the IC (CIC) of blast animals (Fig. 5.10, mid row, left panel), while in sham animals, GAD concentrated at dorsal CIC, dorsal cortex (DCIC), and external cortex of the IC (ECIC. Fig. 5.10, mid row, mid panel). No difference in acrolein was observed in any of the auditory structures from 7 days onward.

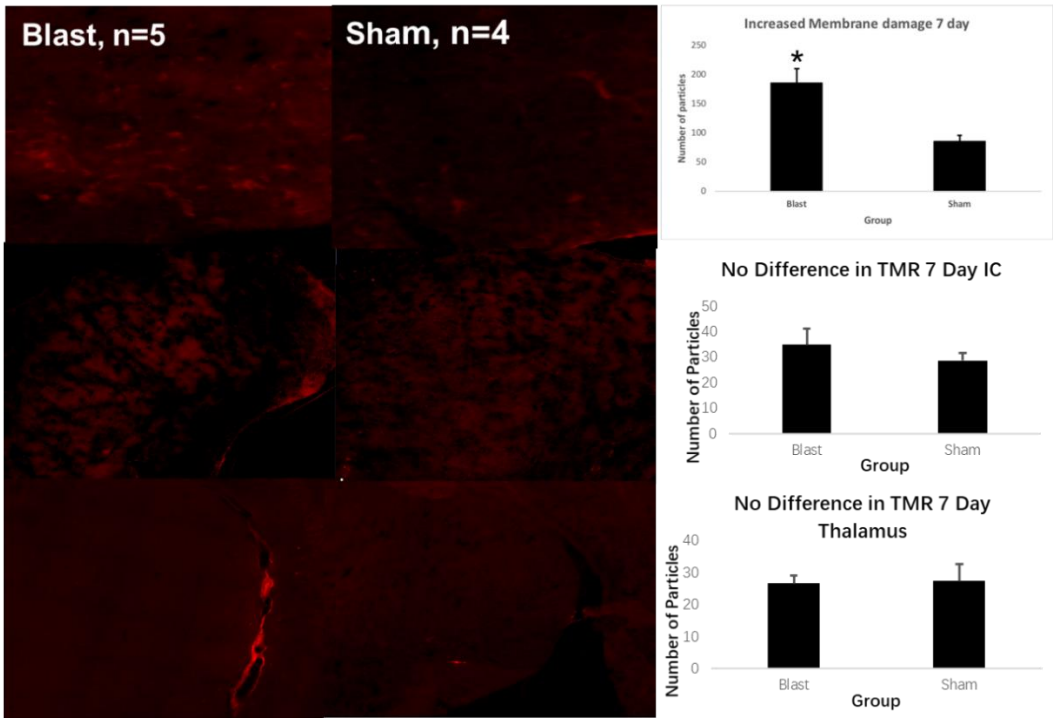

Figure 5.9. Significantly increased TMR observed in blast-exposed SOC compared to sham, but not in the IC or thalamus.

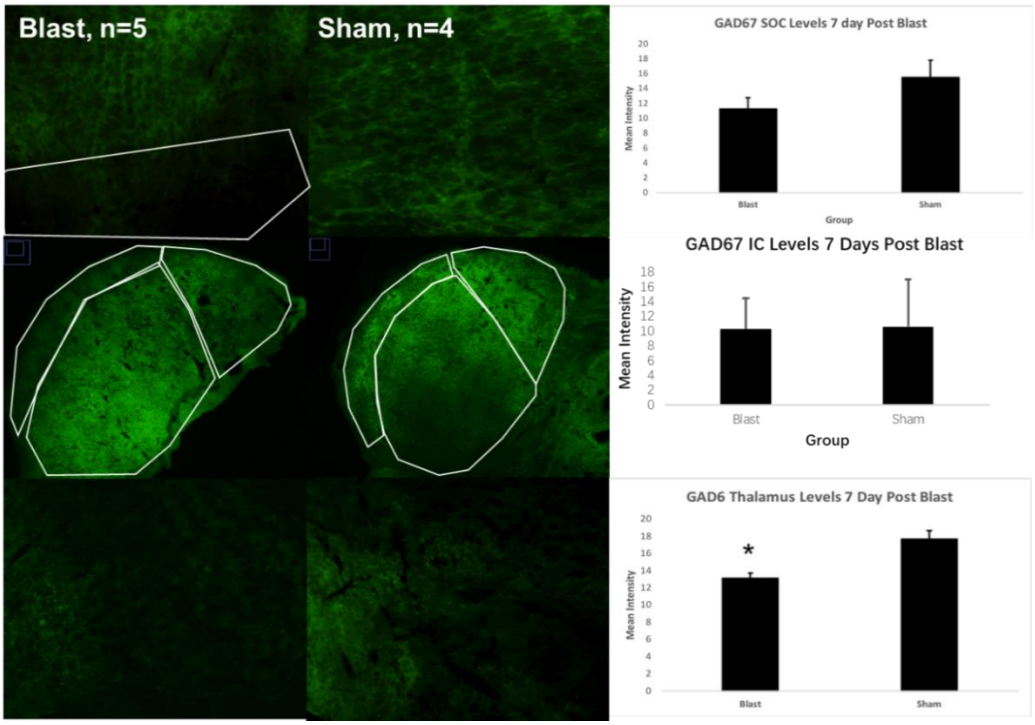

Figure 5.10. Significantly decreased GAD observed in blast-exposed thalamus compared to sham, but not in the IC or SOC. Notably, differential GABA distributions were seen in the IC, with GABA preferentially distributed in ventral CIC for blast, but in DCIC, ECIC and dorsal CIC in sham.

At 14 days post-exposure, however, all three structures displayed reversed trends in GAD compared to 2 days post-exposure. GAD decreased in the IC (Blast: Intensity =9.351194; Sham: Intensity =20.70094. p=0.094) and increased in the SOC (Blast: Intensity =33.990; Sham: Intensity =12.896. p=0.219) and thalamus (Blast: Intensity =19.497; Sham: Intensity =5.818. p=0.295) respectively, though the trends were not significant (Figure 11, left column). In all three structures, a elevation of TMR in blast compared to sham was observed in blast animals compared to sham animals, though the trend was only significant in the thalamus (Figure 11, mid column. SOC: Blast N=1679.916, Sham N=942.0087, p=0.252; IC: Blast N=1328.418, Sham N=1007.824, p=0.051; Thalamus: Blast N=1539.147, Sham N=385.518, p=0.045). Notably, variance at 14 days was high for blast animals in the SOC and the thalamus (TMR: SOC variance=483913.9, Thalamus variance=216633.3; GAD: SOC variance=316.916, Thalamus variance=209.520), showing a great degree of individuality in the recovery process of each blast animals.

5.3.5 Treatment

The effect on threshold, wave ratio and latency following HZ systemic administration to blast-exposed animals from the time of exposure to day6 post-exposure (7 days in total) were measured. IP administration of HZ had no effect on blast-induced threshold changes, showing no Time*Treatment interaction effects and no simple main effect at any point post-exposure between HZ and PBS groups. No significant repeated measures effect was observed in wave III/I and wave V/I ratios at both 80 dB SPL and 30 dB SL. In terms of wave I latency, the only significant repeated measures effect was the effect of Time ($F=5.408$, $p=0.034$, $\eta^2_p=0.351$) observed in 8 kHz ABR wave I latency at 80 dB SPL. Although *ex vivo* administration of HZ has proven to be effective in alleviating acrolein-mediated oxidative damage and loss of membrane integrity in spinal cord injury (Hamann et al. 2008b), *in vivo*, systemic administration through IP injection has almost no effect on blast-induced changes in ABR.

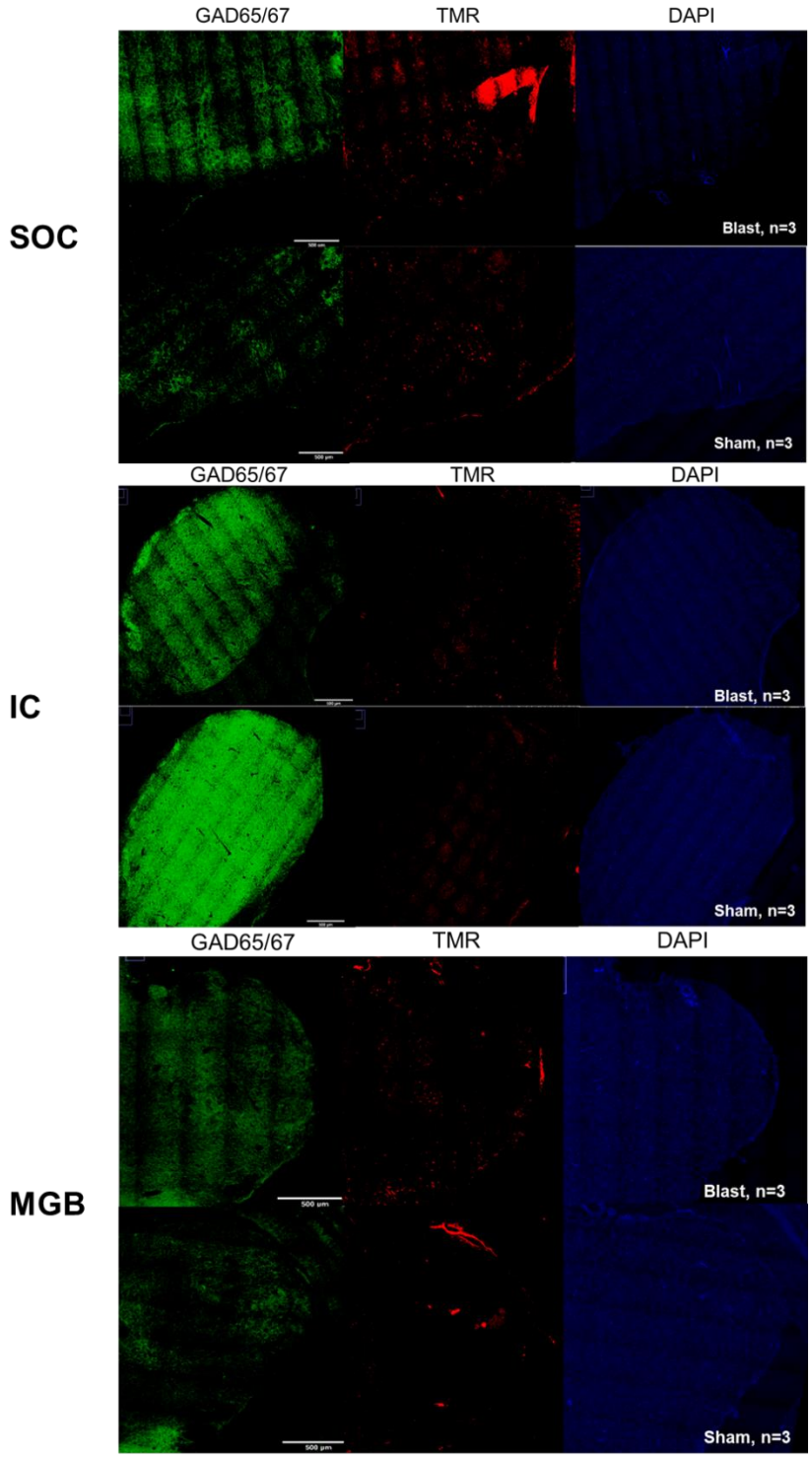

Figure 5.11. GAD (green) and TMR (red) immunohistochemistry of blast-exposed and sham rat auditory structures. Blast animals showed elevated GABA in SOC and auditory thalamus (MGB) and decreased GABA in the IC, but the trends were not significant. The auditory thalamus also showed a significant elevation of TMR. DAPI (blue) staining showed no significant difference in cell counts was observed in all structures of interest.

5.4 Discussion

5.4.1 ABR ratios and MLR amplitudes partially reflected interdependent, time-sensitive changes in subcortical inhibitory neurotransmission.

By comparing AEP wave ratio analysis result with anatomical observations, the current study attempted to pinpoint the putative cellular and neurochemical changes in various auditory structures along the auditory neuraxis that underlie blast-induced hearing deficits, as indicated by our previous studies (Race et al. 2017; Han et al. 2020). Most notably, we demonstrated that two distinct and interdependent waves of excitatory/inhibitory changes took place in the central auditory system, in early (day 1-7) and late (day 14 and onwards) time windows, respectively. The statistics and potential implications of this dynamic pattern are summarized in Figure 5.12. These findings provided novel insights to better understanding and intervention strategies of blast-induced hearing deficits in the acute-subacute and chronic phases post-injury.

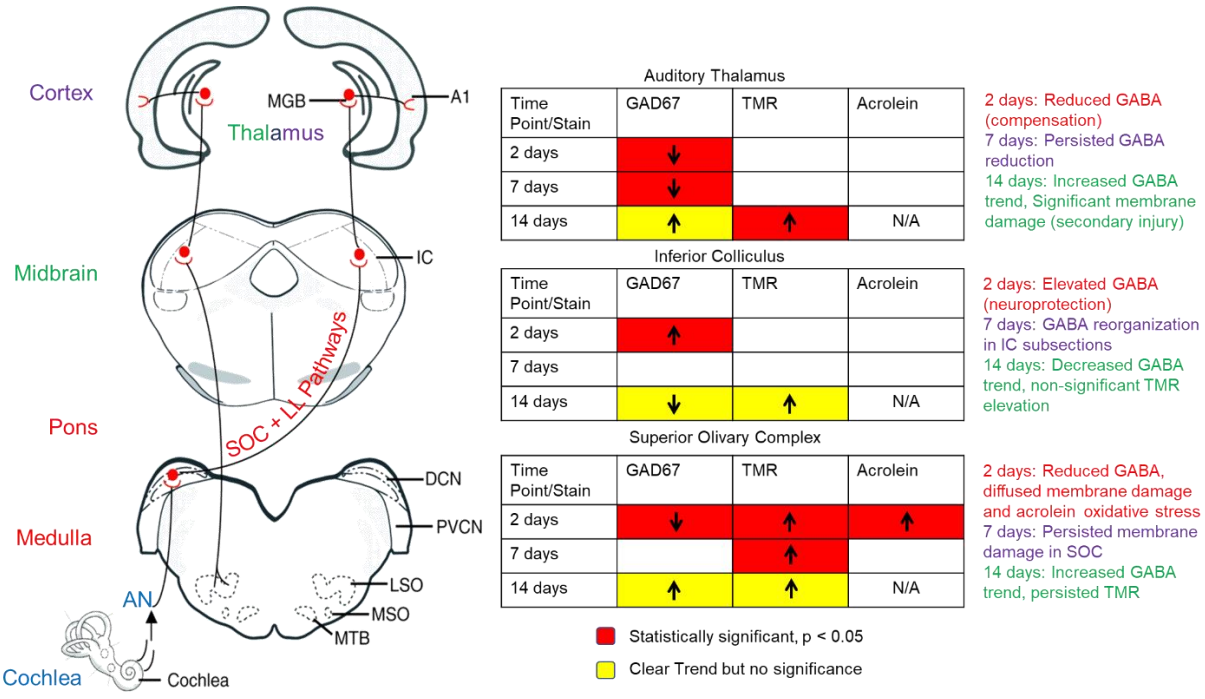

Figure 5.12. Summary schematic of blast-induced inhibitory change, membrane damage and oxidative stress over time. Auditory system drawing was adapted from Caspary et al. (2008) and Race et al. (2017).

Auditory brainstem

Decreased GABA, decreased membrane integrity, as well as a transient acrolein increase, were observed in the auditory brainstem immediately post-blast (Fig. 5.7). Superior olivary complex, being in the ventral auditory brainstem, bore the brunt of primary injuries due to blast, with TMR analysis showing diffuse membrane damage even up to 7 days post-blast. The drastic downregulation of GABA was also diffuse and may extend to the CN, as a loss of GABA inhibitory neurotransmission can be contributing to the drastic increase of wave III/I ratio at day 1 post-blast (Fig. 5.1). Our result is consistent with single-unit recordings in rats, in which blast rats showed hyperexcitability and elevated spontaneous firing rate in the CN in the acute phase (Luo et al. 2014a). Luo et al. (2014a) hypothesized that this increase in excitability could be due to inhibitory loss in the DCN, a symptom often associated with auditory-trauma induced tinnitus (Wang et al. 2009a; Middleton et al. 2011) By comparing the amplitudes of AN and CN activity, our results further strengthened the hypothesis of acute central compensation in the auditory brainstem through inhibitory loss.

Aside from direct damage to the cochlea, one source of blast-induced peripheral deafferentation that led to central excitatory/inhibitory imbalance could be auditory tract axonopathy since the elevation of TMR extends to ventral auditory tracts in the acute phase (Fig. 5.7). As acrolein is known to mediate demyelination and membrane disruption in neural injury (Hamann et al. 2008a; Shi et al. 2011), the acute increase of acrolein level observed in the auditory brainstem could be a key factor in peripheral deafferentation and indirectly contribute to interlocking excitatory/inhibitory imbalance in more central auditory structures.

Inferior colliculus

Conversely, GABA level experienced two waves of changes in the IC: during the acute phase (day 1-4), an increase of GAD65/67 was found in the IC (Fig. 5.7), particularly in the central nucleus of the IC, receiving majorly ascending projections. Although the trend seemed to subside at day 7, differential trends were observed in the IC: elevation remained in ventral CIC, and a relative decrease in dorsal regions, compared to sham (Figure 10). Considering ventral CIC is the high-frequency end of CIC's tonotopy, a lingering elevation in this region could indicate prolonged

excitotoxicity from corresponding high-frequency regions of the auditory brainstem when lower frequency regions are already recovering.

On day 14, a trend of GAD65/67 decrease was observed in the IC (Figure 5.11), though not significant (p=0.094). Because channel 2 is not favorable in measuring wave III, and channel 1 is not favorable in measuring wave V (Parthasarathy and Bartlett 2012), the electrophysiological change in central gain between the CN and the IC cannot be directly compared through our method of ABR measurement. But anatomical trends in sub-chronic and chronic phases were partially reflected in the substantial but not statistically significant increase in wave V/I ratio in Click and 8 kHz ABR at 80 dB SPL, as well as Click ABR at 30 dB SL.

Very little differences in TMR and acrolein were observed in the auditory midbrain throughout the time points of interest. It is suggested in studies using the same mild blast model (Song et al. 2015; Walls et al. 2016) that the dorsal brain, including the IC, being cushioned by the rest of the brain, receives little direct injuries compared to the ventral brain and showed negligible damage in membrane integrity. The acute upregulation of GABA in the IC was most likely secondary, a response to drastic changes in the peripheral auditory system, not dissimilar to the increase of GABA in the IC immediately after noise trauma (Abbott et al. 1999). This upregulation of GABA can be understood as a neuroprotective measure, not exclusive to the auditory system, as induced upregulation of GABA in the same acute period was beneficial to the survival and cognitive performance of TBI-impacted rats (O'Dell et al. 2000).

Auditory thalamus

Curiously, the trend of excitatory/inhibitory imbalance in the auditory thalamus was in the opposite direction to its direct upstream structure, the IC. The auditory thalamus displayed a drastic downregulation of GAD over the entire acute and sub-acute phase of blast injury, likely a result of the inhibitory increase in the IC during this period. Later on, as the trend of GABA upregulation in the IC started to turn around day 14 post-blast, the trend in the blast-exposed thalamus also turned direction to higher than sham (Fig. 5.11), though not significant (p=0.295), suggesting an excitatory/inhibitory reorganization in the thalamus in reaction to the neurochemical conditions of later post-blast stage. The reorganization process was likely still ongoing, as threshold recovery, changes in MLR and significant differences in complex sound EFR are known to appear between 14 days and 30 days post-blast (Race et al. 2017; Han et al. 2020). This is in stark contrast to the

aging auditory system, as reduced GABA neurotransmission was seen throughout the aging auditory system, from the auditory brainstem to the auditory cortex (Caspary et al. 1990, 2008, 2013; Richardson et al. 2013; Xiong et al. 2017; Caspary and Llano 2019).

Acrolein assessments also showed that changes in oxidative stress in the thalamus, at any time point of interest in this study, were non-significant. However, a significant increase in TMR particles was observed in the auditory thalamus ($p=0.045$). This later stage increase in TMR, after no significant difference was observed on day 2 and 7, suggested that this wave of compromised membrane integrity was not directed caused by primary, mechanical injury from the blast but belonged to a secondary wave of more widespread biochemical injuries and neurodegeneration that were still likely ongoing.

The reduced MLR peak amplitudes at 80 dB SPL displayed compromised thalamic, thalamocortical and cortical activation (Fig. 5.6). This is in direct comparison to the noise-induced increase in thalamocortical and cortical waves observed by Popelar et al. (Popelar et al. 2008). Blast exposure produced a compound injury to multiple structures within the auditory brainstem, producing greater compromise of transmission and activity at cortical and thalamic levels that was unable to compensate for at equal sound levels. Only at equal sensation levels, especially at later time points, did thalamocortical and cortical waves display substantial compensation (Fig. 6B).

Variance in blast AEP and anatomy

One issue in assessing blast-induced hearing loss, and blast injuries in general, was the variance between individuals, both in the distribution and the severity of injuries. Controlled blast models using animals are, therefore, necessary to isolate the various factors in blast exposure, such as blast intensity, blast angles, the age, physique, and life experience of the subjects, in order to gain a more objective understanding of blast-induced hearing loss. However, even in controlled blast exposure models, variance remains to be substantial in many auditory parameters of blast animals. The variable nature of blast injury was reflected in this current study through both electrophysiology and anatomical results. Variance in ABR threshold and spontaneous firing rate was also observed to be larger in blast-exposed rats than in control rats (Luo et al. 2014a, 2014b). These observations call into the spotlight the importance of variance between individuals when assessing blast-induced hearing deficits and blast-induced injury in general.

Because of the current study's design, we were unable to match anatomical and electrophysiological results of individual animals, as obtaining anatomical results would require the animals to be sacrificed at earlier time points, thus disabling non-invasive, longitudinal electrophysiological recordings. As the current study and our previous work (Han et al. 2020) have narrowed down the few critical turning points of blast-induced hearing loss and blast injury development in general, future studies of non-longitudinal nature that match electrophysiological and anatomical profiles of individual animals are called for, with special focus on acute and 7-10 days sub-acute time windows.

5.4.2 ABR latencies demonstrated limited blast-induced changes to neural transmission efficacy at cochlea and AN levels.

Both mechanical and neural transmission time contributes to ABR latency, which is known to decrease with increased sensation level and frequency (Neely et al. 1988; Henry et al. 2011). Blast exposure induces diffuse mechanical and biochemical changes that are hypothesized to contribute to multilocal synaptopathy, axonopathy, and demyelination (Garman et al. 2011; Walls et al. 2016; Hickman et al. 2018), all of which impact neural transmission time and may disrupt precise coding of temporal information. As such, AEP peak latencies are important parameters to look at when assessing blast-induced mechanical and biochemical damage at different levels along the auditory neuraxis.

Wave I usually exhibit a shortened latency in noise-induced hearing loss (Henry et al. 2011; Mehraei et al. 2016). The single noise exposure in our mild blast model was not enough to elicit a similar change in sham animals. Therefore, the increase of click wave I latency even at 30 dB SL in blast animals (Fig. 5.3A) was mainly the result of blast shockwave impact. Disruption in transmission latency at least partially shares the same cause as threshold increase, the source of which is likely in acute blast-induced AN neuropathy.

The difference in wave I latency disappears for the most part after day 7 post-blast (Fig. 5.3A and 5.3B), consistent with many ABR recordings in long or uncertain-term post-TBI human subjects (Podoshin et al. 1990; Gallun et al. 2012a; Washnik et al. 2019). Gallun et al. (2012a) noted that while ABR amplitudes are different between blast and non-blast subjects, neither of wave I, III or V latencies are significantly different between groups. This is in stark contrast to the significant increases in late latency response (LLR) N100 and P300 latencies between groups.

Compared to previous studies, our results highlighted the transient increase of wave I latency, as well as confirmed the lack of ABR latency changes along the auditory neuraxis between AN and the IC. It should be noted that Podoshin et al. (1990) observed that ABR latencies, especially inter-wave latencies (wave I-III, I-V and III-V latencies) in post-mTBI individuals, were sensitive to fast ABR presentation rate (55/s, compared to 10/s. The presentation rate for ABR in the current study was 33/s), suggesting the existence of complex and multilocal lesion in the white matter in TBI that may not be properly revealed through slower presentation rate.

The more significant increase of wave I latency in click compared to 8 kHz ABR could result from blast-induced damage to high-frequency auditory fibers, which through ABR latency have shown to have shorter latencies in human (Neely et al. 1988), rodents (Overbeck and Church 1992) and cats (Rhode and Smith 1985). This is consistent with our previous observation that broadband stimuli could reveal blast-induced hearing deficits more robustly than pure tone stimuli due to them encompassing these short-latency high-frequency fibers (Han et al. 2020).

Click wave I latency at equal suprathreshold SL appeared to be positively correlated with click threshold for both blast and sham (Fig 5.3B). This correlation holds true for 8 kHz wave I latencies of sham animals but not blast animals (Fig. 5.4B). A specific temporal property alteration for the 8 kHz region was likely to have taken place in the blast-exposed cochlea, resulting in shorter AN latency, as suggested by click-8 kHz latency correlation at equal sensation levels. This indication, coupled with the hypothesized damage to high-frequency auditory fibers as seen through broadband auditory measurements, suggests a novel insight towards blast-induced hearing deficits that are underrepresented in AEP tests (Gallun et al. 2012a; Bressler et al. 2017): If unequal temporal alterations happen at different frequency regions as a result of blast exposure, the disruption of synchronized temporal processing across frequency range could affect the perception of speech and other spectrotemporally complex sounds, without significant changes in simple, pure-tone auditory measurements such as ABR and EFR. This idea is in consistency with our previous study, in which deficits in speech-like iterated rippled noise processing extend beyond the first 7 days post-blast when wave I latency showed differences (Han et al. 2020). More detailed investigations into frequency-specific temporal property changes and their effect on complex sound processing are called for.

Because ABR wave I is hard to measure in human (Mehraei et al. 2016; Plack et al. 2016), previous research has established that wave V is effective in measuring noise-induced AN fiber

loss and cochlear neuropathy in rodents (Henry et al. 2011; Mehraei et al. 2016), which can be easily translated to human subjects. Our study demonstrated that at least with mild to moderate blast exposure, there was no significant difference in wave I-III or I-V latency. ABR wave III and V latencies may prove to be an effective and accessible tool in diagnosing early blast-induced cochlear and AN neuropathy in human patients.

5.4.3 Acrolein and treatment

Our results suggested that changes in acrolein oxidative marker in the auditory neuraxis are predominantly limited to the auditory brainstem. Acrolein increase was significant but transient in the auditory brainstem of blast-impacted animals, disappeared at day 7. This observation is consistent with previous research in the same mild blast rat model (Walls et al. 2016). The secondary injuries from acrolein in this mild blast model were comparably milder to spinal cord injury models in which acrolein level remained significantly elevated at 14 days post-trauma (Zheng et al. 2013; Due et al. 2014).

Administration of Hydralazine was proven to be effective in reducing acrolein levels in the spinal cord (Hamann et al. 2008b; Due et al. 2014). The lack of treatment effect, even in structures highly likely to subject to primary blast-induced oxidative stress, could be due to differences in HZ transportation to the brain compared to localized delivery in the spinal cord (Due et al. 2014), resulting in a concentration too low for effective acrolein scavenge, as suggested by Hamann et al. (2008b; 2009). Systemic administration may prove to be a suboptimal method of HZ delivery, calling for research into therapeutics with more localized delivery or more efficient pharmacokinetic properties.

5.4.4 Limitations

A series of limitations was evident in our study due to time constraints, study design and presuppositions based on previous studies.

The electrophysiological half of the current study maintained that in a controlled model of blast exposure, blast-induced changes should be similar between individual blast animals. Therefore our focus, as was in our previous studies (Race et al. 2017; Han et al. 2020), was primarily on the longitudinal recordings of blast-induced changes over time, with parallel

documentations of anatomical markers at key time points conducted separately. This focus led to our inability to match animal electrophysiology with anatomy before the end of the 60 days observation period. However, our presupposition turned out to be not true, as both AEP amplitudes and anatomical markers we observed showed considerable variation between individual animals. Our findings called for future investigations that match the electrophysiology of individual animals with their anatomical features. Notably, single-unit recording of auditory structures, combined with auditory responses such as local field potentials (LFP), was able to uncover age-related central gain mechanisms and their impact on temporal coding in the aging IC (Herrmann et al. 2017; Parthasarathy et al. 2019b). The non-recovery nature of such studies is well-suited for immediate anatomical observation after the recording session. By applying these methods at key time points post-blast, future studies may provide a better understanding of the mechanisms in which excitatory/inhibitory changes affect the coding of temporally modulated sounds.

In the current study, as well as our previous study (Han et al. 2020), our choice of method to compensate for blast-induced threshold changes was through equal sensation level at 30 dB SL, with the presupposition that changes to suprathreshold AEP amplitude-intensity function would be negligible. AEP amplitude-intensity function is a factor that could impact the effectiveness of threshold compensation through the standardization of suprathreshold sensation level. A previous study by Luo et al. observed that ABR wave I amplitude-intensity curve was only significantly altered for blast rats at 26-28 kHz (Luo et al. 2014a). Unknown changes in the amplitude-intensity function due to blast may reduce the effectiveness of our selected threshold compensation method, which was measuring at matched sensation level, with broadband carriers being more affected. This limitation could be mitigated in future studies through wave I amplitude-matching, as used in studies on age-related hearing loss (Lai et al. 2017; Lai and Bartlett 2018).

Finally, a limited time frame could not enable us to investigate the anatomical properties of several key auditory structures, such as CN and primary auditory cortex, as well as later time points of interest (30 days and 60 days). Our findings at 14 days suggested that neurochemical reorganization was likely still taking place in various auditory structures, further emphasizing the importance of anatomical observations in later time points. This limitation could be overcome through following anatomical studies, which, together with the current study, shall provide a fuller picture of the changes in excitatory/inhibitory balance as well as its impact on post-blast auditory performances.

5.5 Conclusion

By directly comparing anatomical evidence at key time points to electrophysiological recordings of blast-induced hearing deficits, we provided insights into the time-sensitive mechanisms in which the post-blast subcortical central auditory system reacts and reorganizes itself. Blast-induced cochlear neuropathy and damage to the auditory brainstem kickstart an interlocking cascade of excitatory/inhibitory changes along the auditory neuraxis. Blast injury is a sudden assault with rapidly unfolding multilocal impacts throughout the brain (Garman et al. 2011; Song et al. 2015; Walls et al. 2016), unlike the gradual, non-traumatic neurodegeneration happening in age-related hearing loss which is theorized to induce overall loss of inhibitory neurotransmission (Caspary et al. 2008). Compared to reduced pre-thalamic wave amplitudes and hyperactivity in thalamic and cortical structures in noise-induced hearing loss (Popelar et al. 2008), primarily thought to be driven by noise-induced damage limited at the levels of cochlea and AN (Hickox and Liberman 2014), the extent of blast-induced injuries also far exceeds that of noise trauma only. Most importantly, the patterns of excitatory/inhibitory within different subcortical auditory structures is compounded by blast-specific injuries to the auditory brainstem, especially to ventral structures such as the SOC and ventral axon tracks.

Our findings provided a unique synthesis of previously established mechanisms of auditory-related neurochemical changes, as manifested in the rapidly developing conditions in blast-induced hearing loss. With this time-sensitive mechanism in mind, further investigations on complex sound processing as well as individualized links between electrophysiology and anatomy is called for to facilitate the development of better diagnostic and therapeutic measures of blast injury.

CHAPTER 6. CONCLUDING REMARKS

6.1 Conclusion

Age-related deficits in central temporal processing have been previously observed in electrophysiology on a population level at various AM frequencies and various AM depths (Parthasarathy et al. 2010; Parthasarathy and Bartlett 2011, 2012). A loss of GABAergic neurotransmission in response to age-related peripheral deafferentation has been proposed to be a key driver of this central temporal processing deficit. However, in the IC, single-unit studies on AM responses from aged animals or with GABA blockage have not demonstrated this reduction of AM phase-locking performance at a given MF (Burger and Pollak 1998; Caspary et al. 2002). Chapter 3 of this dissertation described our post hoc analysis of young and aged single-unit AM responses to attenuated modulation depth. Alongside previous studies such as Herrmann et al. (2017) and Parthasarathy et al. (2019b), we addressed the apparent paradox of AM responses in aged animals: High VS in single-unit but low FFT amplitude in AMFR and LFP. Through circular analysis, we observed the effect of ARHL in AM responses manifesting as two phenomena in the IC: Across AMF decrease in excitatory neurotransmission, as assessed by reduced firing rates, that was not fully compensated by GABAergic loss, resulting in sparse spikes that overly concentrated at peak input, but at the cost of reduced dynamic range and loss of off-peak firing, evident from circular analysis; and a discrepancy between response latency, likely due to age-related neurodegeneration, resulting in peak phase discrepancies between individual aged IC neurons, which could contribute to reduced population response.

Unlike the gradual process of ARHL, BIHL is the result of sudden, traumatic assault(s), which damages not only the PAS but gradually manifests itself into a series of lasting, multilocal central auditory deficits (Gallun et al. 2012b; Race et al. 2017). Because of the sudden nature and lasting deficits, it is crucial to investigate the time course of BIHL development and recovery. In Chapter 4, we documented various AEP measurements of simple transient sounds and complex, sustained stimuli in blast-exposed animals over a two-month period, with a special focus on the acute (day 1-7) and sub-acute (day 7-14) periods. We uncovered significant changes in auditory pathophysiology and proposed a potential multi-stage recovery process in BIHL. Although simple, tonal auditory parameters mostly recovered after 2 weeks, broadband, temporally complex and

speech-like stimuli revealed that even a single mild blast could result in lasting changes in temporal processing in the CAS.

With knowledge gained from previous chapters, we proposed that an excitatory/inhibitory imbalance mechanism would contribute to BIHL. Chapter 5 aimed to link our observation of blast-induced changes in electrophysiology, as observed in Chapter 4, to anatomical markers of GABA inhibitory neurotransmission, membrane damage and acrolein-mediated oxidative stress. In stark contrast to general inhibitory loss along the auditory neuraxis observed in ARHL (Caspary et al. 1990, 2008, 2013; Richardson et al. 2013; Xiong et al. 2017; Caspary and Llano 2019), blast trauma kickstarted a dynamic and interdependent cascade of excitatory/inhibitory changes along the auditory neuraxis. Primary injuries, manifesting as loss of membrane integrity and trauma-induced acrolein oxidative stress, were mostly limited to the PAS and auditory brainstem. However, evidence showed that secondary injuries, as well as gradual excitatory/inhibitory reorganization take place in more central structures (the IC and auditory thalamus) at later stage post-blast, which was likely a main contributor to complex temporal processing deficits observed in Chapter 4.

6.2 Future Works

The findings from our first aim were complementary to similar studies from our group such as Herrmann et al. (2017) and Parthasarathy et al. (2019b), in which single-unit responses to temporally complex sounds were analyzed alongside presynaptic activity representation LFP (Bullock 1997; Buzsáki et al. 2012), with temporal periodicity and stimuli correlation in mind. Taken together, these studies illustrated potential mechanisms in which excitatory/inhibitory changes in the IC, as observed by many and theorized to affect the coding of envelope shapes in speech and other natural sounds (Caspary et al. 1995, 2008; Milbrandt et al. 1996; Helfert et al. 1999; Rabang et al. 2012). A logical future step would be to use an improved computational model of IC single-unit, based on previous studies such as Rabang et al. (2012) and Coventry et al. (2017), to recreate young and aged-like IC responses by manipulating presynaptic inputs with reference to our LFP observations. We hypothesize that through altering presynaptic input level and synaptic conductance of NMDA, AMPA and GABA to fit the age-related changes as observed in Chapter 3 and previous studies (Herrmann et al. 2017; Parthasarathy et al. 2019b), replicating the increase in VS, reduction in dynamic range modulation depth sensitivity would be possible. This would confirm the theories as illustrated by our previous studies, and provide insights to novel therapeutic

applications such as improved algorithms for hearing aids and auditory midbrain implants (Lim et al. 2009).

The study for our second aim carefully documented the electrophysiological properties of blast-exposed rats at various time points post exposure. This study, a natural expansion on Race et al. (2017), identified the physiological and clinical importance of the acute period immediate following exposure (day 1 – 7), where drastic changes in electrophysiological responses in the auditory system take place, as suggested by previous anatomical studies (Song et al. 2015; Walls et al. 2016), as well as the period between day 7 and 14, where the auditory system experiences a wave of early recovery. The study of our third aim further confirmed that this recovery period is a turning point in blast-induced excitatory/inhibitory imbalance. However, in both aim 2 and aim 3 studies, variance between individual animals, even in a controlled blast model, presented a major limitation to the significance in our findings, thereby limiting the application of these findings on human patients, whose conditions of blast injuries could only be more variable. Although variability in the extent of primary injuries can been accounted for through careful implementation of dose-response curves, similar to the Bowen curves used in pulmonary blast models (Bowen et al. 1968), it has been noted that these curves are ill-fitted predicting secondary and chronic biological changes (Watts et al. 2019). Minuscule differences in initial condition and during recovery, through multivariate interaction with the complex and dynamic process of blast injury development, can lead to significant variance in late-term symptoms. In the current study, this variance is present in both electrophysiology and anatomy. Therefore, it is reasonable to hypothesize that electrophysiological performances in an individual blasted animal should correlate closely to its anatomical profiles. As our studies have identified key post-blast time points, future studies could reduce the time points of interest to only day 1 or 2, day 7, and later time points such as day 14, 30 and 60, and conduct immunohistochemistry studies from harvested brain immediately after collecting electrophysiological data at one of these key time points.

Among potential electrophysiological studies to accompany individual anatomical profiling, single-unit recording on blast-exposed rats at key points, with LFP and circular analysis in mind, would be a perfect candidate. Although chapter 4 of this dissertation, as well as AMFR research focusing on blast-impacted human patients (Bressler et al. 2017) have shown mixed results, our results in IRN periodicity-tracking and stimuli cross-correlation have certainly showed promise in temporally complex stimuli uncovering blast-induced temporal processing deficits. An array of

temporally modulated and speech-like stimuli, such as AM ramp-damp envelope shape stimuli and voice-onset time stimuli that have been used in age-related hearing loss research (Herrmann et al. 2017; Parthasarathy et al. 2019b), can be easily incorporated into single-unit BIHL studies. Blast-induced central hearing deficits may manifest in excitatory/inhibitory change models that are vastly different from that of ARHL. Specifically, in mild blast cases without sustained, clinically significant shifts in hearing thresholds, an increase of excitability and activity is common in auditory structures, as observed by Luo et al. (2014a, 2014b, 2017); whereas general neurodegeneration and reduced excitatory and inhibitory neurotransmission in ARHL results in an across-the-board reduction in auditory-evoked activity. Future study may utilize these single-unit temporal modulation paradigms to uncover the precise mechanisms in which different auditory structures alter their temporal coding properties as a result of blast-specific and time-sensitive excitatory/inhibitory imbalance.

As a part of the study for aim 3, we tested the efficacy of HZ in treating acrolein-mediated oxidative stress in the blast-exposed rat auditory system. IP administration of HZ had little result on blast-induced hearing threshold change, ABR amplitudes and ABR latencies. As HZ has been proved to be effective in treating TBI-induced acrolein oxidative stress damage in an *ex vivo* spinal cord injury model (Hamann et al. 2008b), and that acrolein is strongly present in blast-exposed auditory midbrain, the reason that our administration of HZ had no effect on ABR could thereby lie in delivery method. Ewert et al. (2012) were successful in delivering N-acetylcysteine (NAC) and 2,4 - disulfonyl α-phenyl tertiary butyl nitrone (HPN-07) to the cochlea with observed effects alleviating blast-induced cochlear damage and hearing loss. Similarly, oral administration of aldosterone has been effective in enhancing spiral ganglion cell survival, preventing autoimmune hearing loss and age-related cochlear apoptosis (Trune et al. 2000; Frisina et al. 2016). However, HZ could follow a different pharmacokinetic mechanism, thereby rendering systemic administration less effective in auditory structures, as Hamann and Shi (2009) suggested. Future studies interested in utilizing the acrolein-scavenging property of HZ and other hydrazines should consider localized delivery methods in order to achieve better effect. An accompanying immunohistochemistry investigation on the auditory structures of HZ-treated blast-exposed animals would further help us determine the transportation, metabolism, and effect of HZ in the auditory system.

Since blast injury is a rapidly developing condition, biochemical changes that are results of damage and changes that are responsive or protective could exist simultaneously, complicating our understanding towards the mechanisms of blast injury and recovery. The co-localization of membrane damage and oxidative stress with neurochemical changes in the SOC observed in Chapter 5 provided potential causes of certain excitatory/inhibitory alterations, and the results generally echoed with previous studies on blast-induced change in inhibitory neurotransmission (Cantu et al. 2015; Guerriero et al. 2015; Wang et al. 2018). However, these results were not sufficient to directly determine whether these changes were pathological, or protective measures towards the injuries, or compensatory responses towards hearing deficits. One way to obtain direct evidence on the role of GABA in the blast-exposed brain is through positive and negative regulation of GABA neurotransmission at different time points. Through the use of $GABA_A$ positive modulator diazepam, and GABA antagonist bicuculline, O'Dell et al. (2000) demonstrated the effect of time-sensitive GABA regulation on TBI-induced mortality and behavioral deficits, providing evidence of the neuroprotective role of GABA in TBI. Future studies may employ GABA-modulating drugs at key time points of BIHL development laid out by Chapter 4 and 5, and through anatomical, electrophysiological, and behavioral comparisons, will be able to separate pathological, responsive, and protective excitatory/inhibitory changes in BIHL.

APPENDIX. SUPPLEMENTARY FIGURES

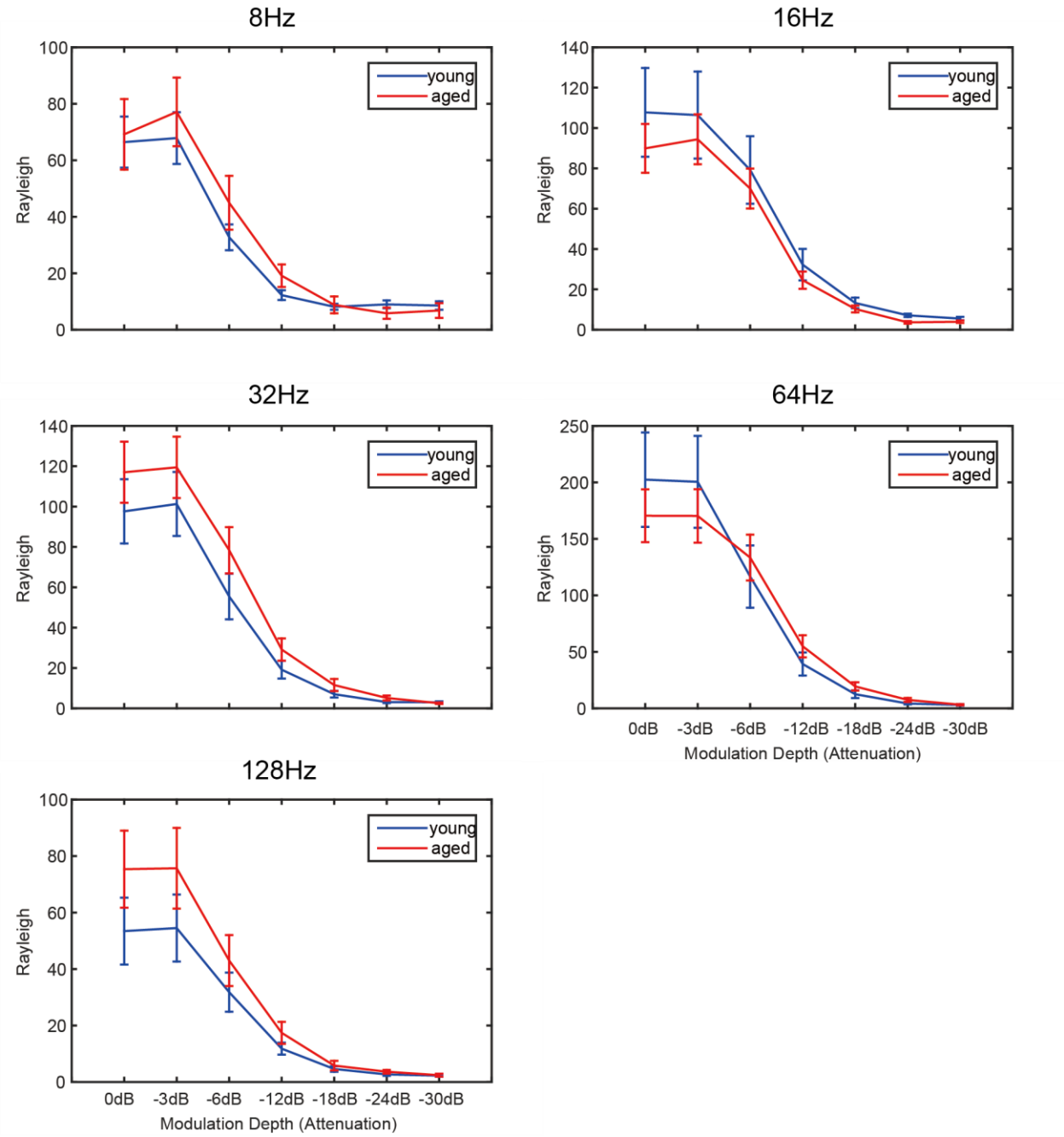

Figure A1. Rayleigh statistics of young and aged AM depth units, breakdown by modulation frequency.

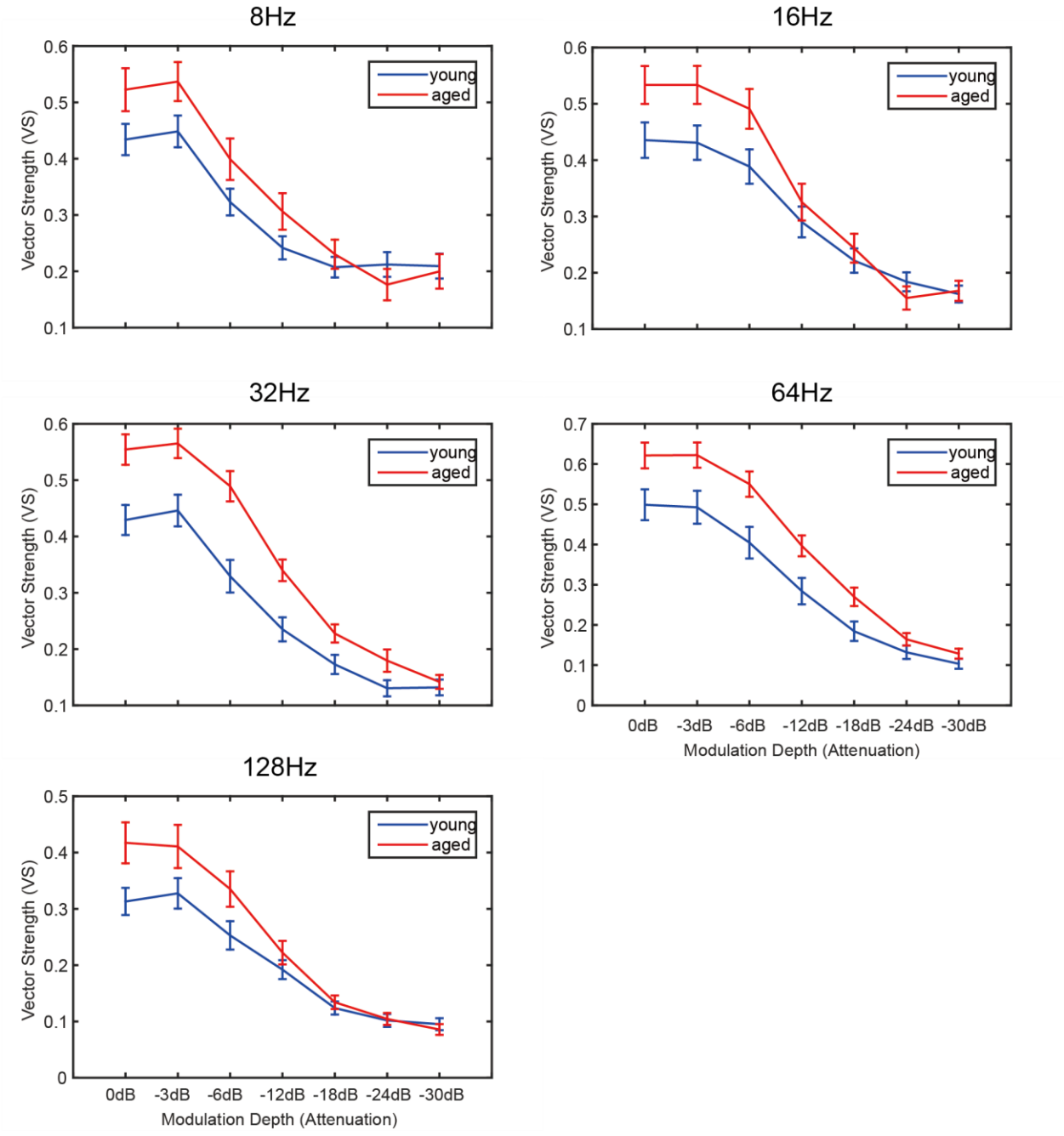

Figure A2. Vector strength of young and aged AM depth units, breakdown by modulation frequency.

REFERENCES

Abbott SD, **Hughes LF**, **Bauer CA**, **Salvi R**, **Caspary DM**. Detection of glutamate decarboxylase isoforms in rat inferior colliculus following acoustic exposure. *Neuroscience* 93: 1375–1381, 1999.

Adams JC. Ascending projections to the inferior colliculus. *J Comp Neurol* 183: 519–538, 1979.

Alsindi S, **Patterson RD**, **Sayles M**, **Winter IM**. The responses of single units to simple and complex sounds from the superior olivary complex of the Guinea pig. In: *Acta Acustica united with Acustica*. S. Hirzel Verlag GmbH, 2018, p. 856–859.

Alvarado JC, **Fuentes-Santamaría V**, **Jareño-Flores T**, **Blanco JL**, **Juiz JM**. Normal variations in the morphology of auditory brainstem response (ABR) waveforms: A study in wistar rats. *Neurosci Res* 73: 302–311, 2012.

Anderson S, **Parbery-Clark A**, **White-Schwoch T**, **Drehobl S**, **Kraus N**. Effects of hearing loss on the subcortical representation of speech cues. *J Acoust Soc Am* 133: 3030–3038, 2013a.

Anderson S, **Parbery-Clark A**, **White-Schwoch T**, **Kraus N**. Aging affects neural precision of speech encoding. *J Neurosci* 32: 14156–14164, 2012.

Anderson S, **Parbery-Clark A**, **White-Schwoch T**, **Kraus N**. Auditory brainstem response to complex sounds predicts self-reported speech-in-noise performance. *J Speech, Lang Hear Res* 56: 31–43, 2013b.

Anderson S, **Skoe E**, **Chandrasekaran B**, **Kraus N**. Neural timing is linked to speech perception in noise. *J Neurosci* 30: 4922–4926, 2010.

Ayala YA, **Malmierca MS**. The effect of inhibition on stimulus-specific adaptation in the inferior colliculus. *Brain Struct Funct* 223: 1391–1407, 2018.

Banay-Schwartz M, **Lajtha A**, **Palkovits M**. Changes with aging in the levels of amino acids in rat CNS structural elements II. Taurine and small neutral amino acids. *Neurochem Res* 14: 563–570, 1989.

Barbour DL, **Wang X**. Auditory cortical responses elicited in awake primates by random spectrum stimuli. *J Neurosci* 23: 7194–206, 2003.

Barth DS, **Shi Di**. The functional anatomy of middle latency auditory evoked potentials. *Brain Res* 565: 109–115, 1991.

Bartlett EL. The organization and physiology of the auditory thalamus and its role in processing acoustic features important for speech perception. *Brain Lang* 126: 29–48, 2013.

Bartlett EL, **Sadagopan S**, **Wang X**. Fine frequency tuning in monkey auditory cortex and thalamus. *J Neurophysiol* 106: 849–859, 2011.

Bartlett EL, **Stark JM**, **Guillery RW**, **Smith PH**. Comparison of the fine structure of cortical and collicular terminals in the rat medial geniculate body. *Neuroscience* 100: 811–828, 2000.

Bartlett EL, **Wang X**. Correlation of neural response properties with auditory thalamus subdivisions in the awake marmoset. *J Neurophysiol* 105: 2647–67, 2011.

Bauer CA, **Brozoski TJ**, **Holder TM**, **Caspary DM**. Effects of chronic salicylate on GABAergic activity in rat inferior colliculus. *Hear Res* 147: 175–182, 2000.

Bauer CA, **Turner JG**, **Caspary DM**, **Myers KS**, **Brozoski TJ**. Tinnitus and inferior colliculus activity in chinchillas related to three distinct patterns of cochlear trauma. *J Neurosci Res* 86: 2564–2578, 2008.

Le Beau FE, **Rees A**, **Malmierca MS**. Contribution of GABA- and glycine-mediated inhibition to the monaural temporal response properties of neurons in the inferior colliculus. *J Neurophysiol* 75, 1996.

Bendor D, **Wang X**. The neuronal representation of pitch in primate auditory cortex. *Nature* 436: 1161–1165, 2005.

Berens P. CircStat: A MATLAB toolbox for circular statistics. *J Stat Softw* 31: 1–21, 2009.

Berger G, **Finkelstein Y**, **Avraham S**, **Himmelfarb M**. Patterns of hearing loss in non-explosive blast injury of the ear. *J Laryngol Otol* 111: 1137–1141, 1997.

Bharadwaj HM, **Masud S**, **Mehraei G**, **Verhulst S**, **Shinn-Cunningham BG**. Individual differences reveal correlates of hidden hearing deficits. *J Neurosci* 35: 2161–2172, 2015.

Bidelman GM, **Villafuerte JW**, **Moreno S**, **Alain C**. Age-related changes in the subcortical-cortical encoding and categorical perception of speech. *Neurobiol Aging* 35: 2526–2540, 2014.

Boettcher F a, **Poth E a**, **Mills JH**, **Dubno JR**. The amplitude-modulation following response in young and aged human subjects. *Hear Res* 153: 32–42, 2001.

Bowen IG, **Fletcher ER**, **Richmond DR**. *Estimate of man's tolerance to the direct effects of air blast*. 1968.

Boyen K, **de Kleine E**, **van Dijk P**, **Langers DRM**. Tinnitus-related dissociation between cortical and subcortical neural activity in humans with mild to moderate sensorineural hearing loss. *Hear Res* 312: 48–59, 2014.

Bramhall NF, **Konrad-Martin D**, **McMillan GP**, **Griest SE**. Auditory Brainstem Response Altered in Humans with Noise Exposure Despite Normal Outer Hair Cell Function. *Ear Hear* 38: e1–e12, 2017.

Bramhall NF, **Niemczak CE**, **Kampel SD**, **Billings CJ**, **McMillan GP**. Evoked Potentials Reveal Noise Exposure–Related Central Auditory Changes Despite Normal Audiograms. *Am J Audiol* 29: 152–164, 2020.

Bregman AS, **Liao C**, **Levitan R**. Auditory grouping based on fundamental frequency and formant peak frequency. *Can J Psychol* 44: 400–413, 1990.

Bressler S, **Goldberg H**, **Shinn-Cunningham B**. Sensory coding and cognitive processing of sound in Veterans with blast exposure. *Hear Res* 349: 98–110, 2017.

Brett B, **Krishnan G**, **Barth DS**. The effects of subcortical lesions on evoked potentials and spontaneous high frequency (gamma-band) oscillating potentials in rat auditory cortex. *Brain Res* 721: 155–166, 1996.

Bullock TH. Signals and signs in the nervous system: The dynamic anatomy of electrical activity is probably information-rich. *Proc Natl Acad Sci U S A* 94: 1–6, 1997.

Burcham PC, **Kerr PG**, **Fontaine F**. The antihypertensive hydralazine is an efficient scavenger of acrolein. *Redox Rep* 5: 47–49, 2000.

Burcham PC, **Pyke SM**. Hydralazine inhibits rapid acrolein-induced protein oligomerization: Role of aldehyde scavenging and adduct trapping in cross-link blocking and cytoprotection. *Mol Pharmacol* 69: 1056–1065, 2006.

Burger RM, **Pollak GD**. Analysis of the role of inhibition in shaping responses to sinusoidally amplitude-modulated signals in the inferior colliculus. *J Neurophysiol* 80: 1686–1701, 1998.

Burianova J, **Ouda L**, **Profant O**, **Syka J**. Age-related changes in GAD levels in the central auditory system of the rat. *Exp Gerontol* 44: 161–9, 2009.

Buzsáki G, **Anastassiou CA**, **Koch C**. The origin of extracellular fields and currents-EEG, ECoG, LFP and spikes. *Nat. Rev. Neurosci.* 13Nature Publishing Group: 407–420, 2012.

Cant NB, **Benson CG**. Parallel auditory pathways: Projection patterns of the different neuronal populations in the dorsal and ventral cochlear nuclei. *Brain Res. Bull.* 60Elsevier Inc.: 457–474, 2003.

Cantu D, **Walker K**, **Andresen L**, **Taylor-Weiner A**, **Hampton D**, **Tesco G**, **Dulla CG**. Traumatic Brain Injury Increases Cortical Glutamate Network Activity by Compromising GABAergic Control. *Cereb Cortex* 25: 2306–2320, 2015.

Caspary DM, **Holder TM**, **Hughes LF**, **Milbrandt JC**, **McKernan RM**, **Naritoku DK**. Age-related changes in GABA(A) receptor subunit composition and function in rat auditory system. *Neuroscience* 93: 307–12, 1999.

Caspary DM, **Hughes LF**, **Ling LL**. Age-related GABAA receptor changes in rat auditory cortex. *Neurobiol Aging* 34: 1486–96, 2013.

Caspary DM, **Ling L**, **Turner JG**, **Hughes LF**. Inhibitory neurotransmission, plasticity and aging in the mammalian central auditory system. *J Exp Biol* 211: 1781–1791, 2008.

Caspary DM, **Llano DA**. Aging Processes in the Subcortical Auditory System. 2019.

Caspary DM, **Milbrandt JC**, **Helfert RH**. Central auditory aging: GABA changes in the inferior colliculus. *Exp Gerontol* 30: 349–360, 1995.

Caspary DM, **Palombi PS**, **Hughes LF**. GABAergic inputs shape responses to amplitude modulated stimuli in the inferior colliculus. *Hear Res* 168: 163–173, 2002.

Caspary DM, **Raza A**, **Lawhorn Armour BA**, **Pippin J**, **Arneric SP**. Immunocytochemical and neurochemical evidence for age-related loss of GABA in the inferior colliculus: Implications for neural presbycusis. *J Neurosci* 10: 2363–2372, 1990.

Caspary DM, **Schatteman T a**, **Hughes LF**. Age-related changes in the inhibitory response properties of dorsal cochlear nucleus output neurons: role of inhibitory inputs. *J Neurosci* 25: 10952–9, 2005.

Cave K, **Cornish EM**, **Chandler DW**. Blast Injury of the Ear: Clinical Update from the Global War on Terror. *Mil Med* 172: 726–730, 2007.

Chait M, **Greenberg S**, **Arai T**, **Simon JZ**, **Poeppel D**. Multi-time resolution analysis of speech: Evidence from psychophysics. *Front Neurosci* 9: 214, 2015.

Chambers AR, **Resnik J**, **Yuan Y**, **Whitton JP**, **Edge AS**, **Liberman MC**, **Polley DB**. Central Gain Restores Auditory Processing following Near-Complete Cochlear Denervation. *Neuron* 89: 867–879, 2016.

Chavko M, **Watanabe T**, **Adeeb S**, **Lankasky J**, **Ahlers ST**, **McCarron RM**. Relationship between orientation to a blast and pressure wave propagation inside the rat brain. *J Neurosci Methods* 195: 61–66, 2011.

Chen C, **Rodriguez FC**, **Read HL**, **Escabí M a**. Spectrotemporal sound preferences of neighboring inferior colliculus neurons: implications for local circuitry and processing. *Front Neural Circuits* 6: 62, 2012.

Cho HJ, **Sajja VSSS**, **VandeVord PJ**, **Lee YW**. Blast induces oxidative stress, inflammation, neuronal loss and subsequent short-term memory impairment in rats. *Neuroscience* 253: 9–20, 2013a.

Cho S Il, **Gao SS**, **Xia A**, **Wang R**, **Salles FT**, **Raphael PD**, **Abaya H**, **Wachtel J**, **Baek J**, **Jacobs D**, **Rasband MN**, **Oghalai JS**. Mechanisms of Hearing Loss after Blast Injury to the Ear. *PLoS One* 8, 2013b.

Choi CH. Mechanisms and treatment of blast induced hearing loss. *Korean J. Audiol.* 16Korean Audiological Society: 103–107, 2012.

Cohen JT, **Ziv G**, **Bloom J**, **Zikk D**, **Rapoport Y**, **Himmelfarb MZ**. Blast injury of the ear in a confined space explosion: Auditory and vestibular evaluation. *Isr Med Assoc J* 4: 559–562, 2002.

Coventry BS, **Parthasarathy A**, **Sommer AL**, **Bartlett EL**. Hierarchical winner-take-all particle swarm optimization social network for neural model fitting. *J Comput Neurosci* 42: 71–85, 2017.

Dal Cengio Leonardi A, **Keane NJ**, **Bir CA**, **Ryan AG**, **Xu L**, **VandeVord PJ**. Head orientation affects the intracranial pressure response resulting from shock wave loading in the rat. *J Biomech* 45: 2595–2602, 2012.

Daube C, **Ince RAA**, **Gross J**. Simple Acoustic Features Can Explain Phoneme-Based Predictions of Cortical Responses to Speech. *Curr Biol* 29: 1924-1937.e9, 2019.

Davies RA. Audiometry and other hearing tests. In: *Handbook of Clinical Neurology*. Elsevier B.V., 2016, p. 157–176.

Deiber MP, **Ibañez V**, **Fischer C**, **Perrin F**, **Mauguière F**. Sequential mapping favours the hypothesis of distinct generators for Na and Pa middle latency auditory evoked potentials. *Electroencephalogr Clin Neurophysiol Evoked Potentials* 71: 187–197, 1988.

Deng D, **Masri S**, **Yao L**, **Ma X**, **Cao X**, **Yang S**, **Bao S**, **Zhou Q**. Increasing endogenous activity of NMDARs on GABAergic neurons increases inhibition, alters sensory processing and prevents noise-induced tinnitus. *Sci Rep* 10: 1–13, 2020.

DePalma RG, **Burris DG**, **Champion HR**, **Hodgson MJ**. Current concepts: Blast injuries. *N. Engl. J. Med.* 352Massachusetts Medical Society: 1335–1342, 2005.

Di S, **Barth DS**. The functional anatomy of middle-latency auditory evoked potentials: Thalamocortical connections. *J Neurophysiol* 68: 425–431, 1992.

Dimitrijevic A, **Alsamri J**, **John MS**, **Purcell D**, **George S**, **Zeng FG**. Human envelope following responses to amplitude modulation: Effects of aging and modulation depth. *Ear Hear* 37: e322–e335, 2016.

Drullman R, **Festen JM**, **Houtgast T**. Effect of temporal modulation reduction on spectral contrasts in speech. *J Acoust Soc Am* 99: 2358–2364, 1996.

Drummond GB. Reporting ethical matters in *The Journal of Physiology* : standards and advice. *J Physiol* 587: 713–719, 2009.

Du X, **Ewert DL**, **Cheng W**, **West MB**, **Lu J**, **Li W**, **Floyd RA**, **Kopke RD**. Effects of antioxidant treatment on blast-induced brain injury. *PLoS One* 8: e80138, 2013.

Dubno JR, **Eckert MA**, **Lee FS**, **Matthews LJ**, **Schmiedt RA**. Classifying human audiometric phenotypes of age-related hearing loss from animal models. *JARO - J Assoc Res Otolaryngol* 14: 687–701, 2013.

Due MR, **Park J**, **Zheng L**, **Walls M**, **Allette YM**, **White FA**, **Shi R**. Acrolein involvement in sensory and behavioral hypersensitivity following spinal cord injury in the rat. *J Neurochem* 128: 776–786, 2014.

El-Badry MM, **Ding DL**, **McFadden SL**, **Eddins AC**. Physiological effects of auditory nerve myelinopathy in chinchillas. *Eur J Neurosci* 25: 1437–1446, 2007.

Engineer CT, **Perez CA**, **Chen YTH**, **Carraway RS**, **Reed AC**, **Shetake JA**, **Jakkamsetti V**, **Chang KQ**, **Kilgard MP**. Cortical activity patterns predict speech discrimination ability. *Nat Neurosci* 11: 603–608, 2008.

Escabí M a, **Schreiner CE**. Nonlinear spectrotemporal sound analysis by neurons in the auditory midbrain. *J Neurosci* 22: 4114–31, 2002.

Ewert DL, **Lu J**, **Li W**, **Du X**, **Floyd R**, **Kopke R**. Antioxidant treatment reduces blast-induced cochlear damage and hearing loss. *Hear Res* 285: 29–39, 2012.

Felix RA, **Gourévitch B**, **Portfors C V.** Subcortical pathways: Towards a better understanding of auditory disorders. *Hear Res* 362: 48–60, 2018.

Frati A, **Cerretani D**, **Fiaschi AI**, **Frati P**, **Gatto V**, **La Russa R**, **Pesce A**, **Pinchi E**, **Santurro A**, **Fraschetti F**, **Fineschi V**. Diffuse axonal injury and oxidative stress: A comprehensive review. *Int J Mol Sci* 18: 2600, 2017.

Frisina DR, **Frisina RD**. Speech recognition in noise and presbycusis: relations to possible neural mechanisms. *Hear Res* 106: 95–104, 1997.

Frisina RD. Subcortical neural coding mechanisms for auditory temporal processing. *Hear Res* 158: 1–27, 2001.

Frisina RD, **Ding B**, **Zhu X**, **Walton JP**. Age-related hearing loss: Prevention of threshold declines, cell loss and apoptosis in spiral ganglion neurons. *Aging (Albany NY)* 8: 2081–2099, 2016.

Frisina RD, **Walton JP**, **Lynch-Armour MA**, **Byrd JD**. Inputs to a physiologically characterized region of the inferior colliculus of the young adult CBA mouse. *Hear Res* 115: 61–81, 1998.

Frisina RD, **Walton JP**, **Lynch-Armour MA**, **Klotz DA**. Efferent projections of a physiologically characterized region of the inferior colliculus of the young adult CBA mouse. *J Acoust Soc Am* 101: 2741–2753, 1997.

Fulbright ANC, **Le Prell CG**, **Griffiths SK**, **Lobarinas E**. Effects of Recreational Noise on Threshold and Suprathreshold Measures of Auditory Function. *Semin Hear* 38: 298–318, 2017.

Gallun FJ, **Diedesch AC**, **Kubli LR**, **Walden TC**, **Folmer RL**, **Samantha Lewis S**, **McDermott DJ**, **Fausti SA**, **Leek MR**. Performance on tests of central auditory processing by individuals exposed to high-intensity blasts. *J Rehabil Res Dev* 49: 1005–1024, 2012a.

Gallun FJ, **Lewis MS**, **Folmer RL**, **Diedesch AC**, **Aud ;**, **Kubli LR**, **McDermott DJ**, **Walden TC**, **Fausti S a**, **Lew HL**, **Leek MR**. Implications of blast exposure for central auditory function: a review. *J Rehabil Res Dev* 49: 1059–74, 2012b.

Garcia-Lazaro JA, **Belliveau LAC**, **Lesica NA**. Independent population coding of speech with sub-millisecond precision. *J Neurosci* 33: 19362–19372, 2013.

Garman RH, **Jenkins LW**, **Switzer RC**, **Bauman RA**, **Tong LC**, **Swauger P V.**, **Parks SA**, **Ritzel D V.**, **Dixon CE**, **Clark RSB**, **Bayır H**, **Kagan V**, **Jackson EK**, **Kochanek PM**. Blast Exposure in Rats with Body Shielding Is Characterized Primarily by Diffuse Axonal Injury. *J Neurotrauma* 28: 947–959, 2011.

Gates G a, **Mills JH**. Presbycusis. *Lancet* 366: 1111–20, 2005.

Gates GA, **Caspary DM**, **Clark W**, **Pillsbury HC**, **Brown SC**, **Dobie RA**. Presbycusis. *Otolaryngol Neck Surg* 100: 266–271, 1989.

Gaumond RP, **Molnar CE**, **Kim DO**. Stimulus and recovery dependency of cat cochlear nerve fiber spike discharge probability. *J Neurophysiol* 48: 856–873, 1982.

Geneva: World Health Organization. Addressing The Rising Prevalence of Hearing Loss. .

Godfrey DA, **Jin YM**, **Liu X**, **Godfrey MA**. Effects of cochlear ablation on amino acid levels in the rat cochlear nucleus and superior olive. *Hear Res* 309: 44–54, 2014.

Goossens T, **Vercammen C**, **Wouters J**, **van Wieringen A**. Aging affects neural synchronization to speech-related acoustic modulations. *Front Aging Neurosci* 8: 133, 2016.

Goossens T, **Vercammen C**, **Wouters J**, **van Wieringen A**. Neural envelope encoding predicts speech perception performance for normal-hearing and hearing-impaired adults. *Hear Res* 370: 189–200, 2018.

Gorga MP, **Kaminski JR**, **Beauchaine KA**, **Jesteadt W**. Auditory brainstem responses to tone bursts in normally hearing subjects. *J Speech Hear Res* 31: 87–97, 1988.

Greenhouse SW, **Geisser S**. On methods in the analysis of profile data. *Psychometrika* 24: 95–112, 1959.

Grinn SK, **Wiseman KB**, **Baker JA**, **Le Prell CG**. Hidden hearing loss? No effect of common recreational noise exposure on cochlear nerve response amplitude in humans. *Front Neurosci* 11: 465, 2017.

Grose JH, **Buss E**, **Elmore H**. Age-Related Changes in the Auditory Brainstem Response and Suprathreshold Processing of Temporal and Spectral Modulation. *Trends Hear* 23: 233121651983961, 2019.

Grose JH, **Mamo SK**, **Hall JW**. Age effects in temporal envelope processing: Speech unmasking and auditory steady state responses. *Ear Hear* 30: 568–575, 2009.

Guerriero RM, **Giza CC**, **Rotenberg A**. Glutamate and GABA Imbalance Following Traumatic Brain Injury. *Curr Neurol Neurosci Rep* 15: 1–11, 2015.

Guest H, **Munro KJ**, **Prendergast G**, **Millman RE**, **Plack CJ**. Impaired speech perception in noise with a normal audiogram: No evidence for cochlear synaptopathy and no relation to lifetime noise exposure. *Hear Res* 364: 142–151, 2018.

Van Haesendonck G, **Van Rompaey V**, **Gilles A**, **Topsakal V**, **Van de Heyning P**. Otologic Outcomes After Blast Injury: The Brussels Bombing Experience. *Otol Neurotol* 39: 1250–1255, 2018.

Hamann K, **Durkes A**, **Ouyang H**, **Uchida K**, **Pond A**, **Shi R**. Critical role of acrolein in secondary injury following ex vivo spinal cord trauma. *J Neurochem* 107: 712–721, 2008a.

Hamann K, **Nehrt G**, **Ouyang H**, **Duerstock B**, **Shi R**. Hydralazine inhibits compression and acrolein-mediated injuries in ex vivo spinal cord. *J Neurochem* 104: 708–718, 2008b.

Hamann K, **Shi R**. Acrolein scavenging: A potential novel mechanism of attenuating oxidative stress following spinal cord injury. *J Neurochem* 111: 1348–1356, 2009.

Han EX, **Fernandez JM**, **Swanberg C**, **Shi R**, **Bartlett EL**. Longitudinal auditory pathophysiology following mild blast induced trauma. *bioRxiv* bioRxiv2020.

Hannula S, **Bloigu R**, **Majamaa K**, **Sorri M**, **Mki-Torkko E**. Audiogram configurations among older adults: Prevalence and relation to self-reported hearing problems. *Int J Audiol* 50: 793–801, 2011.

Harkrider AW, **Plyler PN**, **Hedrick MS**. Effects of age and spectral shaping on perception and neural representation of stop consonant stimuli. *Clin Neurophysiol* 116: 2153–64, 2005.

Harris KC, **Dubno JR**. Age-related deficits in auditory temporal processing: unique contributions of neural dyssynchrony and slowed neuronal processing. *Neurobiol Aging* 53: 150–158, 2017.

Harris KC, **Wilson S**, **Eckert MA**, **Dubno JR**. Human evoked cortical activity to silent gaps in noise: Effects of age, attention, and cortical processing speed. *Ear Hear* 33: 330–339, 2012.

Hashimoto T, **Maze M**, **Ohashi Y**, **Fujinaga M**. Nitrous oxide activates GABAergic neurons in the spinal cord in Fischer rats. *Anesthesiology* 95: 463–469, 2001.

He N, **Mills JH**, **Ahlstrom JB**, **Dubno JR**. Age-related differences in the temporal modulation transfer function with pure-tone carriers. *J Acoust Soc Am* 124: 3841–3849, 2008.

Heeringa AN, **van Dijk P**. The immediate effects of acoustic trauma on excitation and inhibition in the inferior colliculus: A Wiener-kernel analysis. *Hear Res* 331: 47–56, 2016.

Heil P, **Peterson AJ**. Basic response properties of auditory nerve fibers: a review. *Cell Tissue Res.* 361Springer Verlag: 129–158, 2015.

Helfer KS, **Bartlett EL**, **Popper AN**, **Fay RR**. *Aging and Hearing: Causes and Consequences*. 2020.

Helfert RH, **Krenning J**, **Wilson TS**, **Hughes LF**. Age-related synaptic changes in the anteroventral cochlear nucleus of Fischer-344 rats. *Hear Res* 183: 18–28, 2003.

Helfert RH, **Sommer TJ**, **Meeks J**, **Hofstetter P**, **Hughes LF**. Age-related synaptic changes in the central nucleus of the inferior colliculus of Fischer-344 rats. *J Comp Neurol* 406: 285–298, 1999.

Henry KS, **Heinz MG**. Diminished temporal coding with sensorineural hearing loss emerges in background noise. *Nat Neurosci* 15: 1362–1364, 2012.

Henry KS, **Kale S**, **Heinz MG**. Noise-induced hearing loss increases the temporal precision of complex envelope coding by auditory-nerve fibers. *Front Syst Neurosci* 8: 20, 2014.

Henry KS, **Kale S**, **Heinz MG**. Distorted tonotopic coding of temporal envelope and fine structure with noise-induced hearing loss. *J Neurosci* 36: 2227–2237, 2016.

Henry KS, **Kale S**, **Scheidt RE**, **Heinz MG**. Auditory brainstem responses predict auditory nerve fiber thresholds and frequency selectivity in hearing impaired chinchillas. *Hear Res* 280: 236–244, 2011.

Herrmann B, **Buckland C**, **Johnsrude IS**. Neural signatures of temporal regularity processing in sounds differ between younger and older adults. *Neurobiol Aging* 83: 73–85, 2019.

Herrmann B, **Henry MJ**, **Johnsrude IS**, **Obleser J**. Altered temporal dynamics of neural adaptation in the aging human auditory cortex. *Neurobiol Aging* 45: 10–22, 2016.

Herrmann B, **Parthasarathy A**, **Bartlett EL**. Ageing affects dual encoding of periodicity and envelope shape in rat inferior colliculus neurons. *Eur J Neurosci* 45: 299–311, 2017.

Herrmann B, **Parthasarathy A**, **Han EX**, **Obleser J**, **Bartlett EL**. Sensitivity of rat inferior colliculus neurons to frequency distributions. *J Neurophysiol* 114: jn.00555.2015, 2015.

Hickman TT, **Smalt C**, **Bobrow J**, **Quatieri T**, **Liberman MC**. Blast-induced cochlear synaptopathy in chinchillas. *Sci Rep* 8: 10740, 2018.

Hickox AE, **Liberman MC**. Is noise-induced cochlear neuropathy key to the generation of hyperacusis or tinnitus? *J Neurophysiol* 111: 552–564, 2014.

Holmes E, **Griffiths TD**. 'Normal' hearing thresholds and fundamental auditory grouping processes predict difficulties with speech-in-noise perception. *Sci Rep* 9: 1–11, 2019.

Holt AG, **Asako M**, **Lomax CA**, **MacDonald JW**, **Tong L**, **Lomax MI**, **Altschuler RA**. Deafness-related plasticity in the inferior colliculus: gene expression profiling following removal of peripheral activity. *J Neurochem* 93: 1069–1086, 2005.

Hovens I, **Nyakas C**, **Schoemaker R**. A novel method for evaluating microglial activation using ionized calcium-binding adaptor protein-1 staining: cell body to cell size ratio. *Neuroimmunol Neuroinflammation* 1: 82, 2014.

Hua Y, **Wang Y**, **Gu L**. Primary blast waves induced brain dynamics influenced by head orientations. *Biomed Eng Lett* 7: 253–259, 2017.

Humes LE, **Dubno JR**, **Gordon-Salant S**, **Lister JJ**, **Cacace AT**, **Cruickshanks KJ**, **Gates GA**, **Wilson RH**, **Wingfield A**. Central presbycusis: A review and evaluation of the evidence. *J. Am. Acad. Audiol.* 23: 635–666, 2012.

Ito T, **Bishop D**, **Oliver D**. Two classes of GABAergic neurons in the inferior colliculus. *J Neurosci* 29, 2009.

Ito T, **Oliver DL**. Origins of Glutamatergic Terminals in the Inferior Colliculus Identified by Retrograde Transport and Expression of VGLUT1 and VGLUT2 Genes. *Front Neuroanat* 4: 135, 2010.

Ito T, **Oliver DL**. The basic circuit of the IC: tectothalamic neurons with different patterns of synaptic organization send different messages to the thalamus. *Front Neural Circuits* 6: 48, 2012.

Ito T, **Oliver DL**. Local and commissural IC neurons make axosomatic inputs on large GABAergic tectothalamic neurons. *J Comp Neurol* 00: 1–16, 2014.

Jalali MM, **Nasimidoust Azgomi M**. Metabolic syndrome components and sudden sensorineural hearing loss: a case–control study. *Eur Arch Oto-Rhino-Laryngology* 277: 1023–1029, 2020.

Jørgensen S, **Dau T**. Predicting speech intelligibility based on the signal-to-noise envelope power ratio after modulation-frequency selective processing. *J Acoust Soc Am* 130: 1475–1487, 2011.

Jørgensen S, **Decorsière R**, **Dau T**. Effects of manipulating the signal-to-noise envelope power ratio on speech intelligibility. *J Acoust Soc Am* 137: 1401–1410, 2015.

Joris PX, **Schreiner CE**, **Rees A**. *Neural Processing of Amplitude-Modulated Sounds*. American Physiological Society, 2004.

Joseph AR, **Shaw JL**, **Clouser MC**, **MacGregor AJ**, **Galarneau MR**. Impact of Blast Injury on Hearing in a Screened Male Military Population. *Am J Epidemiol* 187: 7–15, 2018.

Kale S, **Heinz MG**. Temporal modulation transfer functions measured from auditory-nerve responses following sensorineural hearing loss. *Hear Res* 286: 64–75, 2012.

Kathleen Pichora-Fuller M, **Kowalchuk D**, **Lamb M**. Gap detection and the precedence effect in young and old adults. *J Acoust Soc Am* 95: 980–991, 1994.

Kaźmierczak H, **Doroszewska G**. Metabolic disorders in vertigo, tinnitus, and hearing loss. *Int Tinnitus J* 7: 54–58, 2001.

Kelly JB, **Liscum A**, **Van Adel B**, **Ito M**. Projections from the superior olive and lateral lemniscus to tonotopic regions of the rat's inferior colliculus. *Hear Res* 116: 43–54, 1998.

Kerr AG. The effects of blast on the ear. *J Laryngol Otol* 94: 107–110, 1980.

Khouri L, **Lesica NA**, **Grothe B**. Impaired auditory temporal selectivity in the inferior colliculus of aged Mongolian gerbils. *J Neurosci* 31: 9958–70, 2011.

Knudsen SK, **Øen EO**. Blast-induced neurotrauma in whales. *Neurosci Res* 46: 377–386, 2003.

Koch U, **Grothe B**. GABAergic and glycinergic inhibition sharpens tuning for frequency modulations in the inferior colliculus of the big brown bat. *J Neurophysiol* 80: 71–82, 1998.

Krebs B, **Lesica NA**, **Grothe B**. The representation of amplitude modulations in the mammalian auditory midbrain. *J Neurophysiol* 100: 1602–1609, 2008.

Krishna BS, **Semple MN**. Auditory temporal processing: responses to sinusoidally amplitude-modulated tones in the inferior colliculus. *J Neurophysiol* 84: 255–273, 2000.

Krishnan A, **Gandour JT**. The role of the auditory brainstem in processing linguistically-relevant pitch patterns. *Brain Lang.* 110Brain Lang: 135–148, 2009.

Krishnan A, **Gandour JT**, **Bidelman GM**. Brainstem pitch representation in native speakers of Mandarin is less susceptible to degradation of stimulus temporal regularity. *Brain Res* 1313: 124–133, 2010.

Krishnan A, **Gandour JT**, **Suresh CH**. Cortical pitch response components show differential sensitivity to native and nonnative pitch contours. *Brain Lang* 138: 51–60, 2014.

Krishnan A, **Gandour JT**, **Suresh CH**. Pitch processing of dynamic lexical tones in the auditory cortex is influenced by sensory and extrasensory processes. *Eur J Neurosci* 41: 1496–1504, 2015.

Krishnan A, **Gandour JT**, **Xu Y**, **Suresh CH**. Language-dependent changes in pitch-relevant neural activity in the auditory cortex reflect differential weighting of temporal attributes of pitch contours. *J Neurolinguistics* 41: 38–49, 2017a.

Krishnan A, **Suresh CH**, **Gandour JT**. Changes in pitch height elicit both language-universal and language-dependent changes in neural representation of pitch in the brainstem and auditory cortex. *Neuroscience* 346: 52–63, 2017b.

Kubli LR, **Brungart D**, **Northern J**. Effect of Blast Injury on Auditory Localization in Military Service Members. *Ear Hear* 39: 457–469, 2018.

Kujawa SG, **Liberman MC**. Adding insult to injury: Cochlear nerve degeneration after "temporary" noise-induced hearing loss. *J Neurosci* 29: 14077–14085, 2009.

Kujawa SG, **Liberman MC**. Synaptopathy in the noise-exposed and aging cochlea: Primary neural degeneration in acquired sensorineural hearing loss. *Hear Res* 330: 191–199, 2015.

Lai J, **Bartlett EL**. Age-related shifts in distortion product otoacoustic emissions peak-ratios and amplitude modulation spectra. *Hear Res* 327: 186–198, 2015.

Lai J, **Bartlett EL**. Masking Differentially Affects Envelope-following Responses in Young and Aged Animals. *Neuroscience* 386: 150–165, 2018.

Lai J, **Sommer AL**, **Bartlett EL**. Age-related changes in envelope-following responses at equalized peripheral or central activation. *Neurobiol Aging* 58: 191–200, 2017.

Lang H, **Jyothi V**, **Smythe NM**, **Dubno JR**, **Schulte BA**, **Schmiedt RA**. Chronic reduction of endocochlear potential reduces auditory nerve activity: Further confirmation of an animal model of metabolic presbyacusis. *JARO - J Assoc Res Otolaryngol* 11: 419–434, 2010.

Laplaca MC, **Lee VMY**, **Thibault LE**. An in vitro model of traumatic neuronal injury: Loading rate-dependent changes in acute cytosolic calcium and lactate dehydrogenase release. *J Neurotrauma* 14: 355–368, 1997.

Leek MR, **Summers V**. Pitch strength and pitch dominance of iterated rippled noises in hearing-impaired listeners. *J Acoust Soc Am* 109: 2944–2954, 2001.

Leigh-Paffenroth ED, **Fowler CG**. Amplitude-modulated auditory steady-state responses in younger and older listeners. *J Am Acad Audiol* 17: 582–597, 2006.

Leung LY, **VandeVord PJ**, **Dal Cengio AL**, **Bir C**, **Yang KH**, **King AI**. Blast related neurotrauma: A review of cellular injury. *MCB Mol Cell Biomech* 5: 155–168, 2008.

Lew HL, **Garvert DW**, **Pogoda TK**, **Hsu P Te**, **Devine JM**, **White DK**, **Myers PJ**, **Goodrich GL**. Auditory and visual impairments in patients with blast-related traumatic brain injury: Effect of dual sensory impairment on functional independence measure. *J Rehabil Res Dev* 46: 819–826, 2009.

Liberman MC. Noise-induced and age-related hearing loss: New perspectives and potential therapies. *F1000Research* 6: 1–11, 2017.

Liberman MC, **Epstein MJ**, **Cleveland SS**, **Wang H**, **Maison SF**. Toward a differential diagnosis of hidden hearing loss in humans. *PLoS One* 11, 2016.

Liberman MC, **Kujawa SG**. Cochlear synaptopathy in acquired sensorineural hearing loss: Manifestations and mechanisms. *Hear. Res.* 349Elsevier B.V.: 138–147, 2017.

Liégeois-Chauvel C, **Musolino A**, **Badier JM**, **Marquis P**, **Chauvel P**. Evoked potentials recorded from the auditory cortex in man: evaluation and topography of the middle latency components. *Electroencephalogr Clin Neurophysiol Evoked Potentials* 92: 204–214, 1994.

Lim HH, **Lenarz M**, **Lenarz T**. Auditory Midbrain Implant: A Review. *Trends Amplif* 13: 149–180, 2009.

Lin HW, **Furman AC**, **Kujawa SG**, **Liberman MC**. Primary neural degeneration in the guinea pig cochlea after reversible noise-induced threshold shift. *JARO - J Assoc Res Otolaryngol* 12: 605–616, 2011.

Ling LL, **Hughes LF**, **Caspary DM**. Age-related loss of the GABA synthetic enzyme glutamic acid decarboxylase in rat primary auditory cortex. *Neuroscience* 132: 1103–13, 2005.

Liu X, **Chen G-D**, **Salvi R**. Neuroplastic changes in auditory cortex induced by long-duration "non-traumatic" noise exposures are triggered by deficits in the neural output of the cochlea. *Hear Res* 404: 108203, 2021.

Lopez-Poveda EA, **Barrios P**. Perception of stochastically undersampled sound waveforms: a model of auditory deafferentation. *Front Neurosci* 7: 124, 2013.

Lu T, **Wang X**. Temporal discharge patterns evoked by rapid sequences of wide- and narrowband clicks in the primary auditory cortex of cat. *J Neurophysiol* 84: 236–246, 2000.

Luo H, **Pace E**, **Zhang J**. Blast-induced tinnitus and hyperactivity in the auditory cortex of rats. *Neuroscience* 340: 515–520, 2017.

Luo H, **Pace E**, **Zhang X**, **Zhang J**. Blast-Induced tinnitus and spontaneous firing changes in the rat dorsal cochlear nucleus. *J Neurosci Res* 92: 1466–1477, 2014a.

Luo H, **Pace E**, **Zhang X**, **Zhang J**. Blast-induced tinnitus and spontaneous activity changes in the rat inferior colliculus. *Neurosci Lett* 580: 47–51, 2014b.

Mahmood G, **Mei Z**, **Hojjat H**, **Pace E**, **Kallakuri S**, **Zhang JS**. Therapeutic effect of sildenafil on blast-induced tinnitus and auditory impairment. *Neuroscience* 269: 367–382, 2014.

Makary CA, **Shin J**, **Kujawa SG**, **Liberman MC**, **Merchant SN**. Age-related primary cochlear neuronal degeneration in human temporal bones. *JARO - J Assoc Res Otolaryngol* 12: 711–717, 2011.

Malmierca MS. The structure and physiology of the rat auditory system: An overview. In: *International Review of Neurobiology*. Academic Press Inc., p. 147–211.

Malmierca MS. The inferior colliculus: A center for convergence of ascending and descending auditory information. *Neuroembryology Aging* 3Karger Publishers: 215–229, 2004.

Malmierca MS, **Izquierdo MA**, **Cristaudo S**, **Hernández O**, **Pérez-González D**, **Covey E**, **Oliver DL**. A discontinuous tonotopic organization in the inferior colliculus of the rat. *J Neurosci* 28: 4767–4776, 2008.

Manzoor NF, **Gao Y**, **Licari F**, **Kaltenbach JA**. Comparison and contrast of noise-induced hyperactivity in the dorsal cochlear nucleus and inferior colliculus. *Hear Res* 295: 114–123, 2013.

Mao JC, **Pace E**, **Pierozynski P**, **Kou Z**, **Shen Y**, **Vandevord P**, **Haacke EM**, **Zhang X**, **Zhang J**. Blast-induced tinnitus and hearing loss in rats: Behavioral and imaging assays. *J Neurotrauma* 29: 430–444, 2012a.

Mao JC, **Pace E**, **Pierozynski P**, **Kou Z**, **Shen Y**, **VandeVord P**, **Haacke EM**, **Zhang X**, **Zhang J**. Blast-Induced Tinnitus and Hearing Loss in Rats: Behavioral and Imaging Assays. *J Neurotrauma* 29: 430–444, 2012b.

Mardia, **Jupp P**. Directional Statistics. .

Masri S, **Zhang LS**, **Luo H**, **Pace E**, **Zhang J**, **Bao S**. Blast Exposure Disrupts the Tonotopic Frequency Map in the Primary Auditory Cortex. *Neuroscience* 379: 428–434, 2018.

Mayko ZM, **Roberts PD**, **Portfors C V**. Inhibition shapes selectivity to vocalizations in the inferior colliculus of awake mice. *Front Neural Circuits* 6: 73, 2012.

McGee T, **Kraus N**. Auditory development reflected by middle latency response. *Ear Hear* 17: 419–429, 1996.

McGee T, **Kraus N**, **Comperatore C**, **Nicol T**. Subcortical and cortical components of the MLR generating system. *Brain Res* 544: 211–220, 1991.

McGee T, **Kraus N**, **Littman T**, **Nicol T**. Contributions of medial geniculate body subdivisions to the middle latency response. *Hear Res* 61: 147–154, 1992.

Meehan A, **Hebert D**, **Deru K**, **Weaver LK**. Longitudinal study of hyperbaric oxygen intervention on balance and affective symptoms in military service members with persistent post-concussive symptoms. *J Vestib Res Equilib Orientat* 29: 205–219, 2019.

Mehraei G, **Hickox AE**, **Bharadwaj HM**, **Goldberg H**, **Verhulst S**, **Charles Liberman M**, **Shinn-Cunningham BG**. Auditory brainstem response latency in noise as a marker of cochlear synaptopathy. *J Neurosci* 36: 3755–3764, 2016.

Mepani AM, **Verhulst S**, **Hancock KE**, **Garrett M**, **Vasilkov V**, **Bennett K**, **De Gruttola VG**, **Liberman MC**, **Maison SF**. Envelope following responses predict speech-in-noise performance in normal hearing listeners. *J. Neurophysiol.* (March 3, 2021). doi: 10.1152/jn.00620.2020.

Mesgarani N, **Chang EF**. Selective cortical representation of attended speaker in multi-talker speech perception. *Nature* 485NIH Public Access: 233–236, 2012.

Mesgarani N, **Cheung C**, **Johnson K**, **Chang EF**. Phonetic feature encoding in human superior temporal gyrus. *Science (80-)* 343: 1006–1010, 2014.

Middleton JW, **Kiritani T**, **Pedersen C**, **Turner JG**, **Shepherd GMG**, **Tzounopoulos T**. Mice with behavioral evidence of tinnitus exhibit dorsal cochlear nucleus hyperactivity because of decreased GABAergic inhibition. *Proc Natl Acad Sci U S A* 108: 7601–7606, 2011.

Milbrandt J, **Albin R**, **Turgeon S**, **Caspary D**. GABA A receptor binding in the aging rat inferior colliculus. *Neuroscience* 73: 449–458, 1996.

Milbrandt JC, **Holder TM**, **Wilson MC**, **Salvi RJ**, **Caspary DM**. GAD levels and muscimol binding in rat inferior colliculus following acoustic trauma. *Hear Res* 147: 251–60, 2000.

Miller CT, **Hauser MD**. Multiple acoustic features underlie vocal signal recognition in tamarins: Antiphonal calling experiments. *J Comp Physiol A Neuroethol Sensory, Neural, Behav Physiol* 190: 7–19, 2004.

Møller AR, **Rees A**. Dynamic properties of the responses of single neurons in the inferior colliculus of the rat. *Hear Res* 24: 203–215, 1986.

Moore BCJ. Prevalence of Dead Regions in Subjects with Sensorineural Hearing Loss. *Ear Hear* 28: 231–241, 2007.

Moore BCJ. Auditory Processing of Temporal Fine Structure. WORLD SCIENTIFIC, 2014.

Morrison J a, **Farzan F**, **Fremouw T**, **Sayegh R**, **Covey E**, **Faure P a**. Organization and trade-off of spectro-temporal tuning properties of duration-tuned neurons in the mammalian inferior colliculus. *J Neurophysiol* 111: 2047–60, 2014.

Mulders WHAM, **Ding D**, **Salvi R**, **Robertson D**. Relationship between auditory thresholds, central spontaneous activity, and hair cell loss after acoustic trauma. *J Comp Neurol* 519: 2637–2647, 2011.

Mulders WHAM, **Robertson D**. Hyperactivity in the auditory midbrain after acoustic trauma: dependence on cochlear activity. *Neuroscience* 164: 733–746, 2009.

Mulders WHAM, **Robertson D**. Progressive centralization of midbrain hyperactivity after acoustic trauma. *Neuroscience* 192: 753–760, 2011.

Mulders WHAM, **Robertson D**. Development of hyperactivity after acoustic trauma in the guinea pig inferior colliculus. *Hear Res* 298: 104–108, 2013.

Musiek F, **Nagle S**. The middle latency response: A review of findings in various central nervous system lesions. *J. Am. Acad. Audiol.* 29American Academy of Audiology: 855–867, 2018.

Neely ST, **Jesteadt W**, **Norton SJ**, **Gorga MP**. Latency of auditory brain-stem responses and otoacoustic emissio] using tone-burst stimuli. *J Acoust Soc Am* 83: 652–656, 1988.

O'Dell DM, **Gibson CJ**, **Wilson MS**, **DeFord SM**, **Hamm RJ**. Positive and negative modulation of the GABA(A) receptor and outcome after traumatic brain injury in rats. *Brain Res* 861: 325–332, 2000.

Ono M, **Bishop DC**, **Oliver DL**. Identified GABAergic and glutamatergic neurons in the mouse inferior colliculus share similar response properties. *J Neurosci* 37: 8952–8964, 2017.

Overbeck GW, **Church MW**. Effects of tone burst frequency and intensity on the auditory brainstem response (ABR) from albino and pigmented rats. *Hear Res* 59: 129–137, 1992.

Overton JA, **Recanzone GH**. Effects of aging on the response of single neurons to amplitude modulated noise in primary auditory cortex of Rhesus macaque. *J Neurophysiol* : jn.01098.2015, 2016.

Özdamar Ö, **Kraus N**. Auditory middle-latency responses in humans. *Int J Audiol* 22: 34–49, 1983.

Palmer A, **Shamma S**. Physiological Representations of Speech. In: *Speech Processing in the Auditory System*. Springer-Verlag, p. 163–230.

Palombi PS, **Backoff PM**, **Caspary DM**. Responses of young and aged rat inferior colliculus neurons to sinusoidally amplitude modulated stimuli. *Hear Res* 153: 174–180, 2001.

Palombi PS, **Caspary DM**. Physiology of the aged Fischer 344 rat inferior colliculus: Responses to contralateral monaural stimuli. *J Neurophysiol* 76: 3114–3125, 1996.

Parthasarathy A, **Bartlett E**. Two-channel recording of auditory-evoked potentials to detect age-related deficits in temporal processing. *Hear Res* 289: 52–62, 2012.

Parthasarathy A, **Bartlett EL**. Age-related auditory deficits in temporal processing in F-344 rats. *Neuroscience* 192: 619–630, 2011.

Parthasarathy A, **Bartlett EL**, **Kujawa SG**. Age-related Changes in Neural Coding of Envelope Cues: Peripheral Declines and Central Compensation. *Neuroscience* 407: 21–31, 2019a.

Parthasarathy A, **Cunningham PA**, **Bartlett EL**. Age-related differences in auditory processing as assessed by amplitude-modulation following responses in quiet and in noise. *Front Aging Neurosci* 2: 3389, 2010.

Parthasarathy A, **Datta J**, **Torres JAL**, **Hopkins C**, **Bartlett EL**. Age-related changes in the relationship between auditory brainstem responses and envelope-following responses. *JARO - J Assoc Res Otolaryngol* 15: 649–661, 2014.

Parthasarathy A, **Herrmann B**, **Bartlett EL**. Aging alters envelope representations of speech-like sounds in the inferior colliculus. *Neurobiol Aging* 73: 30–40, 2019b.

Parthasarathy A, **Kujawa SG**. Synaptopathy in the aging cochlea: Characterizing early-neural deficits in auditory temporal envelope processing. *J Neurosci* 38: 7108–7119, 2018.

Parthasarathy A, **Lai J**, **Bartlett EL**. Age-Related Changes in Processing Simultaneous Amplitude Modulated Sounds Assessed Using Envelope Following Responses. *JARO - J Assoc Res Otolaryngol* 17: 119–132, 2016.

Parthasarathy A, **Romero Pinto S**, **Lewis RM**, **Goedicke W**, **Polley DB**. Data-driven segmentation of audiometric phenotypes across a large clinical cohort. *Sci Rep* 10: 1–12, 2020.

Patterson JH, **Hamernik RP**. Blast overpressure induced structural and functional changes in the auditory system. 1997.

Patterson RD, **Handel S**, **Yost WA**, **Jaysurya Datta A**. The relative strength of the tone and noise components in iterated rippled noise. *J Acoust Soc Am* 100: 3286–3294, 1996.

Paul BT, **Bruce IC**, **Roberts LE**. Evidence that hidden hearing loss underlies amplitude modulation encoding deficits in individuals with and without tinnitus. *Hear Res* 344: 170–182, 2017.

Paxinos G, **Watson CR**. *The Rat Brain in Stereotaxic Coordinates*. 2007.

Penninger RT, **Chien WW**, **Jiradejvong P**, **Boeke E**, **Carver CL**, **Limb CJ**. Perception of pure tones and iterated rippled noise for normal hearing and cochlear implant users. *Trends Amplif* 17: 45–53, 2013.

Pérez-González D, **Hernández O**, **Covey E**, **Malmierca MS**. GABA A-mediated inhibition modulates stimulus-specific adaptation in the inferior colliculus. *PLoS One* 7: e34297, 2012.

Peter V, **Wong K**, **Narne VK**, **Sharma M**, **Purdy SC**, **McMahon C**. Assessing spectral and temporal processing in children and adults using Temporal Modulation Transfer Function (TMTF), Iterated Ripple Noise (IRN) perception, and Spectral Ripple Discrimination (SRD). *J Am Acad Audiol* 25: 210–218, 2014.

Phillips DJ, **Schei JL**, **Meighan PC**, **Rector DM**. State-Dependent Changes in Cortical Gain Control as Measured by Auditory Evoked Responses to Varying Intensity Stimuli. *Sleep* 34: 1527–1537, 2011.

Phillips SL, **Gordon-Salant S**, **Fitzgibbons PJ**, **Yeni-Komshian G**. Frequency and Temporal Resolution in Elderly Listeners with Good and Poor Word Recognition. *J. Speech, Lang. Hear. Res.* (2000). doi: 10.1044/jslhr.4301.217.

Pickles JO. Auditory pathways: Anatomy and physiology. In: *Handbook of Clinical Neurology*. Elsevier B.V., 2015, p. 3–25.

Picton TW, **Hillyard SA**, **Krausz HI**, **Galambos R**. Human auditory evoked potentials. I: Evaluation of components. *Electroencephalogr Clin Neurophysiol* 36: 179–190, 1974.

Plack CJ, **Barker D**, **Prendergast G**. Perceptual consequences of "hidden" hearing loss. *Trends Hear* 18: 233121651455062, 2014.

Plack CJ, **Léger A**, **Prendergast G**, **Kluk K**, **Guest H**, **Munro KJ**. Toward a Diagnostic Test for Hidden Hearing Loss. *Trends Hear* 20: 1–9, 2016.

Podoshin L, **Ben-David Y**, **Fradis M**, **Sharf B**, **Schwartz M**. Brainstem auditory evoked potential with increased stimulus rate in minor head trauma. *J Laryngol Otol* 104: 191–194, 1990.

Pollak GD, **Gittelman JX**, **Li N**, **Xie R**. Inhibitory projections from the ventral nucleus of the lateral lemniscus and superior paraolivary nucleus create directional selectivity of frequency modulations in the inferior colliculus: A comparison of bats with other mammals. *Hear Res* 273: 134–144, 2011.

Popelar J, **Grecova J**, **Rybalko N**, **Syka J**. Comparison of noise-induced changes of auditory brainstem and middle latency response amplitudes in rats. *Hear Res* 245: 82–91, 2008.

Prendergast G, **Guest H**, **Munro KJ**, **Kluk K**, **Léger A**, **Hall DA**, **Heinz MG**, **Plack CJ**. Effects of noise exposure on young adults with normal audiograms I: Electrophysiology. *Hear Res* 344: 68–81, 2017.

Puel JL, **Ruel J**, **Gervais D'Aldin C**, **Pujol R**. Excitotoxicity and repair of cochlear synapses after noise- trauma induced hearing loss. *Neuroreport* 9: 2109–2114, 1998.

Pujol R, **Puel JL**. Excitotoxicity, synaptic repair, and functional recovery in the mammalian cochlea: A review of recent findings. In: *Annals of the New York Academy of Sciences*. New York Academy of Sciences, p. 249–254.

Rabang CF, **Parthasarathy A**, **Venkataraman Y**, **Fisher ZL**, **Gardner SM**, **Bartlett EL**. A computational model of inferior colliculus responses to amplitude modulated sounds in young and aged rats. *Front Neural Circuits* 6: 77, 2012.

Race N, **Lai J**, **Shi R**, **Bartlett EL**. Differences in postinjury auditory system pathophysiology after mild blast and nonblast acute acoustic trauma. *J Neurophysiol* 118: 782–799, 2017.

Rafaels K, **"Dale" Bass CR**, **Salzar RS**, **Panzer MB**, **Woods W**, **Feldman S**, **Cummings T**, **Capehart B**. Survival Risk Assessment for Primary Blast Exposures to the Head. *J Neurotrauma* 28: 2319–2328, 2011.

Razak KA, **Fuzessery ZM**. GABA shapes selectivity for the rate and direction of frequency-modulated sweeps in the auditory cortex. *J Neurophysiol* 102: 1366–1378, 2009.

Reed AC, **Centanni TM**, **Borland MS**, **Matney CJ**, **Engineer CT**, **Kilgard MP**. Behavioral and Neural Discrimination of Speech Sounds After Moderate or Intense Noise Exposure in Rats. *Ear Hear* 35: e248–e261, 2014.

Rees A, **Møller AR**. Stimulus properties influencing the responses of inferior colliculus neurons to amplitude-modulated sounds. *Hear Res* 27: 129–143, 1987.

Remenschneider AK, **Lookabaugh S**, **Aliphas A**, **Brodsky JR**, **Devaiah AK**, **Dagher W**, **Grundfast KM**, **Heman-Ackah SE**, **Rubin S**, **Sillman J**, **Tsai AC**, **Vecchiotti M**, **Kujawa SG**, **Lee DJ**, **Quesnel AM**. Otologic outcomes after blast injury: The Boston Marathon experience. *Otol Neurotol* 35: 1825–1834, 2014.

Rennies J, **Verhey JL**, **Fastl H**. Comparison of loudness models for time-varying sounds. *Acta Acust united with Acust* 96: 383–396, 2010.

Rhode WS, **Smith PH**. Characteristics of tone-pip response patterns in relationship to spontaneous rate in cat auditory nerve fibers. *Hear Res* 18: 159–168, 1985.

Richardson BD, **Ling LL**, **Uteshev V V.**, **Caspary DM**. Reduced GABAA receptor-mediated tonic inhibition in aged rat auditory thalamus. *J Neurosci* 33: 1218–1227, 2013.

Ritenour AE, **Wickley A**, **Ritenour JS**, **Kriete BR**, **Blackbourne LH**, **Holcomb JB**, **Wade CE**. Tympanic membrane perforation and hearing loss from blast overpressure in Operation Enduring Freedom and Operation Iraqi Freedom wounded. *J Trauma* 64, 2008.

Robertson D, **Bester C**, **Vogler D**, **Mulders WHAM**. Spontaneous hyperactivity in the auditory midbrain: Relationship to afferent input. *Hear Res* 295: 124–129, 2013.

Rodríguez FA, **Read HL**, **Escabí MA**. Spectral and temporal modulation tradeoff in the inferior colliculus. *J Neurophysiol* 103: 887–903, 2010.

Roque L, **Gaskins C**, **Gordon-Salant S**, **Goupell MJ**, **Anderson S**. Age Effects on Neural Representation and Perception of Silence Duration Cues in Speech. (2019). doi: 10.1044/2018_JSLHR-H-ASCC7-18-0076.

Rose JE, **Hind JE**, **Anderson DJ**, **Brugge JF**. Some effects of stimulus intensity on response of auditory nerve fibers in the squirrel monkey. *J Neurophysiol* 34: 685–699, 1971.

Rosen S. Temporal information in speech: acoustic, auditory and linguistic aspects. *Philos. Trans. R. Soc. Lond. B. Biol. Sci.* 336The Royal Society London: 367–373, 1992.

Sajja VSSS, **Galloway M**, **Ghoddoussi F**, **Kepsel A**, **Vandevord P**. Effects of blast-induced neurotrauma on the nucleus accumbens. *J Neurosci Res* 91: 593–601, 2013.

Säljö A, **Mayorga M**, **Bolouri H**, **Svensson B**, **Hamberger A**. Mechanisms and pathophysiology of the low-level blast brain injury in animal models. *Neuroimage* 54: S83–S88, 2011.

Saunders GH, **Frederick MT**, **Arnold M**, **Silverman S**, **Chisolm TH**, **Myers P**. Auditory difficulties in blast-exposed veterans with clinically normal hearing. *J Rehabil Res Dev* 52: 343–360, 2015.

Sayegh R, **Aubie B**, **Fazel-Pour S**, **Faure P a.** Recovery cycle times of inferior colliculus neurons in the awake bat measured with spike counts and latencies. *Front Neural Circuits* 6: 1–20, 2012.

Schaette R, **McAlpine D**. Tinnitus with a normal audiogram: Physiological evidence for hidden hearing loss and computational model. *J Neurosci* 31: 13452–13457, 2011.

Schatteman TA, **Hughes LF**, **Caspary DM**. Aged-related loss of temporal processing: Altered responses to amplitude modulated tones in rat dorsal cochlear nucleus. *Neuroscience* 154: 329–337, 2008.

Schmiedt RA, **Mills JH**, **Boettcher FA**. Age-related loss of activity of auditory-nerve fibers. *J Neurophysiol* 76: 2799–2803, 1996.

Schnupp JWH, **Garcia-Lazaro JA**, **Lesica NA**. Periodotopy in the gerbil inferior colliculus: Local clustering rather than a gradient map. *Front Neural Circuits* 9, 2015.

Schrode KM, **Muniak MA**, **Kim YH**, **Lauer AM**. Central compensation in auditory brainstem after damaging noise exposure. *eNeuro* 5, 2018.

Sergeyenko Y, **Lall K**, **Charles Liberman M**, **Kujawa SG**. Age-related cochlear synaptopathy: An early-onset contributor to auditory functional decline. *J Neurosci* 33: 13686–13694, 2013.

Shannon R V, **Zeng F-GG**, **Kamath V**, **Wygonski J**, **Ekelid M**. Speech recognition with primarily temporal cues. *Science* 270: 303–4, 1995.

Shearer DE, **Molis MR**, **Bennett KO**, **Leek MR**. Auditory stream segregation of iterated rippled noises by normal-hearing and hearing-impaired listeners. *J Acoust Soc Am* 143: 378–387, 2018.

Sheft S, **Ardoint M**, **Lorenzi C**. Speech identification based on temporal fine structure cues. *J Acoust Soc Am* 124: 562–75, 2008.

Shi R, **Rickett T**, **Sun W**. Acrolein-mediated injury in nervous system trauma and diseases. *Mol. Nutr. Food Res.* 55John Wiley & Sons, Ltd: 1320–1331, 2011.

Shofner WP. Responses of cochlear nucleus units in the chinchilla to iterated rippled noises: analysis of neural autocorrelograms. *J Neurophysiol* 81: 2662–2674, 1999.

Simpson G V., **Knight RT**, **Brailowsky S**, **Prospero-Garcia O**, **Scabini D**. Altered peripheral and brainstem auditory function in aged rats. *Brain Res* 348: 28–35, 1985.

Simpson MIG, **Prendergast G**. Auditory magnetic evoked responses. In: *Handbook of Clinical Neurophysiology*. 2013, p. 253–270.

Singh NC, **Theunissen FE**. Modulation spectra of natural sounds and ethological theories of auditory processing. *J Acoust Soc Am* 114: 3394–3411, 2003.

Skoe E, **Kraus N**. Auditory Brain Stem Response to Complex Sounds: A Tutorial. *Ear Hear* 31: 302–324, 2010.

Snell KB, **Frisina DR**. Relationships among age-related differences in gap detection and word recognition. *J. Acoust. Soc. Am.* (2000). doi: 10.1121/1.428446.

Song S, **Race NS**, **Kim A**, **Zhang T**, **Shi R**, **Ziaie B**. A Wireless Intracranial Brain Deformation Sensing System for Blast-Induced Traumatic Brain Injury. *Sci Rep* 5: 1–10, 2015.

Spoendlin H, **Schrott A**. Analysis of the human auditory nerve. *Hear Res* 43: 25–38, 1989.

Stebbings KA, **Lesicko AMH**, **Llano DA**. The auditory corticocollicular system: Molecular and circuit-level considerations. *Hear. Res*. 314Elsevier: 51–59, 2014.

Stevens KN. Toward a model for lexical access based on acoustic landmarks and distinctive features. *J Acoust Soc Am* 111: 1872–1891, 2002.

Strouse a, **Ashmead DH**, **Ohde RN**, **Grantham DW**. Temporal processing in the aging auditory system. [Online]. *J Acoust Soc Am* 104: 2385–99, 1998. http://www.ncbi.nlm.nih.gov/pubmed/10491702.

Sturm JJ, **Zhang-Hooks YX**, **Roos H**, **Nguyen T**, **Kandler K**. Noise trauma-induced behavioral gap detection deficits correlate with reorganization of excitatory and inhibitory local circuits in the inferior colliculus and are prevented by acoustic enrichment. *J Neurosci* 37: 6314–6330, 2017.

Sun W, **Deng A**, **Jayaram A**, **Gibson B**. Noise exposure enhances auditory cortex responses related to hyperacusis behavior. *Brain Res* 1485: 108–116, 2012.

Sun W, **Lu J**, **Stolzberg D**, **Gray L**, **Deng A**, **Lobarinas E**, **Salvi RJ**. Salicylate increases the gain of the central auditory system. *Neuroscience* 159: 325–334, 2009.

Šuta D, **Rybalko N**, **Pelánová J**, **Popelář J**, **Syka J**. Age-related changes in auditory temporal processing in the rat. *Exp Gerontol* 46: 739–746, 2011.

Swaminathan J, **Krishnan A**, **Gandour JT**. Pitch encoding in speech and nonspeech contexts in the human auditory brainstem. *Neuroreport* 19: 1163–1167, 2008.

Syka J, **Rybalko N**. Threshold shifts and enhancement of cortical evoked responses after noise exposure in rats. *Hear Res* 139: 59–68, 2000.

Tadros SF, **D'Souza M**, **Zettel ML**, **Zhu X**, **Waxmonsky NC**, **Frisina RD**. Glutamate-related gene expression changes with age in the mouse auditory midbrain. *Brain Res* 1127: 1–9, 2007.

Ter-Mikaelian M, **Sanes DH**, **Semple MN**. Transformation of temporal properties between auditory midbrain and cortex in the awake Mongolian gerbil. *J Neurosci* 27: 6091–6102, 2007.

Thomas ME, **Friedman NHM**, **Cisneros-Franco JM**, **Ouellet L**, **De Villers-Sidani É**. The prolonged masking of temporal acoustic inputs with noise drives plasticity in the adult rat auditory cortex. *Cereb Cortex* 29: 1032–1046, 2019.

Thompson W, **Marozeau J**. Auditory Stream Segregation: Boundaries. In: *Music in the Social and Behavioral Sciences: An Encyclopedia*. 2014.

Tichko P, **Skoe E**. Frequency-dependent fine structure in the frequency-following response: The byproduct of multiple generators. *Hear Res* 348: 1–15, 2017.

Tremblay KL, **Piskosz M**, **Souza P**. Effects of age and age-related hearing loss on the neural representation of speech cues. *Clin Neurophysiol* 114: 1332–1343, 2003.

Trune DR, **Kempton JB**, **Kessi M**. Aldosterone (mineralocorticoid) equivalent to prednisolone (glucocorticoid) in reversing hearing loss in MRL/MpJ-Fas(lpr) autoimmune mice. *Laryngoscope* 110: 1902–1906, 2000.

Tukey JW. Comparing Individual Means in the Analysis of Variance. *Biometrics* 5: 99, 1949.

Unnikrishnan G, **Mao H**, **Sundaramurthy A**, **Bell ED**, **Yeoh S**, **Monson K**, **Reifman J**. A 3-D Rat Brain Model for Blast-Wave Exposure: Effects of Brain Vasculature and Material Properties. *Ann Biomed Eng* 47: 2033–2044, 2019.

Vaden KI, **Matthews LJ**, **Eckert MA**, **Dubno JR**. Longitudinal Changes in Audiometric Phenotypes of Age-Related Hearing Loss. *JARO - J Assoc Res Otolaryngol* 18: 371–385, 2017.

Valderrama JT, **Beach EF**, **Yeend I**, **Sharma M**, **Van Dun B**, **Dillon H**. Effects of lifetime noise exposure on the middle-age human auditory brainstem response, tinnitus and speech-in-noise intelligibility. *Hear Res* 365: 36–48, 2018.

Viana LM, **O'Malley JT**, **Burgess BJ**, **Jones DD**, **Oliveira CACP**, **Santos F**, **Merchant SN**, **Liberman LD**, **Liberman MC**. Cochlear neuropathy in human presbycusis: Confocal analysis of hidden hearing loss in post-mortem tissue. *Hear Res* 327: 78–88, 2015.

Wagner L, **Plontke SK**, **Rahne T**. Perception of Iterated Rippled Noise Periodicity in Cochlear Implant Users. *Audiol Neurotol* 22: 104–115, 2017.

Wallace MN, **Shackleton TM**, **Palmer AR**. Morphological and physiological characteristics of laminar cells in the central nucleus of the inferior colliculus. *Front Neural Circuits* 6: 55, 2012.

Wallaert N, **Moore BCJ**, **Lorenzi C**. Comparing the effects of age on amplitude modulation and frequency modulation detection. *J Acoust Soc Am* 139: 3088–3096, 2016.

Walls MK, **Race N**, **Zheng L**, **Vega-Alvarez SM**, **Acosta G**, **Park J**, **Shi R**. Structural and biochemical abnormalities in the absence of acute deficits in mild primary blast-induced head trauma. *J Neurosurg* 124: 675–686, 2016.

Walton JP. Timing is everything: Temporal processing deficits in the aged auditory brainstem. *Hear Res* 264: 63–69, 2010.

Walton JP, **Simon H**, **Frisina RD**. Age-related alterations in the neural coding of envelope periodicities. *J Neurophysiol* 88: 565–78, 2002.

Wan G, **Corfas G**. Transient auditory nerve demyelination as a new mechanism for hidden hearing loss. *Nat Commun* 8: 1–13, 2017.

Wang C, **Dallos P**. Latency of Whole-Nerve Action Potentials: Influence of Hair-Cell Normalcy. *J Acoust Soc Am* 52: 1678–1686, 1972.

Wang H, **Brozoski TJ**, **Turner JG**, **Ling L**, **Parrish JL**, **Hughes LF**, **Caspary DM**. Plasticity at glycinergic synapses in dorsal cochlear nucleus of rats with behavioral evidence of tinnitus. *Neuroscience* 164: 747–759, 2009a.

Wang H, **Turner JG**, **Ling L**, **Parrish JL**, **Hughes LF**, **Caspary DM**. Age-related changes in glycine receptor subunit composition and binding in dorsal cochlear nucleus. *Neuroscience* 160: 227–239, 2009b.

Wang W, **Zinsmaier AK**, **Firestone E**, **Lin R**, **Yatskievych TA**, **Yang S**, **Zhang J**, **Bao S**. Blocking Tumor Necrosis Factor-Alpha Expression Prevents Blast-Induced Excitatory/Inhibitory Synaptic Imbalance and Parvalbumin-Positive Interneuron Loss in the Hippocampus. *J Neurotrauma* 35: 2306–2316, 2018.

Wang X, **Lu T**, **Bendor D**, **Bartlett E**. Neural coding of temporal information in auditory thalamus and cortex. *Neuroscience* 154: 294–303, 2008.

Wang Y, **Urioste RT**, **Wei Y**, **Wilder DM**, **Arun P**, **Sajja V**, **Gist ID**, **Fitzgerald TS**, **Chang W**, **Kelley MW**, **Long JB**. Blast-induced hearing impairment in rats is associated with structural and molecular changes of the inner ear. *Sci Rep* 10: 1–12, 2020.

Washnik NJ, **Anjum J**, **Lundgren K**, **Phillips S**. A Review of the Role of Auditory Evoked Potentials in Mild Traumatic Brain Injury Assessment. *Trends Hear* 23: 1–13, 2019.

Watts S, **Kirkman E**, **Bieler D**, **Bjarnason S**, **Franke A**, **Gupta R**, **Leggieri MJ**, **Orru H**, **Ouellet S**, **Philippens M**, **Sarron JC**, **Skriudalen S**, **Teland JA**, **Risling M**, **Cernak I**. Guidelines for using animal models in blast injury research. *J. R. Army Med. Corps* 165: 38–40, 2019.

Vander Werff KR. Auditory Dysfunction Among Long-Term Consequences of Mild Traumatic Brain Injury (mTBI). *Perspect Hear Hear Disord Res Diagnostics* 16: 3, 2012.

Wiegrebe L, **Winter IM**. Temporal Representation of Iterated Rippled Noise as a Function of Delay and Sound Level in the Ventral Cochlear Nucleus. *J Neurophysiol* 85: 1206–1219, 2001.

Willott JF, **Parham K**, **Hunter KP**. Response properties of inferior colliculus neurons in young and very old CBA/J mice. *Hear Res* 37: 1–14, 1988a.

Willott JF, **Parham K**, **Hunter KP**. Response properties of inferior colliculus neurons in middle-aged C57BL/6J mice with presbycusis. *Hear Res* 37: 15–27, 1988b.

Witcher KG, **Bray CE**, **Chunchai T**, **Zhao F**, **O'Neil SM**, **Gordillo AJ**, **Campbell WA**, **McKim DB**, **Liu X**, **Dziabis JE**, **Quan N**, **Eiferman DS**, **Fischer AJ**, **Kokiko-Cochran ON**, **Askwith C**, **Godbout JP**. Traumatic brain injury causes chronic cortical inflammation and neuronal dysfunction mediated by microglia. *J Neurosci* 41: JN-RM-2469-20, 2021.

Wong ACY, **Ryan AF**. Mechanisms of sensorineural cell damage, death and survival in the cochlea. *Front. Aging Neurosci.* 7Frontiers Research Foundation: 58, 2015.

Wu PZ, **Liberman LD**, **Bennett K**, **de Gruttola V**, **O'Malley JT**, **Liberman MC**. Primary Neural Degeneration in the Human Cochlea: Evidence for Hidden Hearing Loss in the Aging Ear. *Neuroscience* 407: 8–20, 2019.

Xing Y, **Samuvel DJ**, **Stevens SM**, **Dubno JR**, **Schulte BA**, **Lang H**. Age-related changes of myelin basic protein in mouse and human auditory nerve. *PLoS One* 7: e34500, 2012.

Xiong B, **Alkharabsheh A**, **Manohar S**, **Chen G Di**, **Yu N**, **Zhao X**, **Salvi R**, **Sun W**. Hyperexcitability of inferior colliculus and acoustic startle reflex with age-related hearing loss. *Hear Res* 350: 32–42, 2017.

Yang S, **Weiner BD**, **Zhang LS**, **Cho SJ**, **Bao S**. Homeostatic plasticity drives tinnitus perception in an animal model. *Proc Natl Acad Sci U S A* 108: 14974–14979, 2011.

Yeend I, **Beach EF**, **Sharma M**. Working Memory and Extended High-Frequency Hearing in Adults: Diagnostic Predictors of Speech-in-Noise Perception. *Ear Hear* 40: 458–467, 2019.

Yost WA. Pitch of iterated rippled noise. *J Acoust Soc Am* 100: 511–518, 1996a.

Yost WA. Pitch strength of iterated rippled noise. *J Acoust Soc Am* 100: 3329–3335, 1996b.

Zheng L, **Park J**, **Walls M**, **Tully M**, **Jannasch A**, **Cooper B**, **Shi R**. Determination of urine 3-HPMA, a stable acrolein metabolite in a rat model of spinal cord injury. *J Neurotrauma* 30: 1334–1341, 2013.

Zhou X, **Jen PHS**. The effect of bicuculline application on azimuth-dependent recovery cycle of inferior collicular neurons of the big brown bat, Eptesicus fuscus. *Brain Res* 973: 131–141, 2003.

Zook JM, **Casseday JH**. Convergence of ascending pathways at the inferior colliculus of the mustache bat,pteronotus parnellii. *J Comp Neurol* 261: 347–361, 1987.

VITA

EMILY XIAO HAN

Education

Department of Biological Sciences, Purdue University, *West Lafayette, IN USA* 2012/08 – Present

School of Life Science, Tsinghua University, *Beijing, China* 2008/8 – 2012/7

Bachelor of Science, Biological Sciences

Research Experiences

Research Assistant, *Central Auditory Processing Lab (Advisor: Dr Edward Bartlett)* 2013/4 - Present

Purdue University, West Lafayette, IN USA

Impact of blast-induced mild traumatic brain injury on central auditory processing

- Recorded auditory brainstem response and two-channel auditory evoked potential AEP) in blast-exposed rats;
- Performed acute craniotomy for *in vivo* SU recording on blast-exposed inferior colliculus;
- Devised measurements utilizing speech-tone iterated rippled noise (IRN) for blast-induced hearing loss assessment.

Single-unit (SU) response to reduced depth amplitude modulation in the aged inferior colliculus

- Recorded *in vivo* single-unit responses in anesthetized rats;
- Analyzed age-related changes in spectral and temporal processing ability of rat inferior colliculus.

Mentoring

- Trained graduate students on two-channel AEP;
- Supervised graduate students on operating TDT OpenEx system for acute SU recording.

Undergraduate Research Trainee, *Developmental Neurobiology Lab (Advisor: Dr Hong Luo)* 2011–2012

School of Life Sciences, Tsinghua University

Skills and Training

Animal Models

Familiar with *Rattus norvegicus* and *Drosophila melanogaster* neurophysiological model

Laboratory

In vivo single-unit electrophysiology (TDT OpenEx system)

Rodent handling, craniotomy and neuroanatomy

Immunofluorescent staining and confocal microscopy

Proficient in basic cellular and molecular biology techniques

Data analysis skill using Matlab

Other Skills

Fluent in English and Mandarin Chinese

Excellent in Microsoft Excel, Adobe Photoshop and Illustrator

Professional Association

Society for Neuroscience

Association for Research in Otolaryngology

Graduate Women in Science Program, Purdue University Fall 2012 – 2016

Teaching Experiences

Teaching Assistant, Purdue University

Neural Mechanisms of Health and Disease Spring 2021

- Graduate level course

Cellular Biology Fall 2013 and Fall 2020

Fundamentals of Biology II Spring 2018

- Held recitations for three classes of 25 students and co-directed two lab classes

First Year Research Experience (FYRE) Fall 2014 & 2015

- Mentored two classes of more than 20 students in the lab
- Prepared and processed tissue for class research projects

Administrative Experiences

School of Life Sciences Men's Soccer Team, *Tsinghua University*

Team Manager 2011/9 – 2012/5

- Communicated with personnel from university's soccer association during the 2011-2012 *Ma Yuehan Cup* intramural soccer tournament
- Managed photographic recording and promotion for the team

School of Life Sciences Student Union, *Tsinghua University*

Vice President of Event Promotion 2011/2 – 2011/12

- Implemented new work request rules between Department of Event Promotion and sister departments;
- Trained department recruits on visual design basics;
- Directed the advertisements and visual designs for the annual Student Festival event series;
- Awarded Social Activity Scholarship by School of Life Sciences.

Department Head of Event Promotion 2010/2 – 2010/12

- Co-founded Department of Event Promotion to provide promotional materials for sister departments effectively;
- Directed and Designed the advertisements and visual designs for the annual Student Festival event series;
- Awarded Outstanding Student Leader by School of Life Sciences.

Publications

Herrmann B.*, Parthasarathy A., **Han E.X.,** Obleser J., Bartlett E.L., "Sensitivity of rat inferior colliculus neurons to frequency distributions", Journal of Neurophysiology Sep 2015, DOI: 10.1152/jn.00555.2015

Abstracts

Oral Presentations

Han E.X., "Auditory processing deficits correspond to secondary injuries along the auditory pathway following mild blast induced trauma". *Blast Injury Conference 2019,* London, United Kingdom, 2019

Posters

Han E.X., Fernandez J., Shi R., Bartlett E.L., "Auditory Processing Deficits Correspond to Secondary Injuries along the Auditory Pathway Following Mild Blast Induced Trauma", *Annual MidWinter Meeting of the Association for Research in Otolaryngology (ARO),* Baltimore MD, 2019

Han E.X., Lai J., Race N., Shi R., Bartlett E.L., "Short-term Neural Response Changes to Sounds in Noise and Speech-like Sounds Following Blast Exposure", *Neuroscience 2017,* San Diego CA, 2017

Coventry B.S., Han E.X., Parthasarathy A, Bartlett E.L., "In Vivo and Modeling Study of Age-Related Changes in Frequency Tuning and Spontaneous Activity in the Inferior Colliculus", *Annual MidWinter Meeting of the Association for Research in Otolaryngology (ARO),* San Diego CA, 2014

Coventry B.S., Han E.X., Parthasarathy A, Bartlett E.L., "In Vivo and Modeling Study of Age-Related Changes in Frequency Tuning and Spontaneous Activity in the Inferior Colliculus", *Aging and Speech Communication (ASC) Conference,* Bloomington IN, 2013